Marine Physical Laboratory

VAST AEL Error Analysis

E.D. Wolin, D.E. Ensberg, J. Murray,
and W. S. Hodgkiss

Supported by the
Office of Naval Research
Contract N00014-89-D-0142(DO#1)

MPL Technical Memorandum 437

MPL-U-14/94
January 1994

Approved for public release; distribution is unlimited.

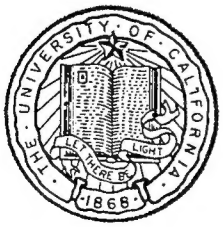

University of California, San Diego
Scripps Institution of Oceanography

REPORT DOCUMENTATION PAGE

Form Approved OMB No. 0704-0188

1. Agency Use Only (Leave Blank).	2. Report Date.	3. Report Type and Dates Covered.
	January 1994	MPL Technical Memorandum

4. Title and Subtitle.
VAST AEL Error Analysis

5. Funding Numbers.
N00014-89-D-0142 (DO#1)

Project No.
Task No.

6. Author(s).
E.D. Wolin, D.E. Ensberg, J. Murray, and W.S. Hodgkiss

7. Performing Monitoring Agency Names(s) and Address(es).
University of California, San Diego
Marine Physical Laboratory
Scripps Institution of Oceanography
San Diego, California 92152-5000

8. Performing Organization Report Number.
MPL TM-437
MPL-U-14/94

9. Sponsoring/Monitoring Agency Name(s) and Address(es).
Chief of Naval Research
Ballston Tower One
800 North Quincy Street
Arlington, VA 22217-5660 (Code 321)

10. Sponsoring/Monitoring Agency Report Number.

11. Supplementary Notes.

12a. Distribution/Availability Statement.
Approved for public release; distribution is unlimited.

12b. Distribution Code.

13. Abstract (Maximum 200 words).

The following report summarizes the types and effects of errors in navigating the vertical line array deployed by the Marine Physical Laboratory in the Northeast Pacific in July 1989. We argue that the overall root mean squared error (RMSE) in navigating array element positions is less than 3 m.

14. Subject Terms.
Array navigation, array element location, VAST.

15. Number of Pages.
86

16. Price Code.

17. Security Classification of Report.	18. Security Classification of This Page.	19. Security Classification of Abstract..	20. Limitation of Abstract.
Unclassified	Unclassified	Unclassified	None

DISCLAIMER NOTICE

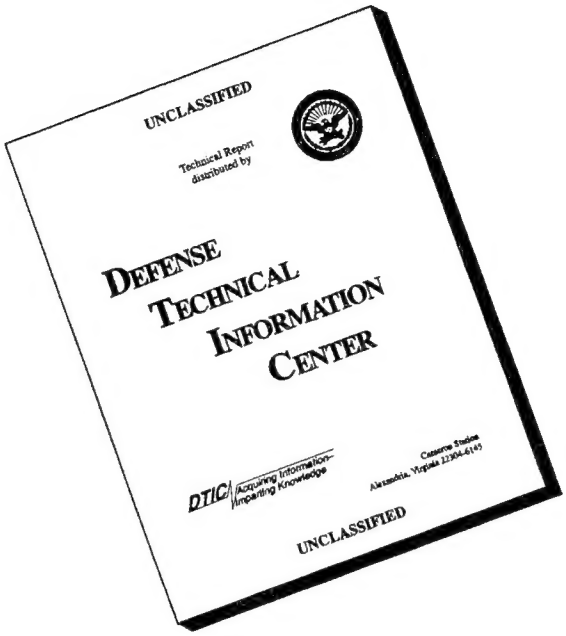

THIS DOCUMENT IS BEST QUALITY AVAILABLE. THE COPY FURNISHED TO DTIC CONTAINED A SIGNIFICANT NUMBER OF PAGES WHICH DO NOT REPRODUCE LEGIBLY.

VAST AEL Error Analysis

E. D. Wolin, D. E. Ensberg, J. Murray, and W. S. Hodgkiss

Marine Physical Laboratory
Scripps Institution of Oceanography
San Diego, CA 92152-6400

ABSTRACT

The following report summarizes the types and effects of errors in navigating the vertical line array deployed by the Marine Physical Laboratory in the Northeast Pacific in July 1989. We argue that the overall root mean squared error (RMSE) in navigating array element positions is less than 3 m.

Table of Contents

Introduction

The VAST MPL vertical line array was deployed in July 1989 in the Northeast Pacific Ocean from the R/P FLIP.

The purpose of this report is to estimate how much navigational error there is in the MPL vertical array positions. Sources of errors are discussed and their magnitudes estimated. How array positions were influenced by these errors is also discussed.

The geometry of the array and the surrounding transponder net is shown in Figures 1-3. The navigation of the array was done in two steps. First the transponders were surveyed in. Then in a second step these "known" transponder positions were used to navigate in the array elements. Figure 18 provides a summary of error sources for each.

Surveying/navigating in the transponders consists of 3-dimensional triangulation using the slant ranges derived from acoustic measurements (travel times). The acoustic travel times were converted into slant ranges using the harmonic mean of the sound speed velocities. This approach assumes that the ray paths are straight lines. However the more misaligned (horizontal) the assumed straight ray path is from the direction of the sound speed gradient, the more the true ray path is curved (see Figure 10). The effects of ray bending were incorporated as a correction term. These terms were calculated with the "Generic Sonar Model" (GSM) and are presented in Figure 11. The correction adds the difference between the straight and curved (true) paths and thus forms the corrected slant ranges using these to triangulate. A more exact method would incorporate the ray bending directly into the least squares solution. As the corrections are relatively small the error from the approximation is quite small (< 1m).

Figure 1 shows how the vertical array was navigated using known transponder positions. A transducer, whose location is described in Figure 2C, pinged to each of four transponders every ten seconds. The transponder interrogation sequence is described in Table 5A. All transponders replied at 12 KHz. These replies were recorded at the 25 navigation elements whose positions are described in Figure 2A.

The geometric picture of how the transponder survey was done is similar to Figure 1, but without the array and with two more transponders (which subsequently failed). For both the ship interrogated the various transponders in a round robin fashion and recorded the transponder replies back at the ship.

I. Transponder Survey Error

An acoustic survey was used to obtain accurate transponder locations. Although (GPS) transponder drop locations were recorded such a survey is necessary since the transponders drift as they descend to the bottom to unknown depth. Further GPS is only accurate to ~15-30m RMS. The final results of the acoustic survey appear in a map in Figure 3 where the ship moved slowly along the course described by the dots. Acoustically navigated transponder positions are also listed

numerically in Table 2. A ship (the USNS Naragansett) attempted to drive over each transponder in the net ranging to as many transponders as possible and recording replies on a chart recorder. (See Figures 5 A,B where 5B demonstrates how traces disappear when the ship is turning.) The number of audible transponders at any one time varies and is primarily a function of distance from the ship to the transponders. Table 4 specifies which transponders were interrogated during the various ship tracks. A unique interrogate/ common reply pinging sequence was used to interrogate the transponders, where the transponders listened at the frequencies listed in Tables 1 and 2. Each transponder replied with a 12 kHz ping. The operators attempted to mark which chart recorder trace corresponded to a given transponder, but were not always successful. The operators also did not record the integral number of seconds per trace. In these cases the chart recorder only provides fractional seconds. The GPS receiver was unavailable during the survey. No record exists of ship latitude/longitude during the survey. Figure 9B demonstrates the sort of possible ambiguity when not enough information is collected, i.e. not enough transponders were interrogated and integral seconds were not recorded by the operators. Further the operators were fooled by a depth varying batwing (transducer towed behind the ship) while the ship was turning, see Figure 8.

A typical survey strategy is to ascertain transponder depth by trying to pass closely over the top of a transponder. For geometrical reasons coming close yields a very accurate depth estimate (see Figure 6). In fact previous software algorithms at MPL fix depth using this technique and don't henceforth allow it to vary. This strategy is often implemented by essentially spiraling in on transponders by "boxing" them in (see Figure 7). Unfortunately this method was not carried out successfully for the first few transponders (see Figures 8 and 9).

A summary of desirable features while performing a transponder survey includes:

1) Initial GPS drop locations.

2) A (SeaBeam) contour map of the bottom for depth estimates.

3) Occasional ship locations during the survey (GPS or range/ bearing to a platform where location is known, e.g. FLIP).

4) A symmetric ship survey (i.e. ship positions symmetrically located around the transponders) with ship positions both close to being over the top of each transponder as well as far away from each transponder. The transponders should at least be ranged to from positions far away and 90 degrees in bearing to reduce geometric dilution of precision (GDOP).

5) The proper correspondence between the chart recorder traces and the interrogated transponder.

6) A record of the integral number of seconds per trace.

7) As many transponders recorded as possible from the various ship locations

While items (1) and (2) were available in this survey the others generally weren't, sometimes resulting in ambiguity. For example Figure 9 demonstrates an interesting scenario. The ship track used during the survey attempted to minimize the ship distance travelled while attempting to pass directly over the top of all the

active transponders. A better survey would have taken more symmetrical ship positions, particularly outside the net so as to minimize bias error. Bias errors, caused by an incorrect sound speed profile or slightly unknown timing delays tend to push the transponders radially inward or outward. However, as the transponders are almost exactly in opposing pairs with respect to the vertical array, most of this bias cancels. This is demonstrated in the simulation section.

Future improvements could also include:

1) Using a detector (preferably digital) rather than a chart recorder output to reduce person time and to increase accuracy.

2) Increasing the signal to noise ratio (SNR) and hence the number of interrogable transponders by improving the batwing design or by using different signals (rather than continuous wave sinusoids (CW)). The batwing was a towed wing that sank ~50 m below the surface of the ocean which contained the transmitter/receiver used to interrogate the transponders and listen for their replies.

3) Measuring the depth of the batwing in order to reduce the number of estimated parameters by one.

4) Using jitter reduction in the transponder interrogation sequences to reduce the transponder recognition time. Jitter in the transponder turn around time is the largest source of random error.

5) Using a transducer on a pole (or a hull mounted transducer) instead of a batwing so its transducer depth would be accurately known.

Verification of the transponder survey results was possible using the motion of the USNS Desteigeur and FLIP, their recorded GPS positions and recorded ranges to their transponders for the lower and upper halves of the transponder net, respectively.

The following procedure was used to navigate the transponders:

1) The recorded round trip travel times were digitized from the chart recorder output.

2) The transponder turn around time and receiver recognition time were subtracted.

3) These round trip travel times were halved to yield one way travel times.

4) These one way travel times were multiplied by their appropriate harmonic mean sound speeds and a small time delay added to account for ray bending. (See Figures 10 and 11 for an explanation of why and how ray bending corrections were made).

5) These data were input into a non-linear least squares (Marquardt) algorithm where the various ship transducer positions (X and Y only as transducer depth was known) and seven (assumed fixed) transponder (X,Y,Z) locations were estimated.

It is not possible to decompose or estimate the random or deterministic components of the transponder positional error directly from the data. This is because the ship is not stationary hence neither are the slant ranges from the ship to the transponders.

Random slant range errors during the transponder survey are estimated to be 2-4 meters RMS. This estimate was obtained from physical considerations. There were two primary sources of random error in the transponder survey. The first was transponder recognition error, i.e. error in turn around time (TAT) which was on the order of one-half to three milliseconds. The second source of error was in picking off the leading edge of the arrivals which constituted up to another two milliseconds of error (see Figure 18).

These random slant range errors propagate as much smaller errors (< 1 meter RMS) when estimating transponder positions (see Figure 19). This simulation demonstrates that most of the random slant range errors cancel themselves rather than contaminating the transponder position estimates due to the many (279) ship positions each derived via triangulation from the various transponders.

Bias errors are the largest source of transponder navigation error. Furthermore, there is no known reference, say a known transponder depth with which to calibrate the bias. Hence these bias errors have been bounded using physical considerations. It is possible however to remove much of the bulk bias in the transponder positions when navigating the array elements. Viewing Figure 1, the transponders are shown to have a lensing effect where moving them outward radially has the same effect as if the transponders were held fixed and the slant ranges shortened roughly equally. This shortening of the slant ranges would cause the array to be translated, primarily downward due to the roughly symmetric transponder placement. The bias errors are caused primarily by error in estimating sound speed precisely combined with any unknown system bias error. Error due to ray bending is a second order concern as this was estimated and corrected for via table lookup (see Figures 10, 11). Further the upper navigation element is constrained by FLIP and the depths of the lower five elements can be estimated via the downward (12 kHz) ping, hence most of the bias was eliminated.

As sound speed error is the primary source of error an upper bound was estimated as well as the effect this upper bound would have on transponder navigation.

This upper bound caused less than one meter/second error in the harmonic means used to convert the travel times into slant ranges. A one meter/second error in harmonic mean causes less than 1.2 meters of differential slant range error; that is error that isn't radially the same for all transponders and hence correctable when navigating array elements (see Figures 28 A-C). There is much more bias in a common/bulk bias due to the symmetric way that the survey was done. In fact this bulk bias is estimated to be about seven meters of primarily radial transponder motion. However, this is corrected when the transponder positions are used to navigate array elements as discussed below.

An attempt was also made to estimate unknown system bias error by varying bias numbers as is done below when navigating array elements. Unfortunately this attempt at bias cancellation failed for the transponder survey as the ship was not stationary and reducing slant ranges continually reduces the RMS error. However as

is discussed below most of the bulk bias (the portion propagated by the incorrect common radial motion of the transponders) was eliminated during array navigation.

II. Array Navigation Error

In order to localize the array elements the following procedure was used:

1. To get slant range travel times from the transponders to the array elements the travel time from FLIP to a transponder was subtracted from the "round trip" travel time from FLIP to a transponder to an array element (the travel time recorded at the array element). The FLIP-to-transponder round trip travel times were derived from the top navigable hydrophone (46m depth), geometry, and the FLIP rotation angle.

2. The ship to transponder time was computed from the round trip travel time collected at FLIP by ST= (SRTTT - TAT - SRR)/2, where SRTTT is the round trip travel time from FLIP to the transponder and then to the array, TAT is the transponder turn around time delay and SRR the array receiver recognition time delay.

3. Then (RTTT - ST - TAT - ARR), where ARR is the array receiver recognition time, was used to compute the travel times from transponder to array element.

4. The four travel time series, one for each transponder were interpolated to every ten seconds then desampled to even minutes.

5. This transponder to array element travel time was multiplied by its harmonic mean sound speed and a small travel time was added to correct for ray bending.

6. These data were then input into a non-linear least squares (Marquardt) algorithm where the various AEL (X,Y,Z) positions were estimated using the slant ranges and the previously derived transponder positions.

7. The depth of the array was adjusted by matching known depths of the top and bottom array elements (the later via a downward 12 kHz ping from FLIP) and correcting the slant ranges by a common bias until the depths matched.

AEL (Array Element Localization) error consists of a combination of errors from both the transponder positioning and then the array positioning based on these transponder positions. Both sources of error may be decomposed into random and deterministic (bias) components.

Unlike the slant range error in the transponder survey the error in the slant ranges from the transponders to the array elements is easy to view and analyze since the array motion is slowly varying. This error is similarly decomposed into random and deterministic components and both bounded by empirical and practical considerations. Furthermore, much of the deterministic component may be removed. The portion of the deterministic component that may be removed is the combination/ sum of the common radial bias in the transponder positions with the common slant range bias.

The random slant range error was bounded by trend removal (high pass filtering) then the resulting high frequency "jitter" examined. Some of this "jitter" was caused by actual array motion; still this provides an upper bound. This random error in the transponder to array element slant ranges is estimated to be one to two meters RMS. This is plotted across time in the "Standard deviations of slant ranges" plots (Figures 23A - 23E). A bound based on physical considerations is also given in Figure 18. Studying the description above as to how the slant ranges are calculated, the random slant range error consists of only 1/2 the random error in the transponder turn-around-time and 1/2 the random receiver recognition error at the ship as well as the random receiver recognition error at the array.

Figure 19A summarizes simulations which demonstrate that AEL positions are affected by random slant range error (error in all slant ranges) by roughly the magnitude of the slant range error. These simulations started with the final transponder and ship positions as acoustically navigated and the exact slant ranges between these ship and transponder positions. Independent identically distributed Gaussian noise sequences with zero mean and different standard deviations (1, 3, 5) were added to the (exact) slant ranges. Two different simulations were run, one with only the transponder X-Y-Z's varying and the other with both the transponder and ship positions varying. Results are similar and show that even with a standard deviation of 5 that the transponders are generally off by much less than a standard deviation of 2. The exception to this is transponder 3 who has a variance slightly greater than 2. Note that the northernmost three transponders were at the start of the survey when the survey ship neglected to pass over the top of the two aforementioned transponders as well as only pinging to three or four of the transponder simultaneously. The key point here is again that even with a large error represented by a Gaussian with a variance of 5 m that the error in estimating the transponder locations is on the order of 2m. This is of course due to the many ship positions used in the survey which results in cancellation of the (random) errors. Note that there are two known sources of random error; there is digitization error from selecting points from the chart recorder (estimated to be less than two meters) and random detection/ recognition error at both the transponder and at the ship (estimated to be less than two meters).

Figures 20.A.1 - 20.A.9, 20.B.1 - 20.B.12 describe how any transponder's X, Y or Z motion would affect array element positioning. In particular they suggest that an incorrect transponder position affect the array by less than two-thirds of the magnitude of the error.

Figure 19B examines how random error in all the transponder positions affects array navigation. It demonstrates that array navigation errors are about the same order of magnitude as the random transponder positional error. As there is potentially only small error (argued above) there should be only a slight array positional error (again note this is a consistently biased error).

Figure 19C shows how random slant range errors affect the array position estimates (here ignoring the fact that we can estimate the array depths fairly well). For a one meter RMS error in the slant ranges we see approximately the same error at the array; for a five meter RMS error in slant ranges we see a three meter RMS error at the array. By fixing depth these errors are reduced by roughly a factor of three as is the case for the aforementioned transponder case. Note the causes of random slant range error are quite similar to those of the transponder navigation error; random digitization error as well as the transponder and array navigation

element random detection error. The *random* is emphasized as bias errors tend to cancel due to the known array navigation element depths. Note in the third and fourth sets of plots the error in Y (North/South) tends to be slightly larger than the error in X (East/West) due to asymmetric transponder locations as two (of originally six) transponders died. Also note there is a greater depth error (and less X-Y error) on the lower navigation phones due to shallow angles (22 degrees at the bottom navigation element).

Figure 19D suggests that bias error in slant ranges affects AEL negligibly except in depth where it has a dramatic effect, particularly at the bottom of the array. Most of this depth error is eliminated as we have very good estimates of the top and bottom of the array and the slant ranges were corrected via a common bias to match these known depths.

Figure 13 displays the FLIP rotation angle. This is needed since the top array element is up 46m and is on one side of FLIP; in order to navigate FLIP this angle and a geometric computation based on angle must be made. Further this data was recorded by the FLIP crew; sometimes every 30 minutes, sometimes with a 3 hour gap. A simulation assumed that the angle is 20 degrees off and demonstrated that the error in navigating the array is still negligible. That 20 degrees is sufficient is obvious from a closer look at the slowly varying time series in Figure 13.

The AEL bias error consists of error produced by having incorrect transponder positions combined with errors caused by an incorrect sound speed when computing harmonic means/ray trace corrections (from the transponders to the array elements) as well as any unknown system delay in either the ship recognition circuit (negligible) or the array recognition circuit. Incorrect transponder positions contribute less than one meter of differential slant range error. The different transponder (to a fixed array element) slant ranges are over very similar depths, hence incorrect sound speed bias is almost identical across the different slant ranges. The system delay is also a bulk bias that is identical for all transponder slant ranges.

As was previously stated most of the common/bulk bias was removed by constraining the slant ranges so that the navigated depths matched depths estimated by the known 46m depth at the top and the depth ascertained from the downward ping at the bottom of the array. The common bias is the combination of the aggregate bias in slant ranges that is common for all four slant ranges, combined with the common radial bias in the placement of the transponders. This bulk bias is estimated to be five meters and this length was subtracted from all (four) slant ranges.

Remaining uncorrected aggregate bias (in slant ranges and incorrect transponder positions) is estimated to be less than three meters and by simulation to affect array navigation by less than two meters (absolute). This number was derived heuristically by adding the worst-case array positioning errors from the two sources of AEL bias error: the differential transponder positions and the differential bias errors in the slant ranges.

There are also several additional errors which are of second order importance:

1) Transponder (conical) motion may translate the array slightly over time (since local currents should be very similar for the 5 transponders). With an estimated

bottom current of 10 cm/sec and a 30 m tether length these discursions are estimated to be less than 1m (absolute).

2) Sound speed variability (primarily in upper 50-100m) may cause slight bias error. All array navigation elements are below this upper level; hence the only time this upper region is used is for navigating the transponders where the travel path was from the ship's transducer (7m) to transponders which were approximately 5000 meters deep. Due to the very long travel paths the effect of the upper region variability is negligible.

3) Both additive and multiplicative biases exist. For example sound speed errors multiply whereas system delays add. Further these are measured as a sum hence we don't know how large each component is. However due to the geometry, the slant ranges are all of similar length, hence error due to correcting one way rather than the other is a second order effect.

III. Conclusions

AEL random errors appear to be on the order of one to three meters RMS.

AEL bias error is estimated to be on the order of two meters (absolute). This was primarily caused by combined uncorrectable differential bias in transponder positions and slant ranges.

IV. Present/Future Considerations

It is desireable to have a symmetrical transponder survey, that is to have ship positions symmetrically located about the transponders. Symmetric ship survey positions assure that the unknown bias (caused by inaccurately measured sound speed and any unknown hardware delays) will push the transponders radially in or out symmetrically. It is also important to collect slant ranges both when the ship is directly above the transponders and when the ship is far away (horizontally) from the transponders. Ship positions directly above a transponder yield depth information, while ship positions far from a transponder will yield information about the transponder in the X-Y plane to the extent that the slant ranges are horizontal (e.g. a 45 degree downward slant range would yield about the same information in Z as in X-Y).

Placing the transponders symmetrically about the array is also important. Having opposing pairs of transponders spaced equally in angle about the array assures that the bias will cause primarily depth errors which may be reduced via a central (upward or downward) transponder. This symmetry combined with an accurate array element depth estimate (say from a calibrated engineering depth sensor) pinpoints array depth, without having to rely on additive constants yielding a minimum mean square error (averaged over long time intervals to eliminate the random component). In VAST the FLIP transducer was used for this purpose. (However the power should have been reduced when pinging down the array (at 12 KHz) as the powerful ping flooded the navigation detector circuits for the first 20 elements, causing no detections.) Knowing transponder depths accurately also simplifies the

problem. Note that in VAST two of the MPL transponders failed, which adversely affected the symmetry. (There is slightly more information in a NNW/SSE direction as one can see from the various error simulations.)

Having redundant transponders is also desirable for two reasons. Navigation error caused by random slant range errors is reduced on the order of the number of transponders. Also having extra transponders allows for successful navigation if transponders fail (as two did in VAST). In general it is very desirable to have at least four transponders as these are used to estimate three parameters, each array element's (X,Y,Z) position. In VAST six transponders were deployed and four eventually used to navigate the MPL array elements.

Jitter reduction, although not used in VAST, would have been beneficial. Jitter reduction uses two interrogation frequencies which enhances a transponder's ability to more accurately detect the leading edge of the interrogation pulse. By using jitter reduction the largest source of random error, transponder turn-around-time, is significantly reduced.

Transducer depth was known for array navigation but not for transponder navigation. Knowing transceiver depth reduces by one the number of parameters to estimate in all least squares calculations. Rather than a towed source on a batwing (where the depth varies as the ship changes speed or turns) a hull mounted transducer is preferable.

Acknowledgements

Dick Harriss and David Ensberg drew several of the descriptive figures. James Murray did the computer simulations in Figures 19, David Ensberg in several of the other figures, and was also responsible for navigating much of the array. Sharon Escher was responsible for computing ray trace corrections, as well as the work involved in figures 11, 27 and 28. This work was supported by the Office of Naval Technology under ONR contract #N000-14-89-D-0142.

Appendix A How Depth of MPL Vertical Array Was Fixed

As the transponder geometry was quite symmetric with respect to the MPL vertical array almost all of the bias cancels if the depth of the array can be estimated correctly.

There were two different methods used to discern the depth at the top and the bottom of the array, respectively. The first method used is that the average depth of the top AEL phone (42.8m) is known with high accuracy as it was tethered to FLIP. This number may be derived from Figures 2A and 2B which show the distance from element 199 to the surface (2 meters), the interelement spacing (14.9 meters), and how the inter-element distance may be derived.

Secondly a 12 KHz ping was sent 50 seconds after the minute on even minutes from the transducer mounted at the bottom (89 meters down) of FLIP (see Figure 2C). Unfortunately as power at various ping frequencies was fixed (to reach transponders which were much farther than the bottom of the array from the transducer) this 12 kHz ping was too powerful to detect for all but the farthest (bottom five) AEL phones. However as this signal was detected on the bottom five phones a very close approximation to their depth (as the array is nearly vertical) may be ascertained by multiplying this travel time by the appropriate harmonic mean, as this is essentially vertical ray path. Further unlike the pings to the various transponders this travel path has no random transponder turn-around-time.

The slant ranges from the transponders to the top and bottom of the array were differentially corrected using ray trace (GSM) results. Approximately 1.5 meters was added to the bottom (more horizontal ray path, see Figure 10), this value was differentially added to each element up the array so that at the top no correction was added. The slant ranges were then adjusted slightly so that results would fit within the estimated top and bottom depths. This was done by averaging over long time segments so that the random error was averaged out. Using this technique the results were quite consistent; this was demonstrated by plotting histograms.

To improve AEL results in future experiments the power of the downward pulse should be reduced and some quick look analysis done to guarantee that the pulse was detected on all navigation phones. This would yield accurate depth estimates of each individual AEL element, simplifying the task of localizing the array and increasing the accuracy of the results. An added benefit, assuming that the downward ping is received on all elements is that the FLIP transducer can be navigated, then the downward pings could be used (with lower standard deviations/ higher weights) in the least squares formulation. This would more accurately constrain the interelement distances since the downward pulse is much more accurate than the FLIP-to-transponder-to-array_element travel path (as the path is much longer, more horizontal, and the transponder turnaround time (the largest source of random error) isn't involved in the downward 12 kHz ping.

Figure Descriptions

Array and Transponder Net Geometry (Figures 1 - 4)

Figure 1 demonstrates how acoustic navigation was done. A unique interrogate/ common reply approach was used where every ten seconds a different transponder was interrogated from a transducer located at the bottom of FLIP (see Figures 2A, 2C, Table 5A). The transponders replied at 12 KHz which was detected back at the transceiver as well as at the array navigation elements. The transceiver also sent a 12 KHz ping as one of the interrogation frequencies, where the detection of this ping at the array allows the transceiver to act as an extra transponder. Unfortunately this ping was sent at the same power as the ping used to interrogate the transponders. The array elements were much closer to the interrogator than the transponders. Hence this 12 kHz ping was only detected at the lower five array elements. As the array was nearly vertical this does fix the depth of the bottom five elements of the array.

The vertical array consisted of 200 acoustic array elements spaced 14.93m apart which produced a 3 km aperture (see Figure 2A). The array was originally designed with a 15 m spacing (lamda/2 = 50 Hz) but this was changed slightly by the addition of vibration isolation rings (see Figure 2B). These rings were added to reduce the effect of cable-strumming which induced low frequency noise into the hydrophones.

The hydrophones were numbered 1 , 2 , ... , 200 with 1 being the bottom hydrophone. Every 8th phone starting with phone 4, i.e. 4, 16, ... , 196 doubled as a navigation phone.

The array acoustic data were sampled at 250 Hz except during Tomography mode. In this mode every fourth phone starting with phone #2, i.e. 2, 6, 10, ... , 198, was sampled at 750 Hz.

The navigation data was always sampled at 250 Hz. However these 8-bit words represented the envelop of the output of an energy detector so that navigation information was effectively obtained every 0.5 ms on every eighth phone.

The topmost navigation phone (at 43m) along with the receiver (at 89m) geometry and FLIP rotation angle were used to navigate FLIP and hence back out the transceiver-to-transponder travel times (see Figures 2A, 2C and 13).

The transponder geometry is described in Figure 3. Transponders were placed in opposing pairs about 5 Km from the array equally spaced in angle. Simulations demonstrated that this was an optimal geometry for reducing navigation error. Transponders were placed on 30 m tethers (i.e. they were 30 m above the bottom) to place them out of any possible shadow zones (see Figure 4). Further the displacement of transponders given typical bottom currents is less than one meter. Such a current would also translate all transponders in the same direction, hence translate the array by less than one meter.

The vertical array has been navigated for nearly the entire experiment using the 21 working navigation hydrophones and has also spacially interpolated to obtain positions for all 198 underwater hydrophones.

Navigating the Transponders (Figures 3 - 13)

These figures demonstrate how the transponders were surveyed.

Navigating the Array (Figures 14 - 16)

These figures demonstrate how the array elements were navigated.

Error Sources/ Error Decomposition (Figures 17 - 18)

These figures demonstrate the sources of error for both transponder and array navigation as well as how this error may be decomposed into determinstic (bias) and random components.

Error Simulations (Figures 19 A-E)

These figures summarize the results of various simulations designed to measure how random errors from various sources propagated into the array element navigation estimation error.

Effect of Deterministic Transponder Error (Figures 20.A,B)

These plots examine the effect absolute transponder error has on AEL navigation. Each transponder was perturbed plus and minus 10m in X, Y, and Z for two cases; a vertical array and an array tilted 2 degrees N/S. This simulates the extremes for the VAST vertical array. Both cases have virtually identical results since the overall geometry essentially is the same. As the results are virtually identical, only one set of plots is given.

In general 10 meters of transponder position error has the effect of moving the array less than 5 meters. This is of course because of the opposing transponder (whose slant range is correct) cancels out about half of the error. The other two transponders affect the AEL error in that it is perpendicular to the line between these other two transponders. Transponder errors in the E/W and NNE/SSW transponders have a symetric response in terms of AEL error.

The following figures describe how transponder motion affects AEL error. Note in the figures that arrow lengths show roughly how the AEL error is less than

the 10 meter transponder error. A dot means up (out of the page), an x down (into the page). Note that the AEL element simply moves as to minimize the least squares fit for all four transponders.

For example in Figure 20.A.4 note how N/S errors in E/W transponders has a negligible effect on array positoning as virtually all the information from transponder 2 (or 4) is in the East/West (and upward) direction.

A more complicated error is in Figure 20.A.3, an eastward error in transponder 3 (or transponder 5). These will tend to move the array north and up in the water column (where there is more upward error at the bottom of the array). The reason for this is that the E/W transponders (2 and 4) constrain the array very tightly in the E/W direction as they are almost due E/W of the array, whereas the other pair (3, 5) are NNE (~32 degrees) and SSW and therefore yield primarily N/S information. The depth error at the bottom of the array being greater than the depth error at the top is explained by the different angles between the transponders and the AEL elements; the angle between any transponder and the top AEL hydrophone is about 45 degrees whereas the angle between any transponder and the bottom AEL hydrophone is about 24 degrees. Due to these angles there is more depth information for the top AEL phone, hence the top element is more constrained in depth than lower ones.

Another example is in Figure 20.A.2, how a 10m eastward or westward error in transponder 2 or 4 affects AEL location. Here the array is heavily constrained in the NNE/SSW direction, hence error is propagated in both X and Y (as well as Z). Note that this X-Y AEL error is perpendicular to the other pair of opposing transponders (3, 5) as previously discussed.

Error Estimation (Figures 21 - 26)

These figures summarize the magnitude of slant range and array element navigation errors.

There were three major types of time-varying navigation errors in the VAST 1989 data. The first and most common type of error in the experiment was that of gaps in the AEL data. Four of the 25 AEL detectors (AEL elements 15, 17, 19, and 24) did not work during the experiment and spatial interpolation was necessary in order to determine their positions. Furthermore, on occasion, the top AEL element (AEL element 25) did not detect the 11 kHz transponder and also was interpolated spatially. Short temporal gaps (< 10 minutes) were interpolated temporally. Gaps typically were caused by an array reset or interrogator box failure. In these cases the RMS error was set to 0 in the navigation results as a flag. When these gaps were large (> 10-30 minutes) interpolation was not a practical alternative.

The second type of error is that the interrogation pulses did not get sent exactly when intended, but were slewed for two of the four transponder frequencies. Figure 21A shows the travel times of the downward pulse received on AEL element 5 over the first six days of the experiment. On days 188, 189, and 190 the ping time was very consistent. For most of day 186 and the first 15 hours of day 187 the ping time delays ramped up for the pulses to two of the four transponders (see Figure 21B) as well as for the 12 kHz (downward) pulse.

To correct this error, a regression line was fit to each problem area (two on day 186 and one on day 187) to determine a trend line. Then an estimated travel time was determined by obtaining an average travel time over many hours of data. The trend line was subtracted out of the data, along with a constant offset if necessary, so that the mean travel time was close to the expected travel time (see Figures 21CD). Once this was applied to the two transponder's travel times, the AEL elements navigated to believable locations.

The third type of error was caused by replacing our primary interrogator box with one which had hardware problems. This was necessary as our primary box needed to be transferred to the tug in order to acoustically survey in the transponders. The substitute box sent pings to only two of the transponders with unknown offsets (see Figures 21E and 21F). Therefore, this data was judged to be unnavigable.

Estimating Sound Speed (Figures 27 A-F)

These figures summarize the error in estimating sound speed

Effect of Sound Speed on Transponder Navigation (Figures 28 A-C)

When the VAST analysis first began, the Chen-Millero sound speed equation was deemed best and used to convert travel times into distances in order to locate the transponders. Later, it was decided that the Del Grosso sound speed equation was more representative of the environmental conditions. Therefore, the following plots were produced to show the relationship of the transponder positions as found by both sound speed profiles and by incorporating ray tracing corrections into the positions.

Three 2-dimensional plots show the directional movement in the XY, XZ and YZ planes. A description of each plot follows.

XY Directional Movement - These plots show a plan (X-Y, looking down) view of the survey (small dots). The transponders are found by using the first sound speed of the second line of the plot title (8 transponders connected by lines). The direction and relative magnitude of motion from the above transponder to the corresponding transponder is found by using the second sound speed in the second line of the plot title (lines extending from the line connecting the 8 transponders). The small square plot shows the net directional movement (vector sum) and actual magnitude of the movement in the XY plane. Transponder positions for both the first and the second sound speeds (in the second line of the title) are also listed on the plot.

YZ Directional Movement - Similar to XY directional movement these plots show a YZ view of the the transponders.

XZ Directional Movement - Similar to XY or YZ directional movement these plots show an XZ view of the the transponders.

Estimating Wind Direction (Figures 29 A-C)

These figures show the magnitude and direction of wind during the VAST experiment.

Array Navigation Block diagram (Figure 30)

This figure summarizes how array element navigation was done.

Table 1 Initial Transponder locations (GPS + depth guess)

Xpdr	Name	X pos	Y pos	Z pos	kHz
1	M6	4944.4	-8713.6	5080.0	10.25
2	M3	7545.5	-4491.8	5080.0	10.00
3	M1	5257.0	-126.2	5050.0	11.00
4	M4	-2461.7	-4353.4	5162.0	10.50
5	M5	-95.7	-8653.4	5133.0	10.75
6	N4	-527.2	-14767.8	5160.0	9.50
7	N3	2518.6	-18506.9	5122.0	10.00
8	N2	7539.1	-17460.0	5100.0	10.50
9	N1	8956.6	-12790.0	5114.0	9.00

The X and Y positions were obtained from the GPS positions of the ship when the transponders entered the water. These were translated to meters with M2 (which died) at (0,0)=(34 2 27.619 lat, 139 59 53.464 long). The depth guess is an estimate of depth from a seabeam contour map and digitized ship survey data.

Table 2 Navigated Transponder Locations (using ship survey)

Xpdr	Name	X pos	Y pos	Z pos	kHz
1	M6	4944.4	-8713.6	5080.0	10.25
2	M3	7745.3	-4507.9	5104.6	10.00
3	M1	5344.0	1.4	5043.5	11.00
4	M4	-2277.2	-4399.6	5170.0	10.50
5	M5	116.9	-8666.2	5154.7	10.75
6	N4	-475.1	-14809.	5167.7	9.50
7	N3	2502.0	-18491.	5131.8	10.00
8	N2	7600.1	-17520.	5101.4	10.50
9	N1	8993.6	-12916.	5113.3	9.00

These values were obtained using digitized data from an acoustic survey where a ship traversed the area interrogating and listening to replies from the transponders. Table 4 refers to which transponders could be heard from which ship locations. A non-linear least-squares algorithm was used to obtain the results (RMSE = 3.16 m)

Table 3 Desteigeur Estimation of Transponder Locations

Xpdr	Name	X pos	Y pos	Z pos	kHz	# of samples	RMSE
5	M5	-6.33	-8695.98	****.**	10.75	66	31.8669
6	N4	-479.67	-14884.08	5177.95	9.50	69	24.2641
7	N3	2482.80	-18421.03	5152.20	10.00	67	14.3028
8	N2	7570.24	-17533.66	5118.45	10.50	56	18.7150
9	N1	8948.77	-12955.47	****.**	9.00	47	21.4778

These values were obtained by using Desteigeur GPS and transceiver data. The large RMSE's in the table are primarily due to the inherent 15 - 30+ meter RMSE in GPS estimated positions (Geometric Dilution Of Precision). Hence these results are less reliable than those in Table 2 (although they are close). Transponders 5 and 9 were unable to iterate on Z (depth) due to insufficient data.

Table 4 Visibility of Transponders from a given survey area

Xpdr Areas	Transponders Visible
2_1	5 2 9
2	2 3 9
3_2	2 3 5
3	2 3 4
4_3	2 3 4 5
4	4 5 6
5_4	4 5 6
5	4 5 6 8 9
5_9	2 5 6 7 8 9
6	6 7 9
6_5	5 6 7 9
7	6 7 8 9
7_6	6 7 8 9
8	7 8 9
8_7	7 8 9
9	7 8 9
9_8	7 8 9

X_Y is the region between transponder X and transponder Y.

Table 5A Transponder Interrogation Sequences (MPL)

MPL before 188 0709		MPL after 188 0709	
Sec	(even min)	Sec	(even min)
00	10.00	00	10.00
10	10.50	10	10.50
20	10.25	20	9.75
30	10.75	30	10.75
40	11.00	40	11.00
50	12.00	50	12.00

The MPL interrogation sequence was repeated every even minute, (e.g. 23:02:00 10 kHz, 23:02:10 10.5 kHz, etc.)

Table 5B Transponder Interrogation Sequences (Norda)

Norda before 187 1520		Norda after 187 1520			
Sec	(odd min)	Sec	1	3	5
00	9.00	00	9.00	10.75	10.00
10	10.50	15	10.50	10.25	9.50
20	10.00	30	10.00	9.00	10.75
30	9.50	45	9.50	10.50	10.25
40	10.75				
50	10.25				

The Norda interrogation sequence was initially repeated every odd minute. (e.g. 23:01:00 9 kHz, 23:01:10 10.5 kHz, etc.) After 187 15:20 Norda changed to a 15 second cycle where they completed a full cycle every 3 of their odd minutes. (e.g. 23:01:00 9 kHz, 23:01:15 10.5 kHz, ..., 23:03:00 10.75 kHz, ..., 23:05:45 10.25 kHz.)

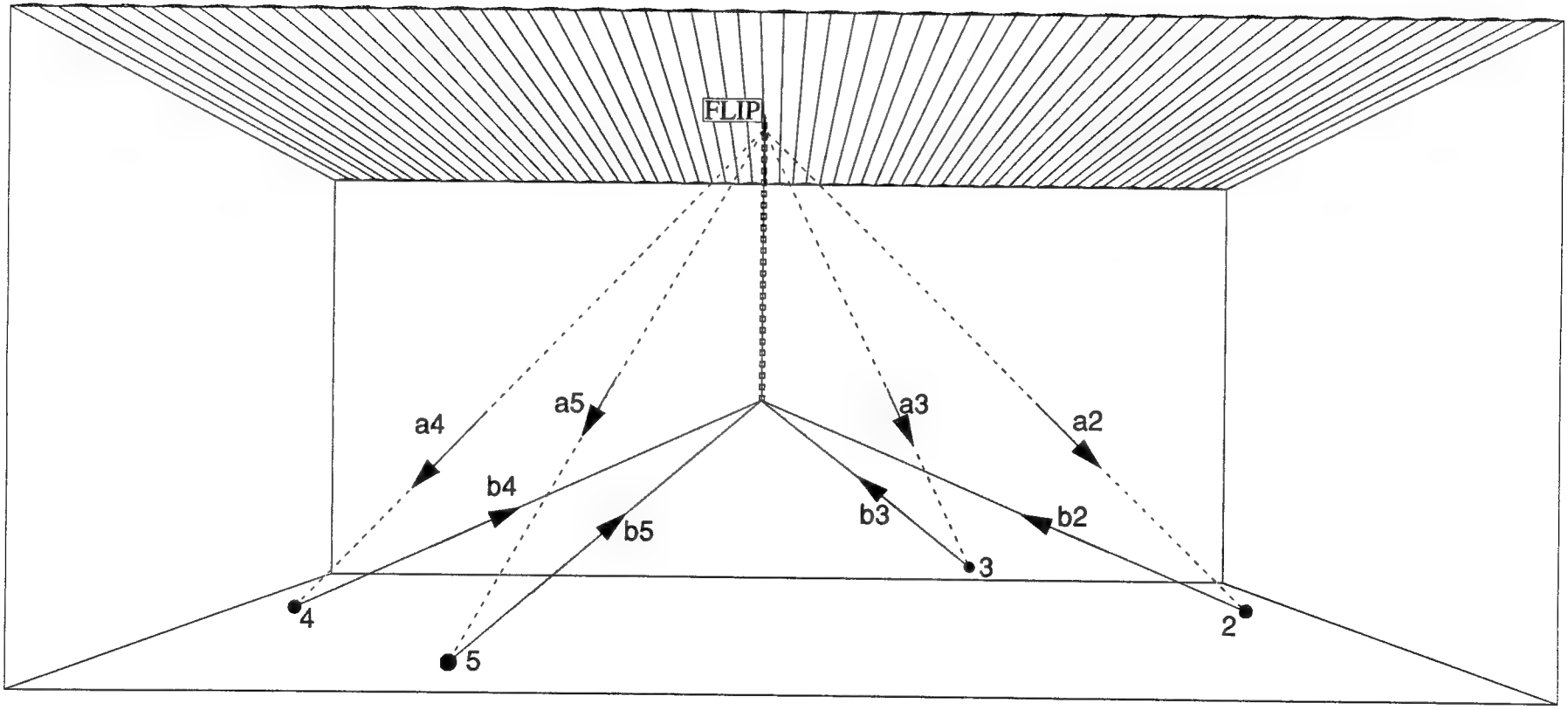

Figure 1 Navigation of the '89 Vast Vertical Array Elements

FLIP pinged in a round robin to four transponders, denoted 2, 3, 4 and 5.
The transponder replies were recorded at the array.

Figure 2A -- MPL VAST vertical array configuration

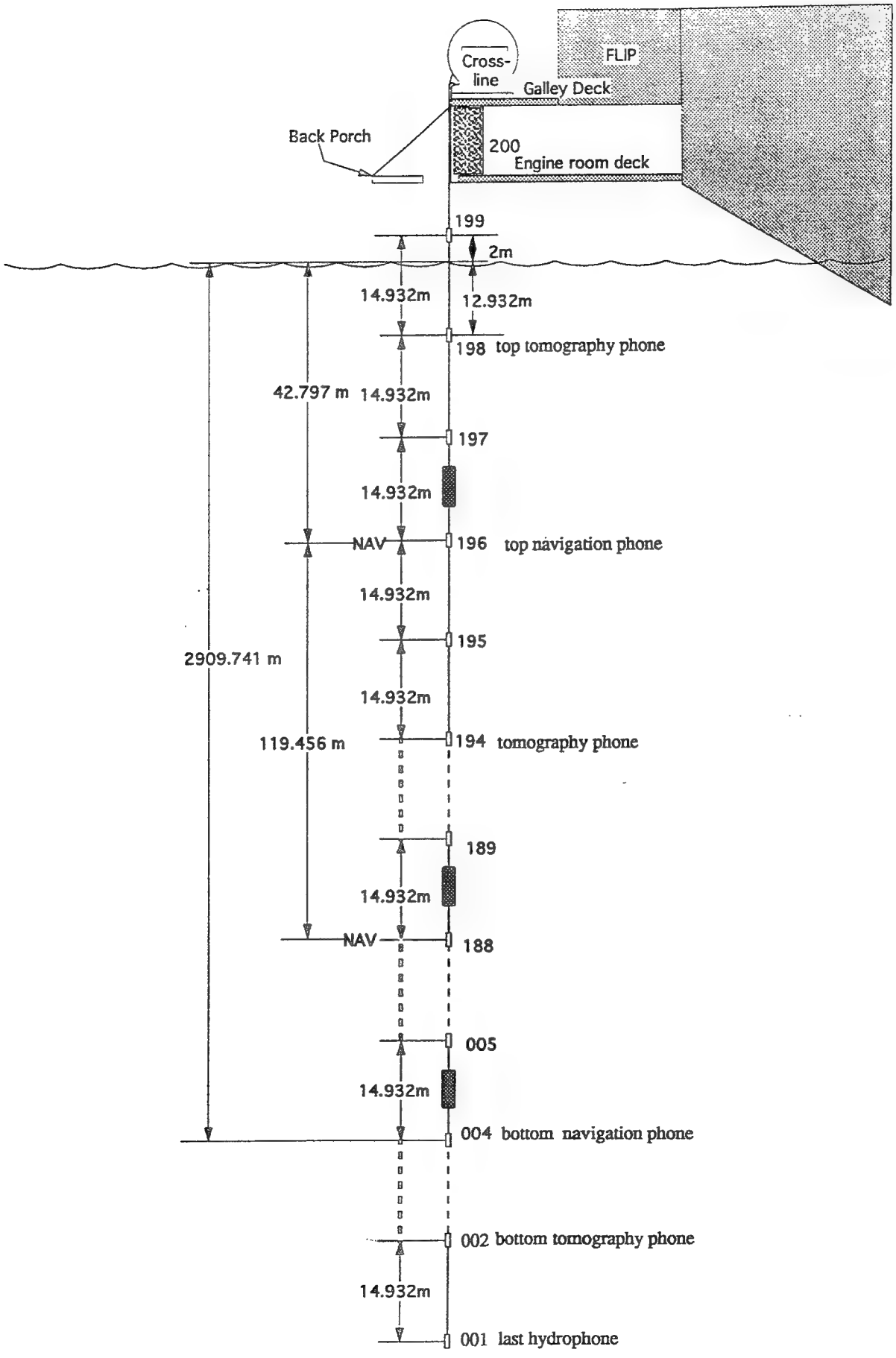

Fig. 2b

How the vibration isolation rings shortened the LVLA array hydrophone spacing from 15m to 14.9m.

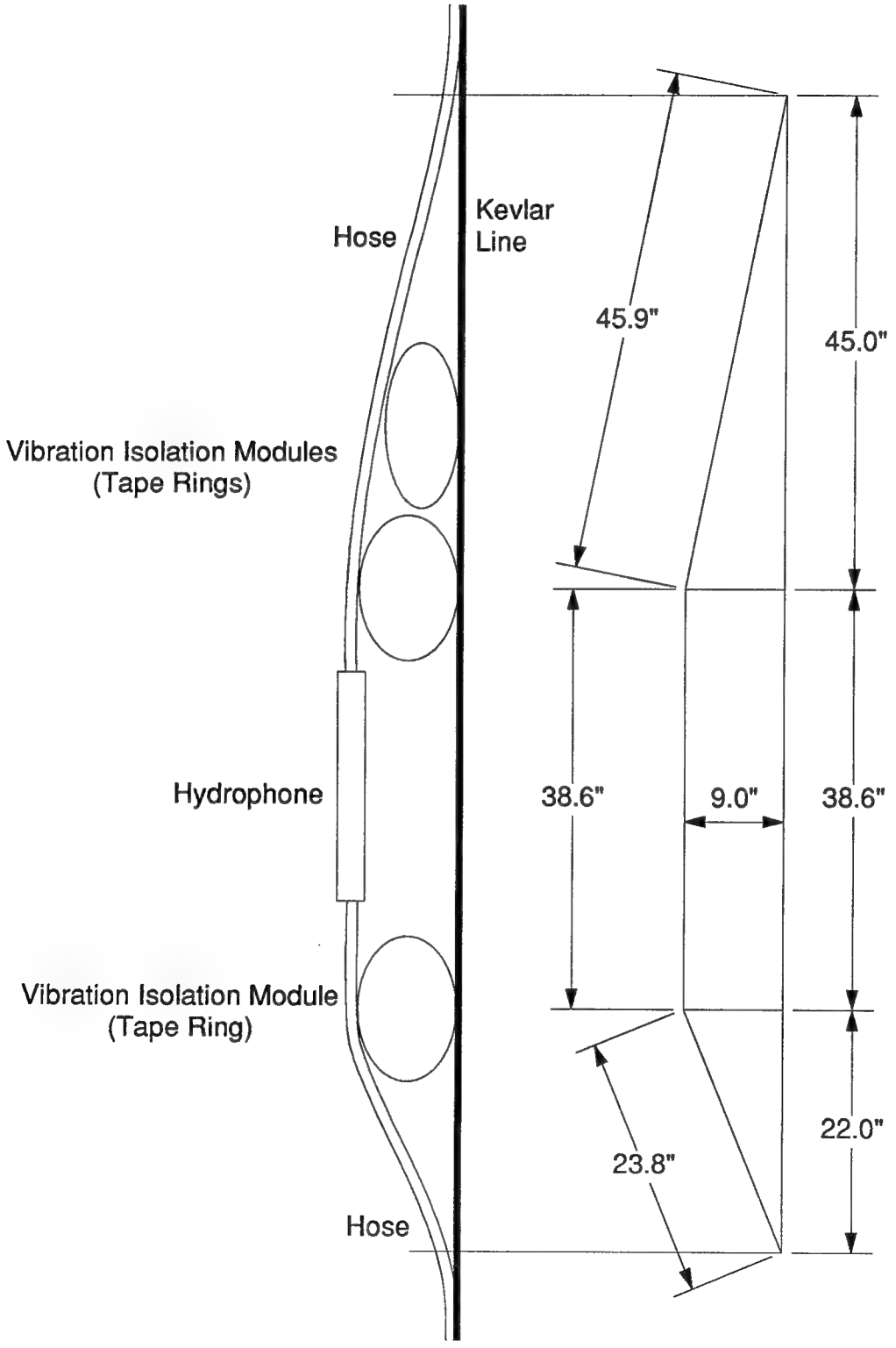

Fig. 2c

FLIP source and receiver geometry. Note that the source was 89 meters deep and the navigation receiver is 46m above the source.

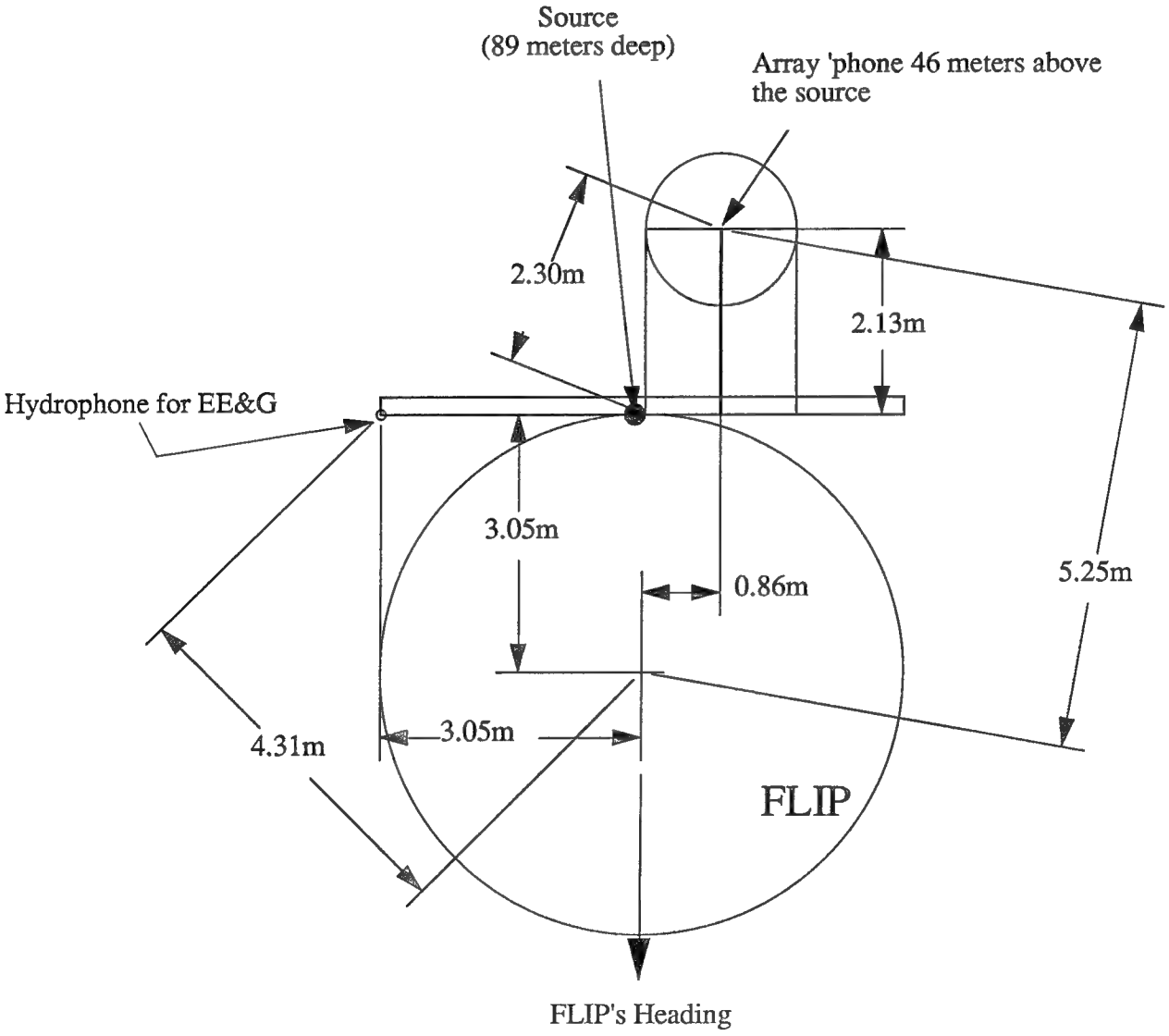

Looking Down

Figure 3 Transponder Positions

- The solid lines indicate the intended ship track, the vertices being the initial transponder drop locations (GPS).
- The X's indicate the navigated transponder locations.
- The dots are navigated ship positions which are samples from the acoustic survey.
- The two circles are transponders that stopped working shortly after the experiment began.

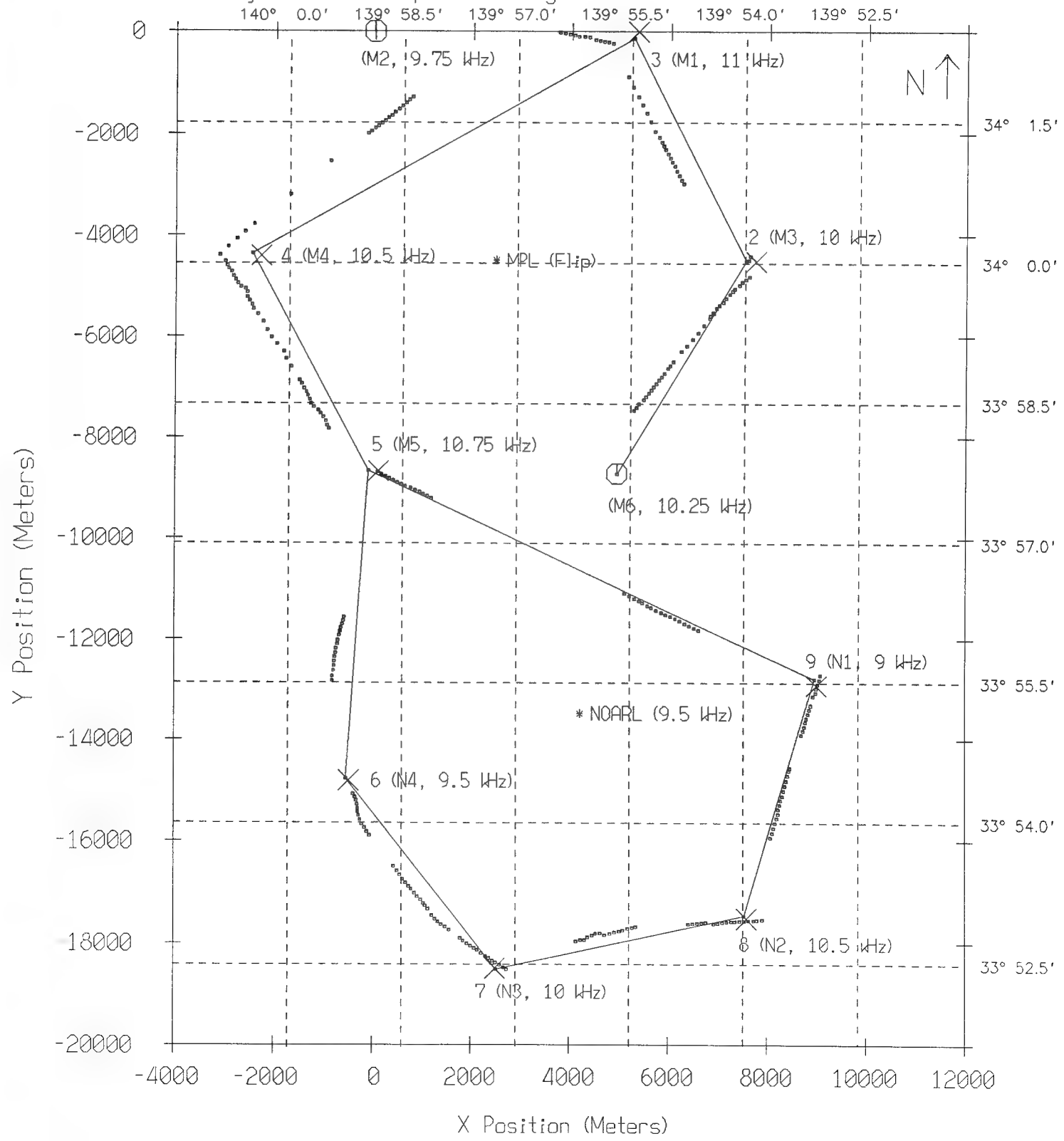

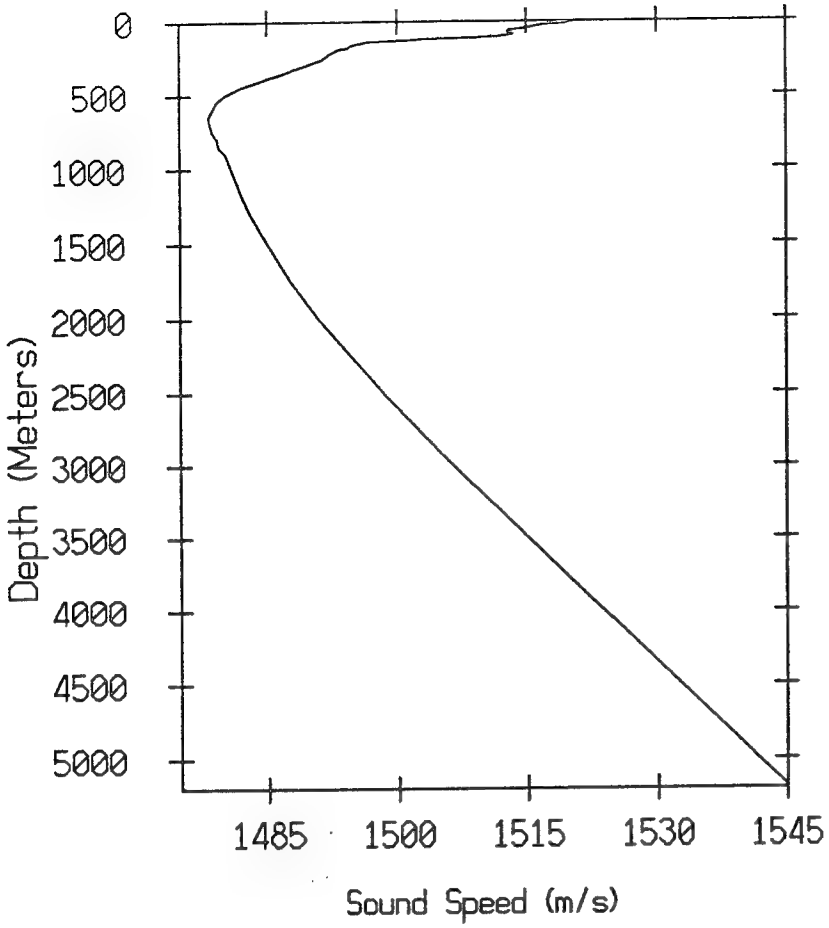

Placing transponders on the bottom:

The ray path in a constant velocity gradient (i.e. > 3500m in the top plot) traces out a circle as shown in the lower plot. Hence below this (circle) is the shadow zone. For example a source and receiver each at 15m depth would be able to communicate at a range of about 3000m.

Note that this result is rather general in that it applies to depths below which pressure takes over in the sound speed equation. For example in the arctic a very similar circle is traced below ~100m.

Figure 4 Determine transponder tether lengths

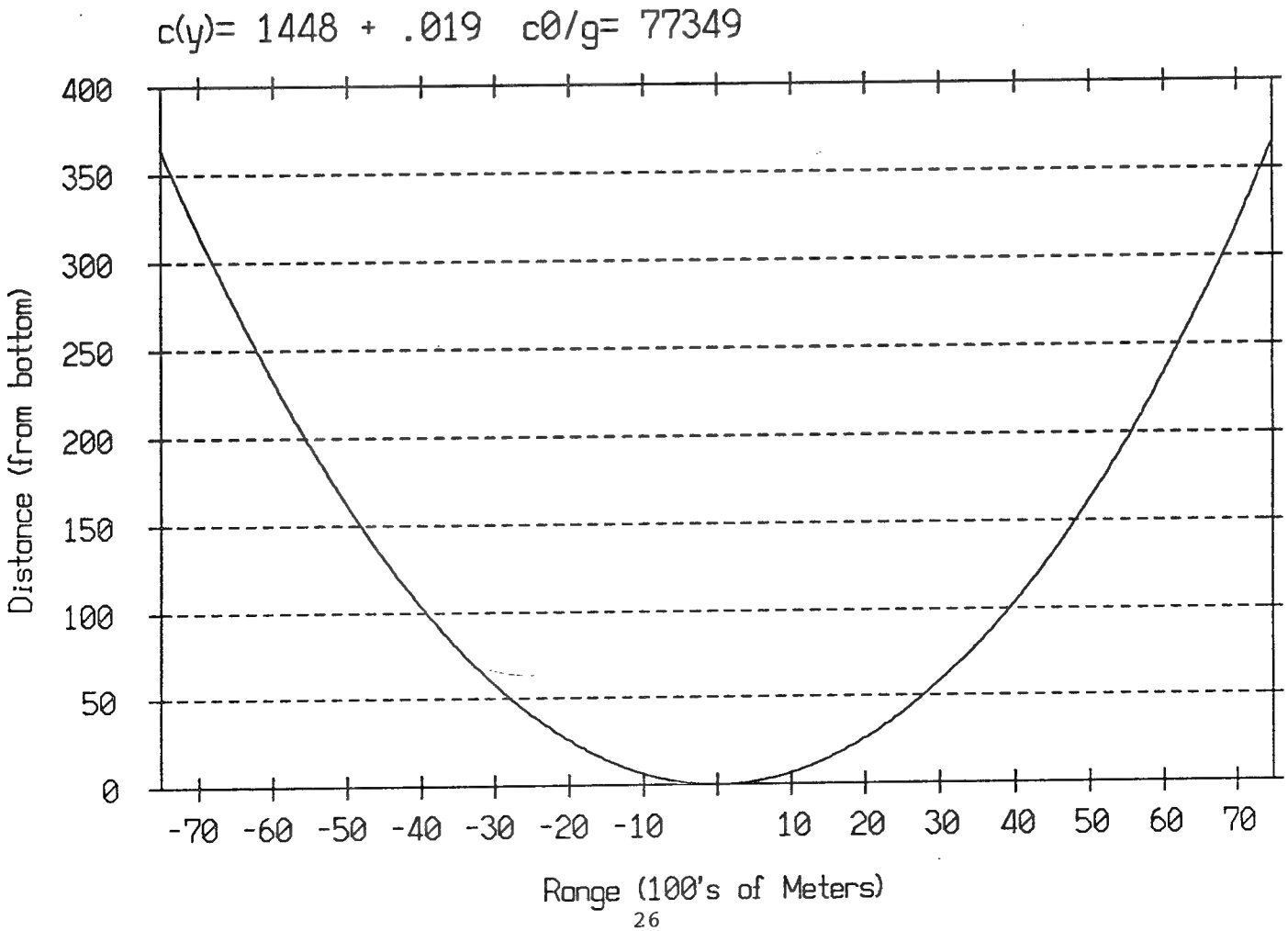

Figure 5A -- Sample Chart Recorder Output

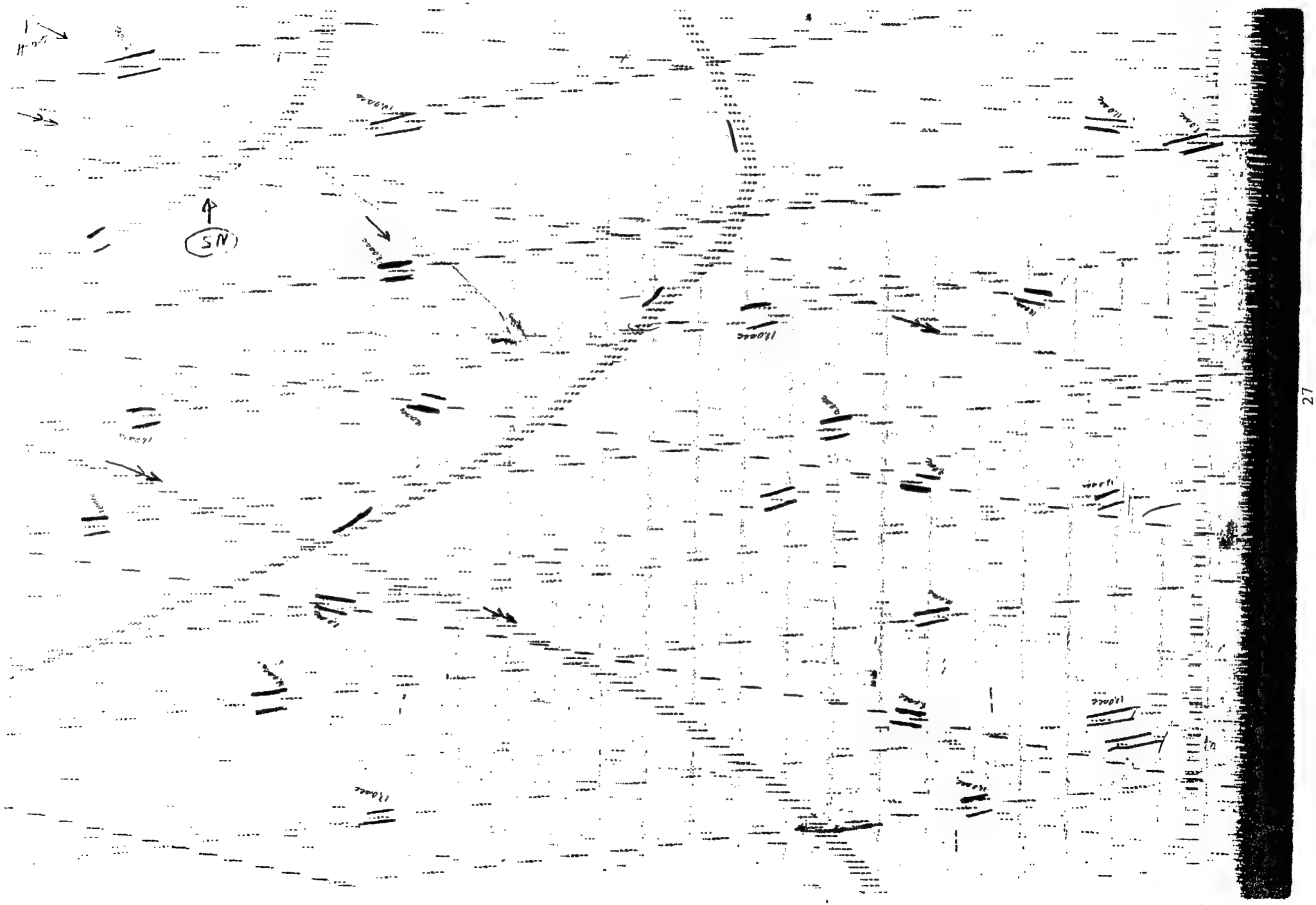

Figure 5B -- Sample Chart Recorder Output (when ship turns)

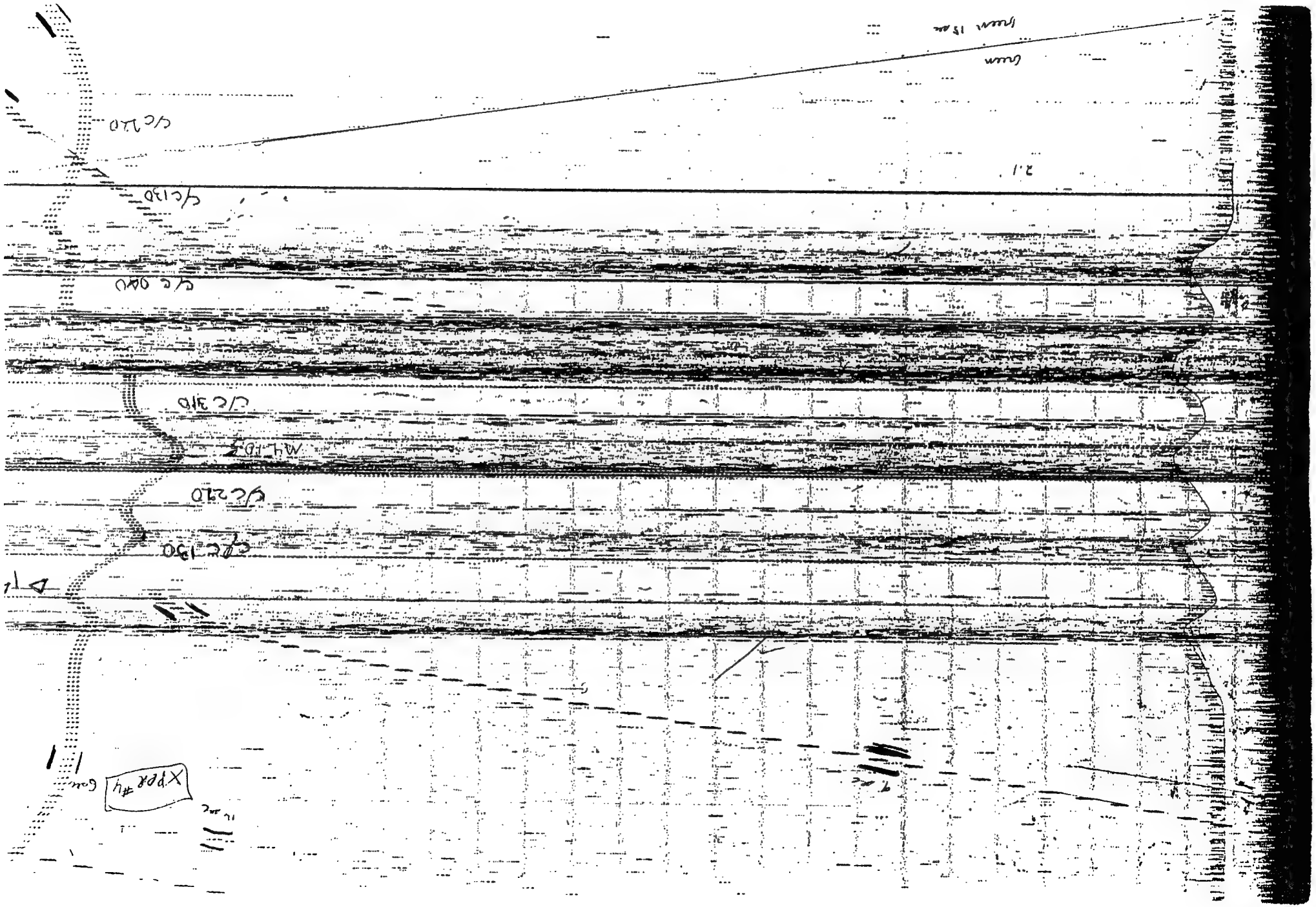

Figure 6:

Error from not passing directly over transponder

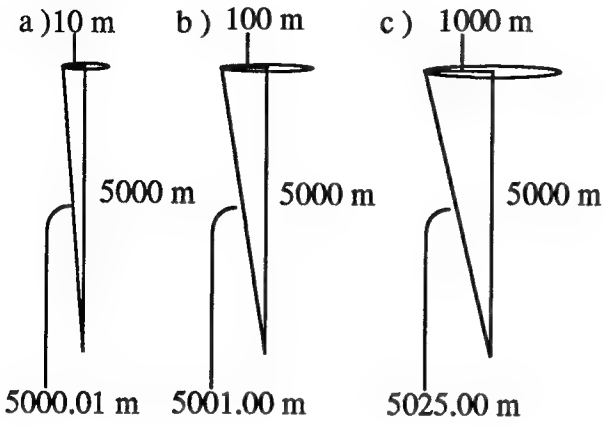

6(a): shows how a ship passing within 10 meters of directly over the top of a transponder will only have an error of +.01 meter in estimated depth.

6(b): shows that passing within 100 meters produces a +1.0 meter error in estimated depth.

6(c): shows that passing within 1000 meters produces a +25 meter error in estimated depth.

Note that in all cases we *over* estimate the depth

Figure 7:

Two methods of "boxing" transponders

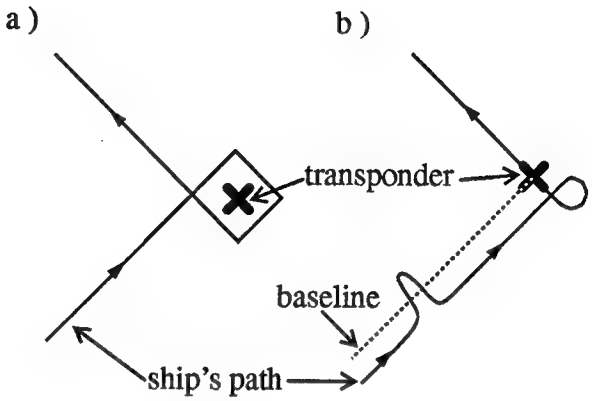

7(a): shows how the ship attempted to box a transponder. The problems with this method are that the 90° turns tend to wash out the detections and the ship never passes directly over the transponder.

7(b): shows a different method. The ship starts turning away from the transponder as soon as it has passed it (the operator sees this by watching the slant ranges, as the ship approachs the transponder the slant range decreases, when the slant ranges start to increase the ship is past the transponder). When the turn is complete the ship will be on a direct path over the transponder. This will provide a more accurate depth measurement since the ship will pass directly over the transponder. Furthermore when passing over the transponder the detections should be much cleaner as the ship is no longer turning. The problem with this method is you must know on which side of the ship the transponder is (in order to know which way to turn). This may be ascertained by crossing the baseline while travelling between two transponders as shown.

Figure 8 How operators thought they were encircling a transponder

The following is digitized chart recorder output from the area where the ship was over transponder M4. The middle trace was used by the operators in an attempt to encircle the transponder. Unfortunately the upper trace described the depth of the source (the surface bounce) and needed to be subtracted which yields the lower trace, the corrected travel times for a source on the surface, which provides evidence that they did not encircle the transponder. (see Figure 3)

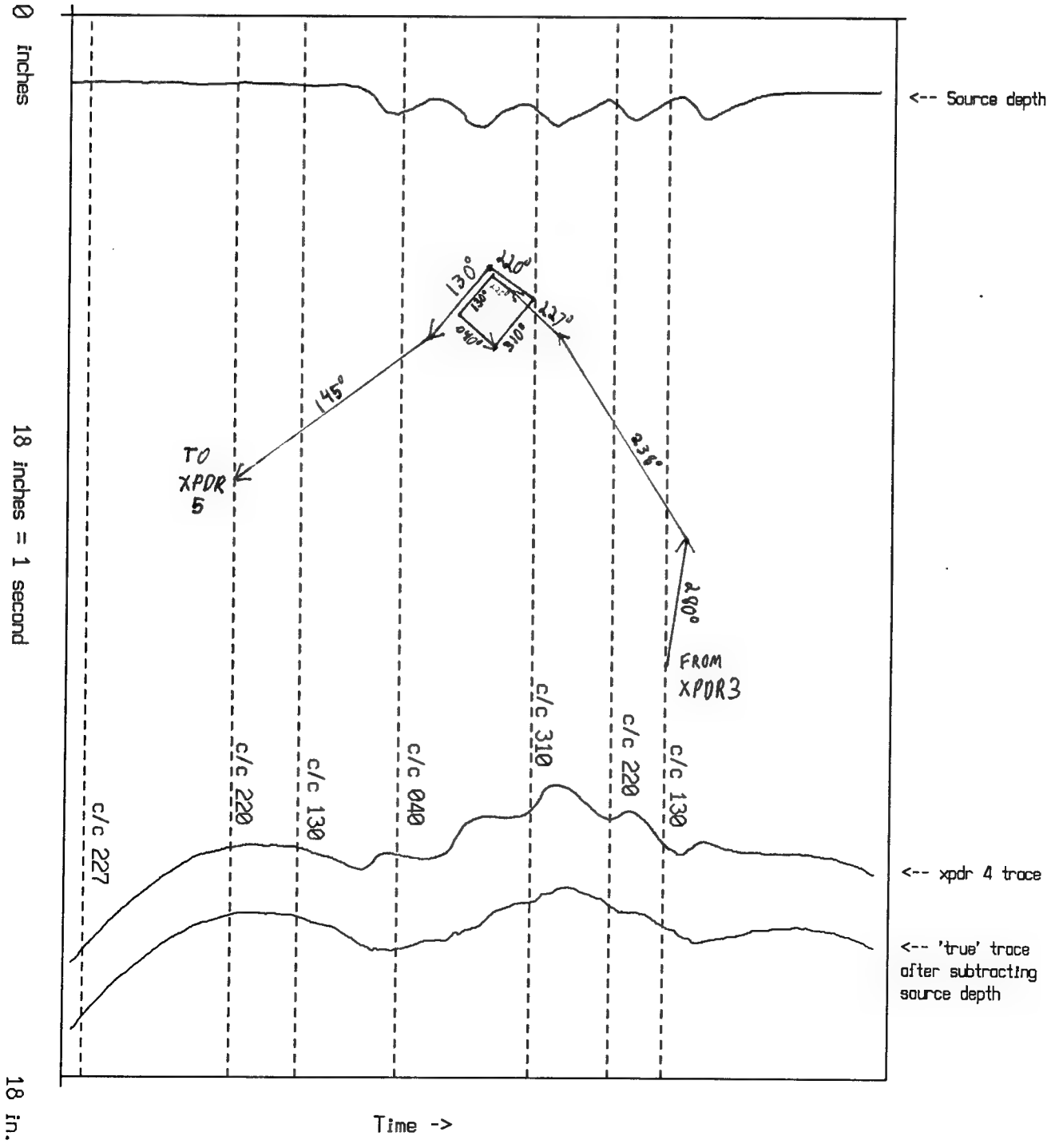

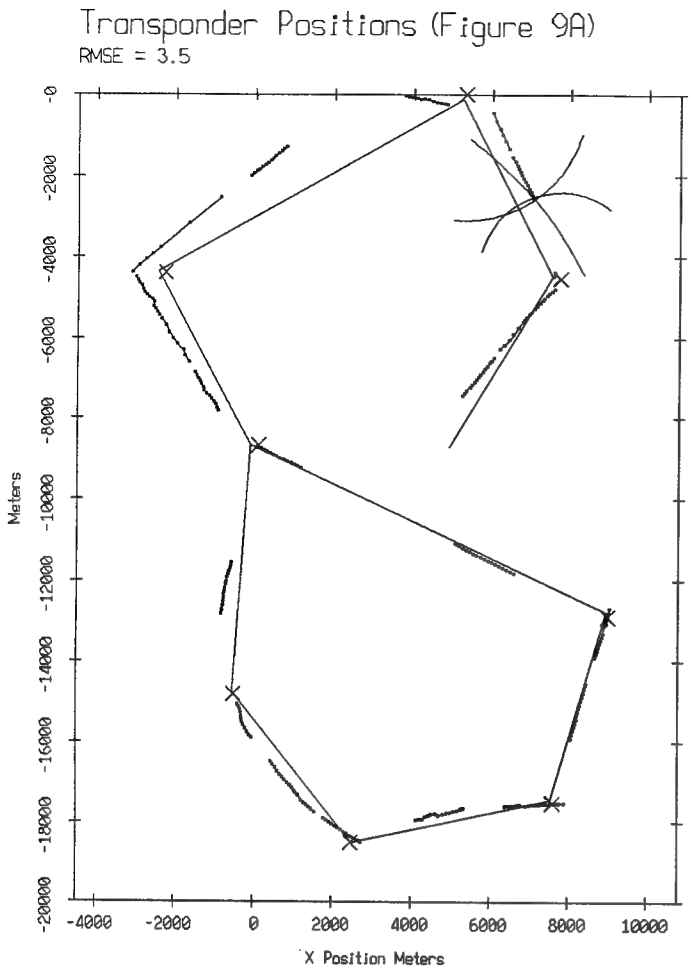

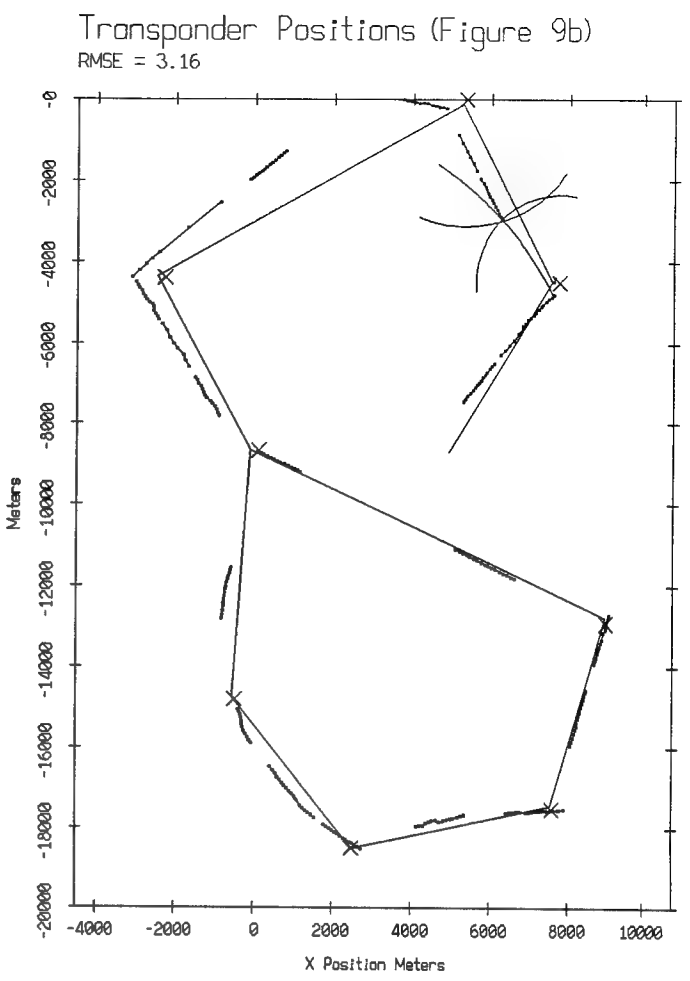

Figure 9A,B - Note the possible ambiguity derived by letting the arc from M5 vary by 1 second. As only fractional seconds were recorded by the operators one needs to guess which scenario is correct. (b) is assumed to be correct as the RMS error is slightly lower and the ship positons make more sense from a continuity argument. Figure 8 also provides evidence for this. Note the transponder locations are affected by this choice.

Figure 10 Ray Trace Corrections

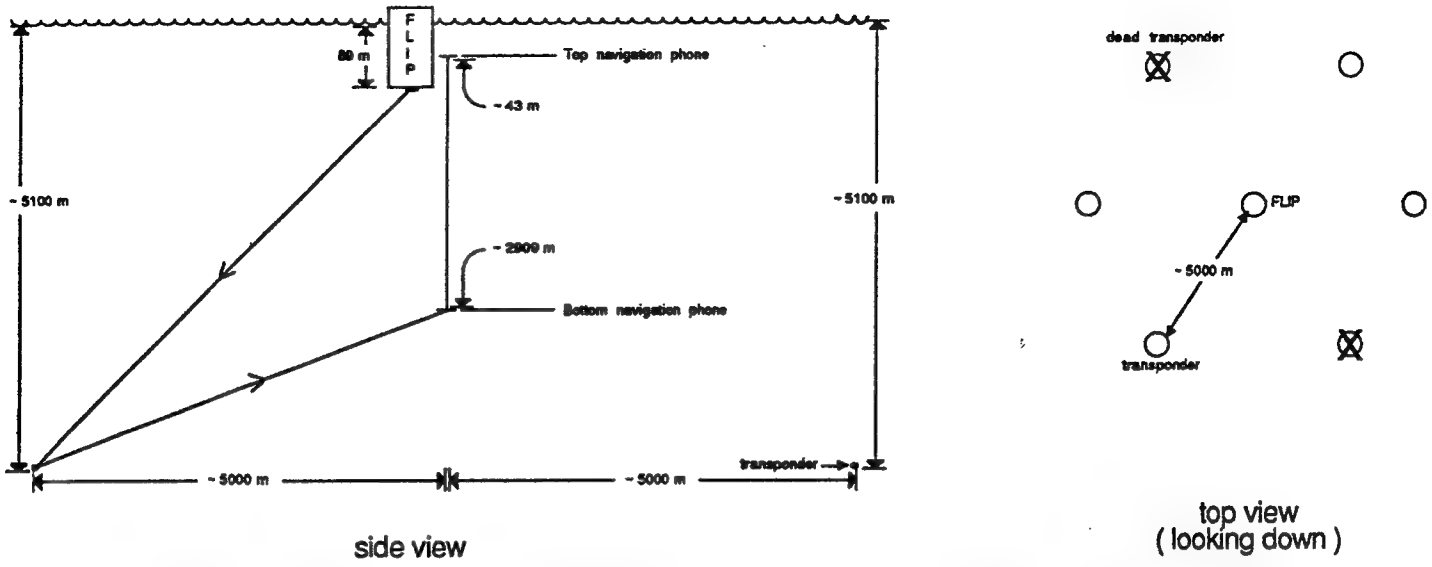

Key Idea: The generic sonar model (GSM,[8]) shows a 1.2 ms difference between straight and actual ray paths from a transponder to the top of the array. Similarly 2.2 ms from a transponder to the bottom of the array. This is a 1 ms/1.5 m difference to be added differentially to the transponder-to-navigation element slant ranges. The same correction works for all four tranponders as they are symetrically placed about the array.

The idea is that rays bend to go as fast as possible the more horizontal the path the more bending:

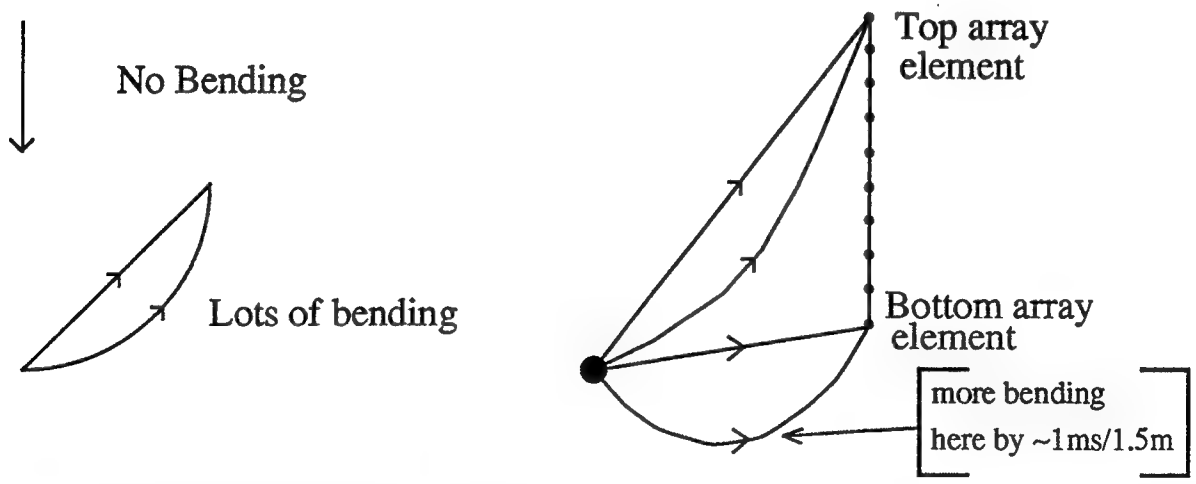

An additive constant was used to match known depths of the top and bottom elements of the array. Symetrically positioned transponders remove most of the other bias (i.e. most of the x-y error cancels).

Note the same ray trace argument is also used in the survey. Figure 11 shows the ray trace travel time corrections as a function of horizontal distance (ship -> transponder).

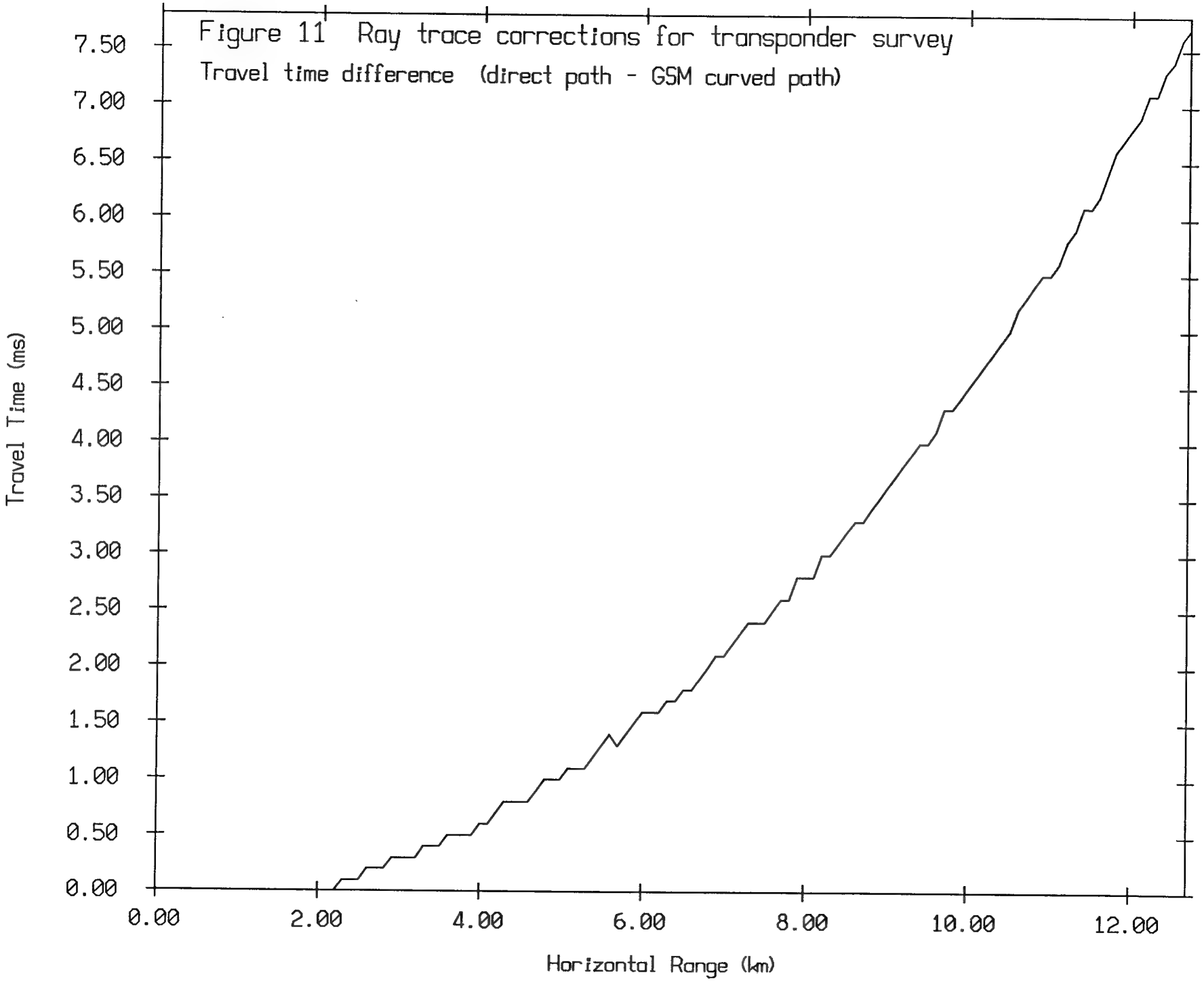
Figure 11 Ray trace corrections for transponder survey
Travel time difference (direct path - GSM curved path)
Travel Time (ms)
7.50
7.00
6.50
6.00
5.50
5.00
4.50
4.00
3.50
3.00
2.50
2.00
1.50
1.00
0.50
0.00
0.00
2.00
4.00
6.00
8.00
10.00
12.00
Horizontal Range (km)

Figure 12 Geodetic Corrections

Navigated Flip vs. GPS FLIP
Xoff = -179.6 Yoff = 31.0 Theta = -7.2

center of rotation = 2432.7 −4342.3 RMSE = 6.1
1989 191 18:12 −> 192 01:44 GMT

N ↑

The following picture shows how the transponder positions were corrected for geocentricity. The transponders drifted from their initial drop locations as they sank to the bottom. The acoustically navigated ship positions were overlayed over GPS ship positions via non−linear least squares. This translated the array ~200m and rotated it ~ −7 degrees.

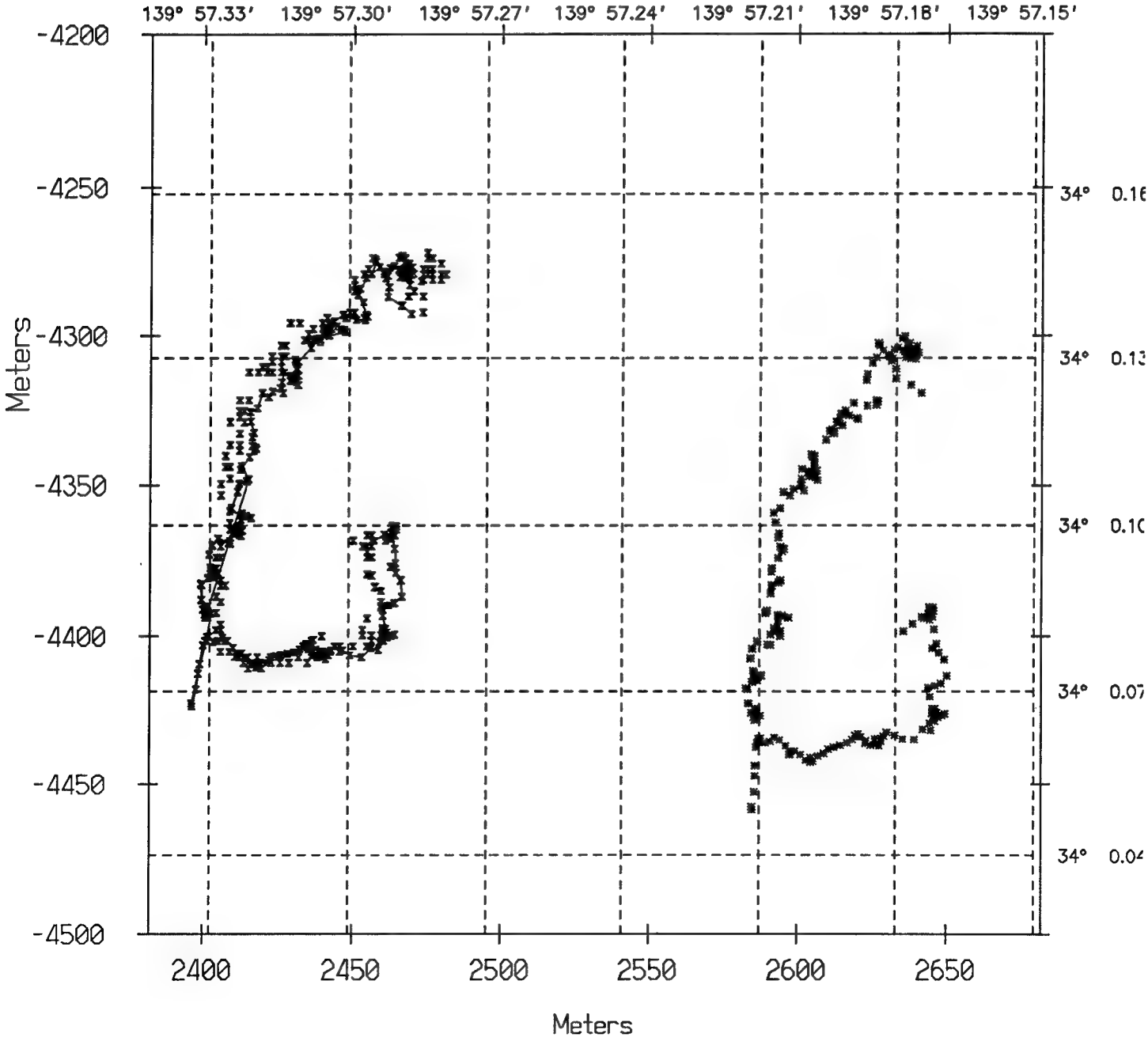

Figure 13 Flip heading for 185 00:00 to 195 13:52

Note FLIP rotation changes very slowly over the days of interest.
A simulation was run which demonstrated that a (huge) 20 degree rotational estimation error caused only ~.15 meters of x-y-z array positional error.

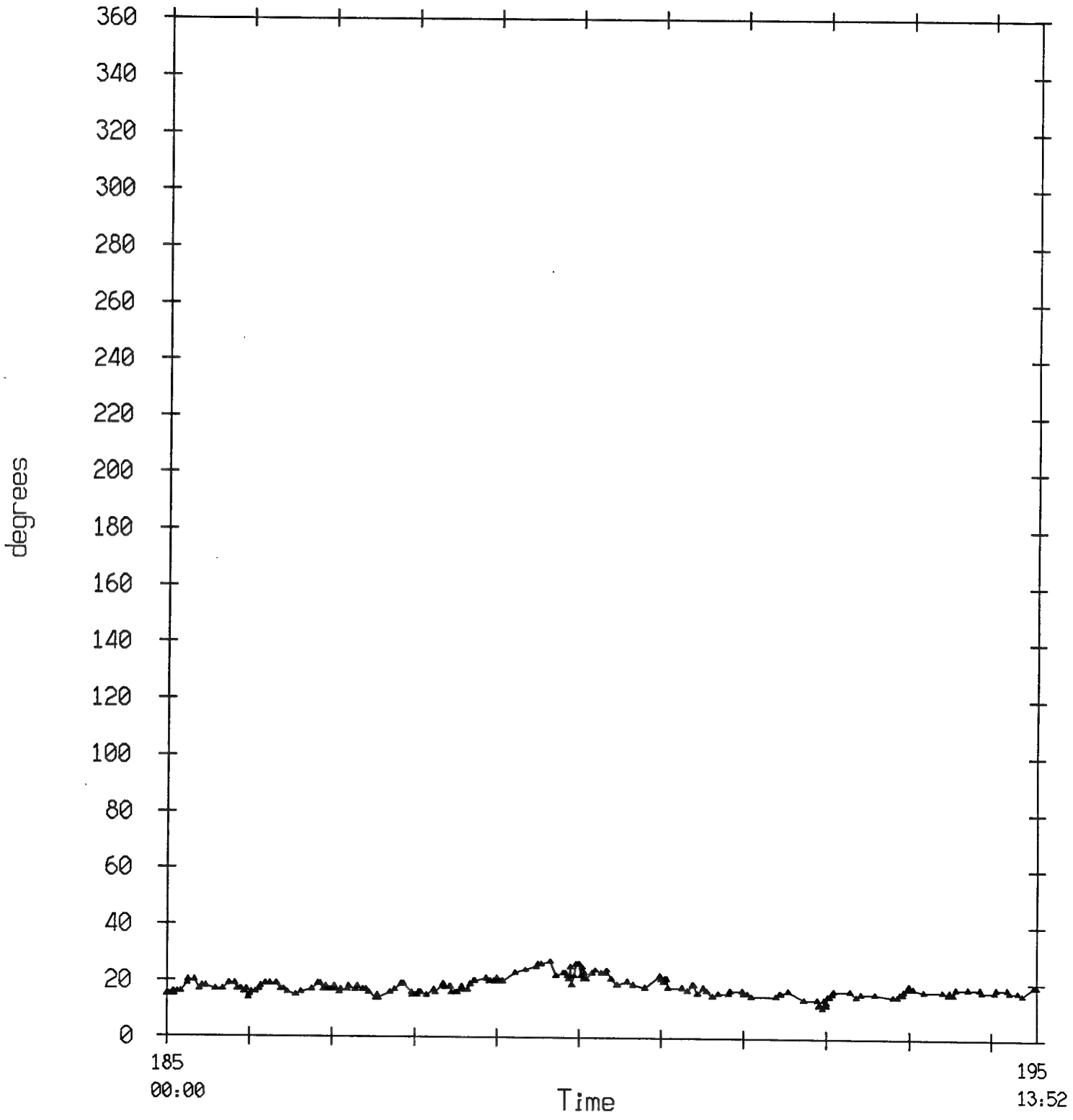

Figure 14 -- Sample detector output

Time: 186_06:06:38.353

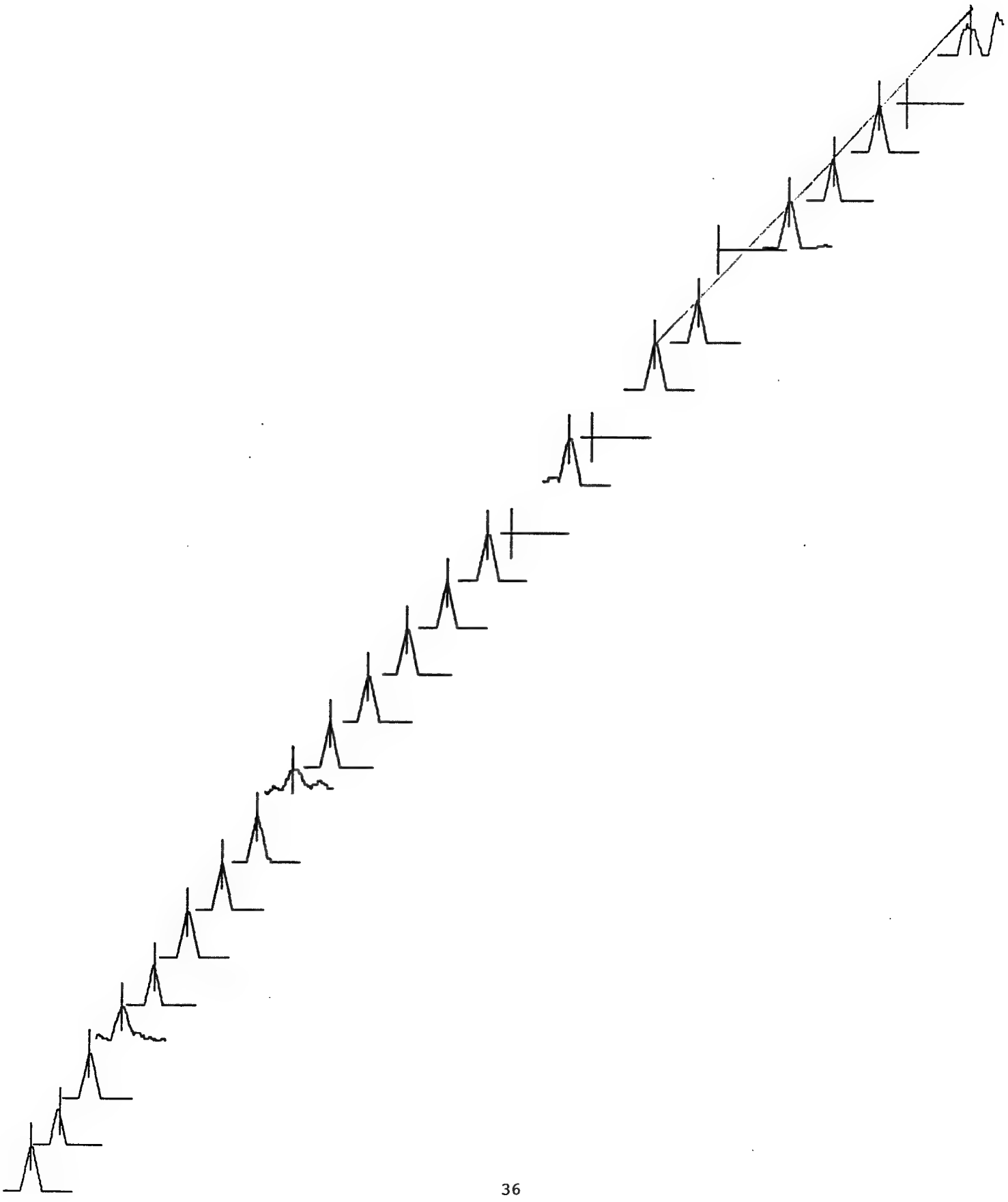

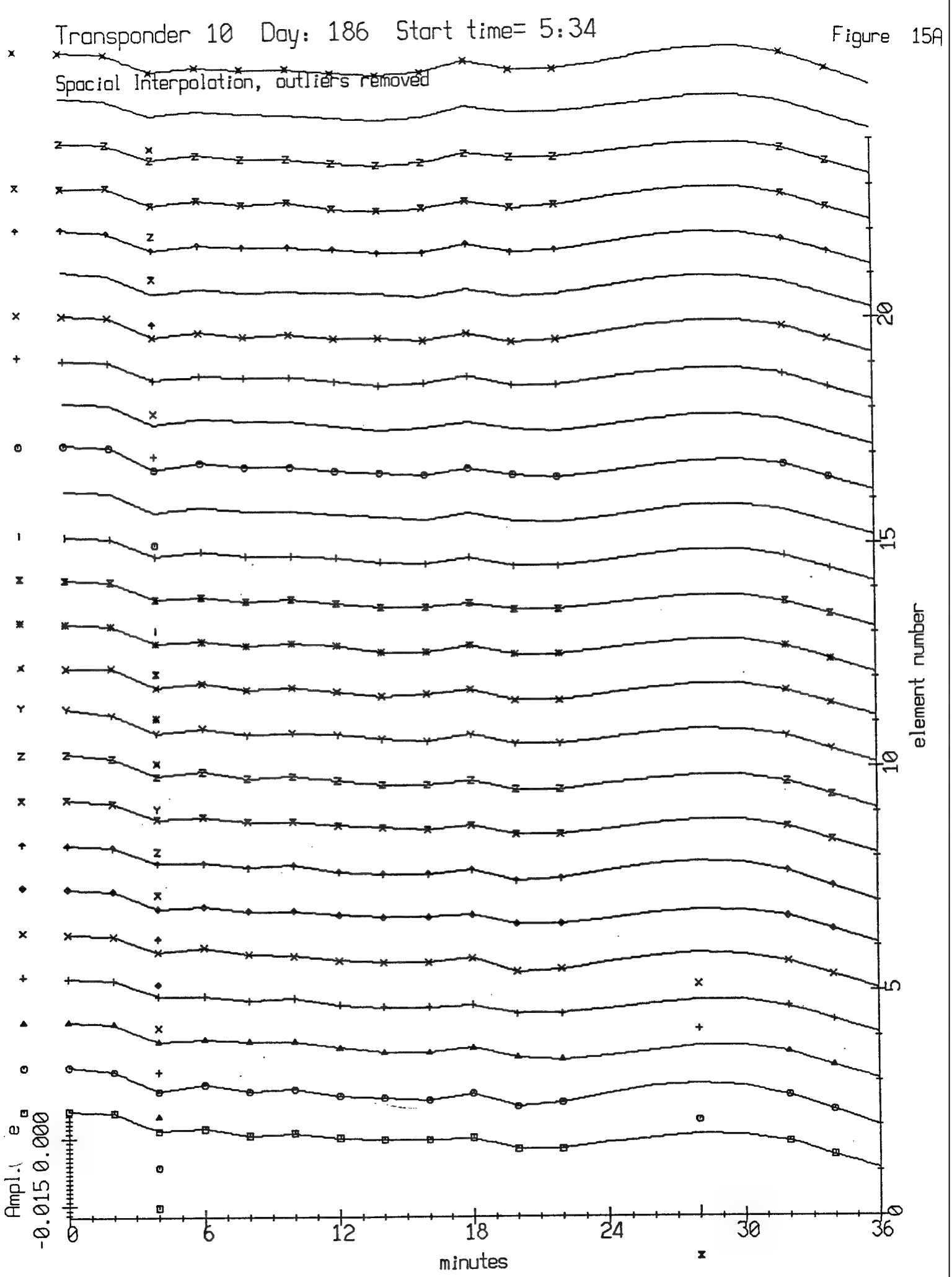
Transponder 10 Day: 186 Start time= 5:34
Spacial Interpolation, outliers removed
element number
minutes
Ampl.
-0.015 0.000
0
6
12
18
24
30
36
0
5
10
15
20

Figure 15A

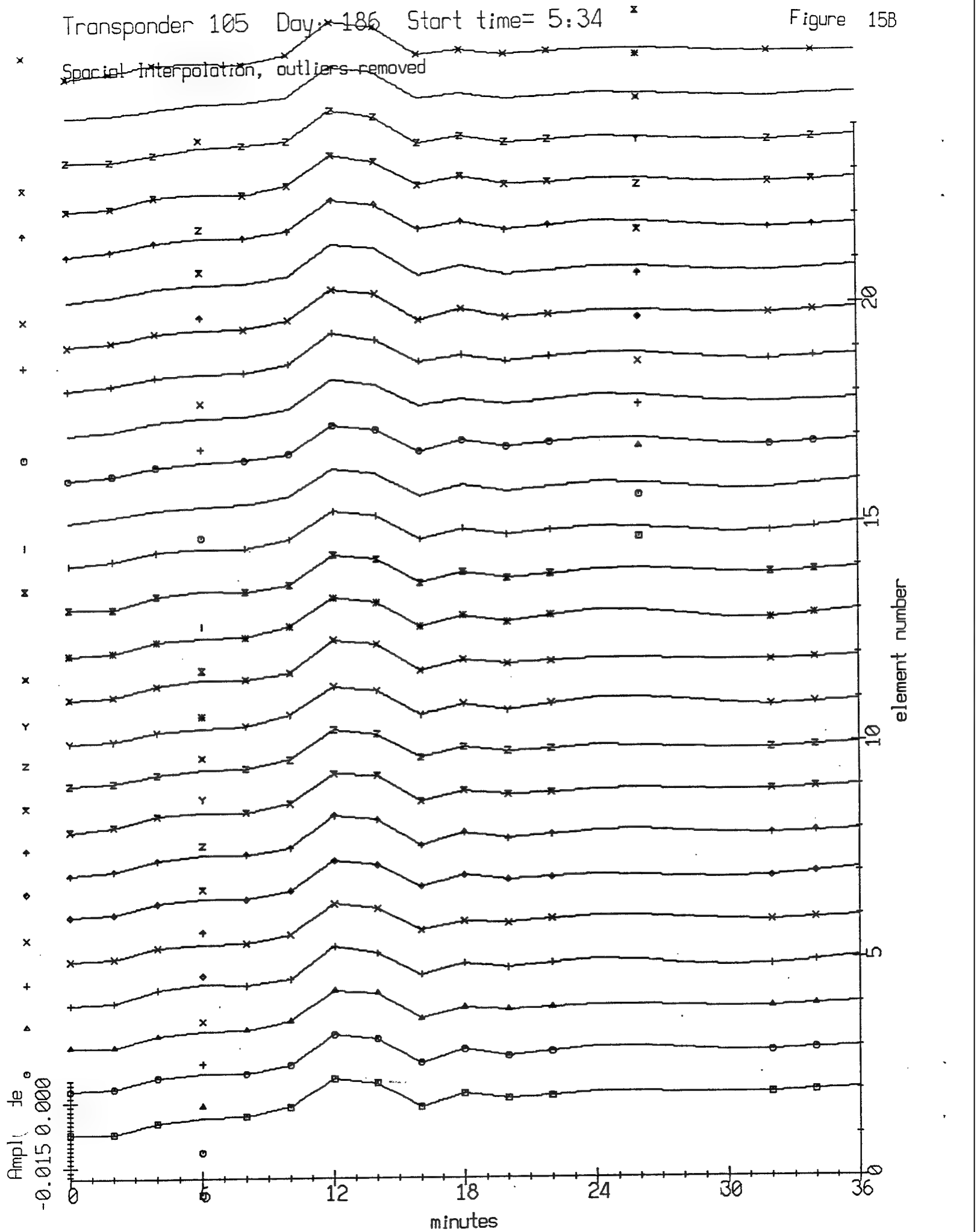
Transponder 105 Day: 186 Start time= 5:34
Figure 15B
Special Interpolation, outliers removed
element number
minutes
0
5
12
18
24
30
36
0
5
10
15
20
-0.015
0.000

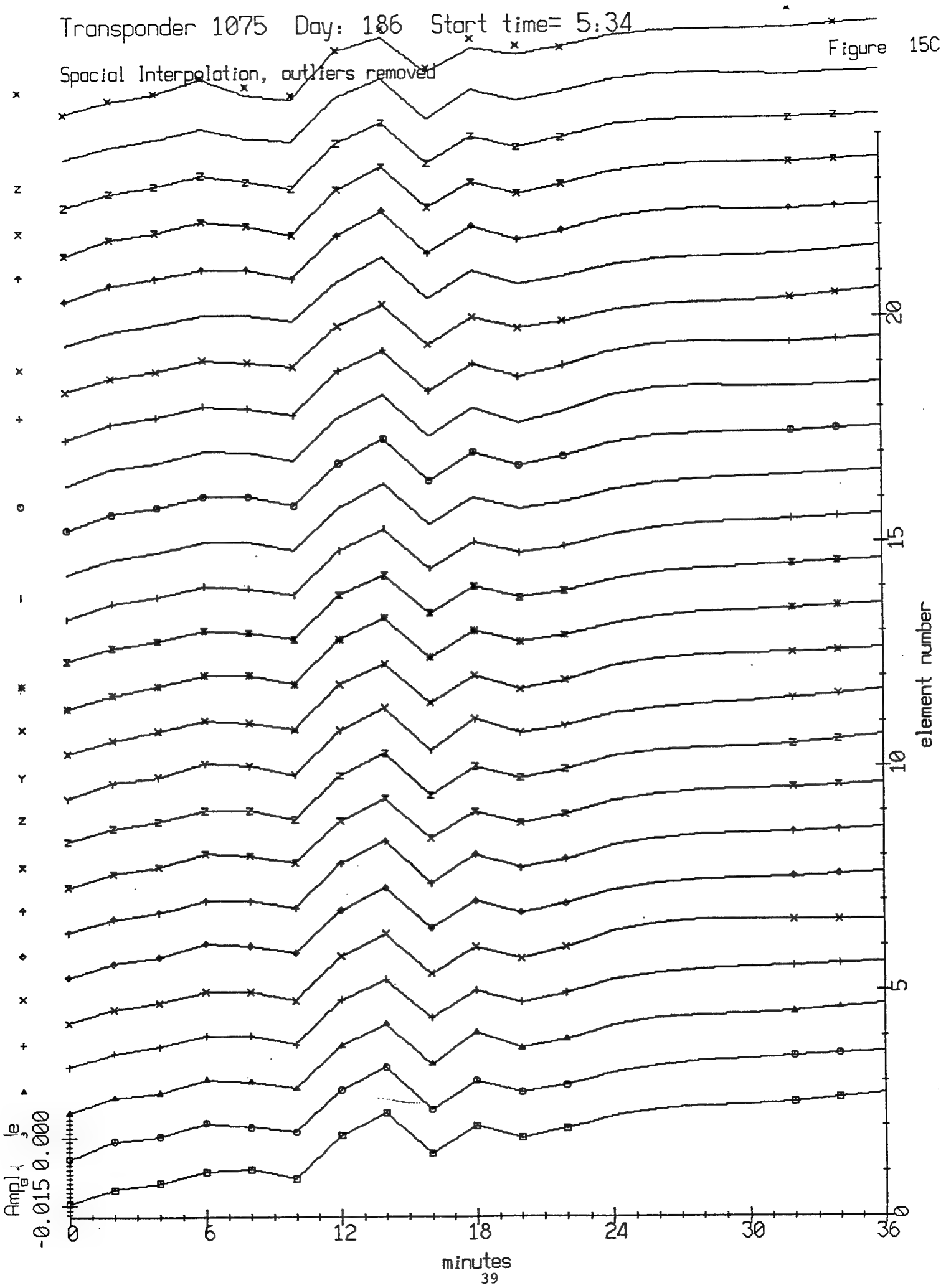
Transponder 1075 Day: 186 Start time= 5:34
Spacial Interpolation, outliers removed
Figure 15C
element number
minutes
Amplitude
-0.015 0.000
0
6
12
18
24
30
36
5
10
15
20

Transponder 11 Day: 186 Start time= 5:34

Figure 15D

Spactal Interpolation, outliers removed

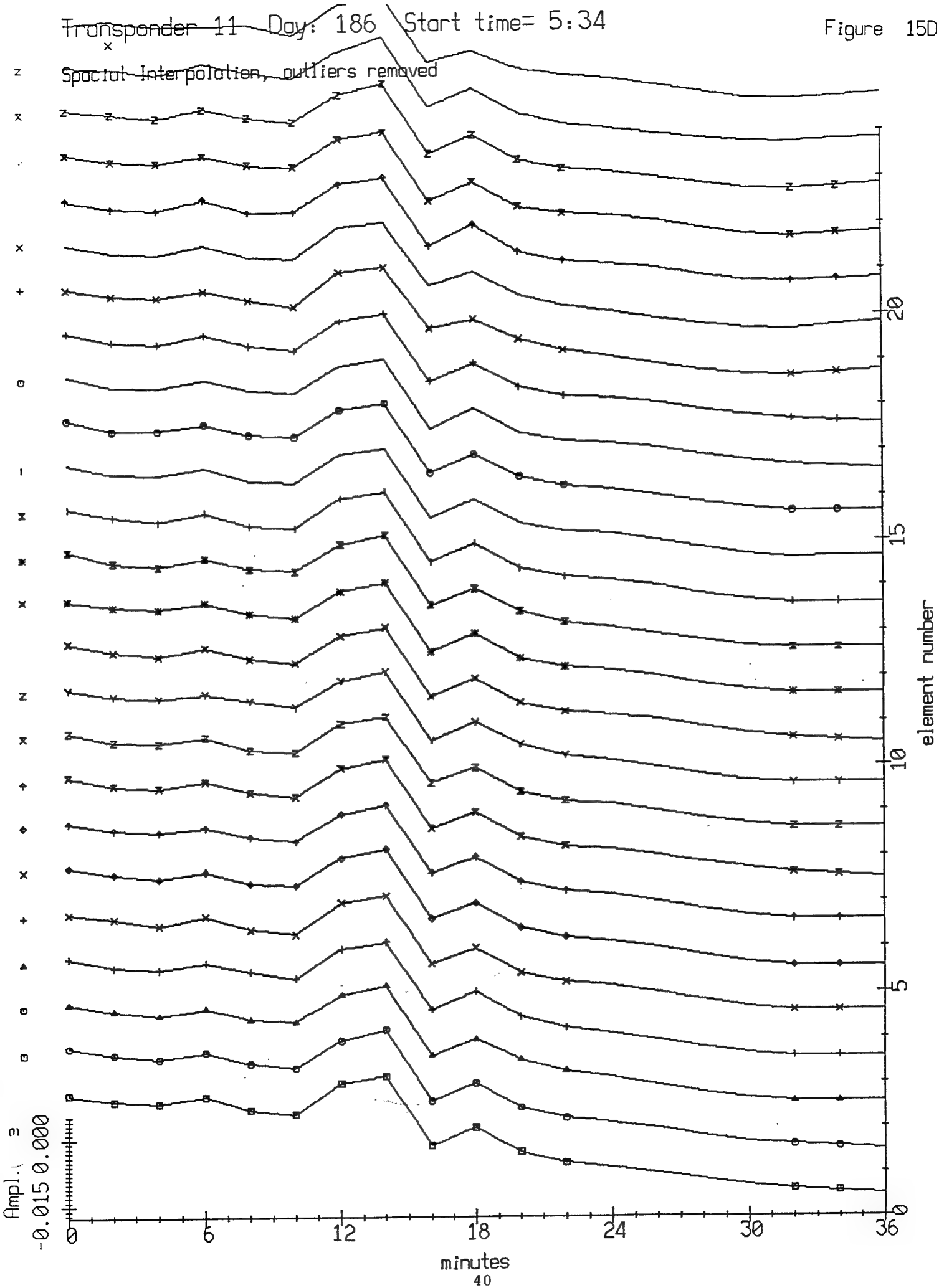

Figure 16A

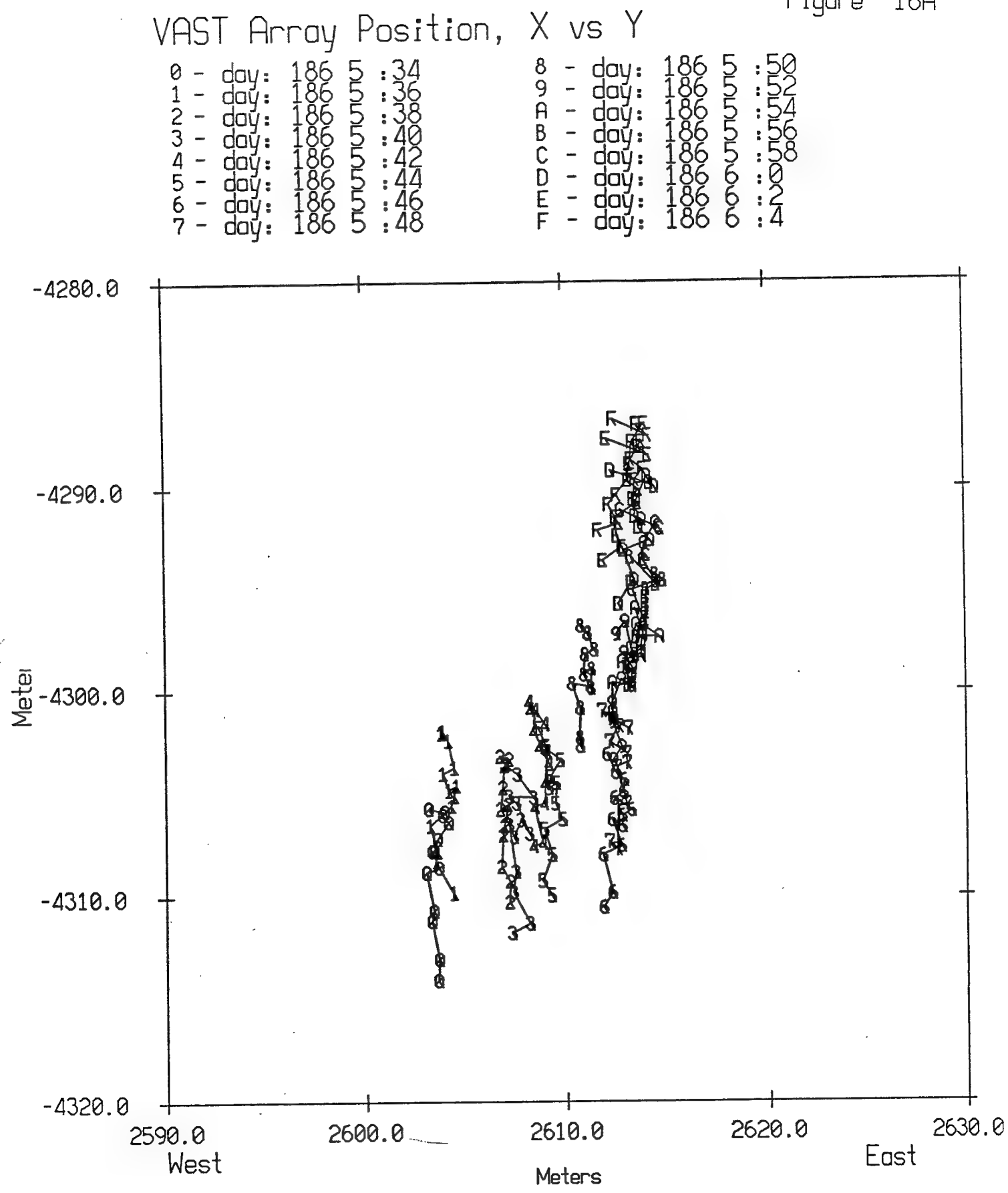
VAST Array Position, X vs Y
0 - day: 186 5 :34
1 - day: 186 5 :36
2 - day: 186 5 :38
3 - day: 186 5 :40
4 - day: 186 5 :42
5 - day: 186 5 :44
6 - day: 186 5 :46
7 - day: 186 5 :48
8 - day: 186 5 :50
9 - day: 186 5 :52
A - day: 186 5 :54
B - day: 186 5 :56
C - day: 186 5 :58
D - day: 186 6 :0
E - day: 186 6 :2
F - day: 186 6 :4
-4280.0
-4290.0
-4300.0
-4310.0
-4320.0
Meters
2590.0
2600.0
2610.0
2620.0
2630.0
West
East
Meters

Figure 16B

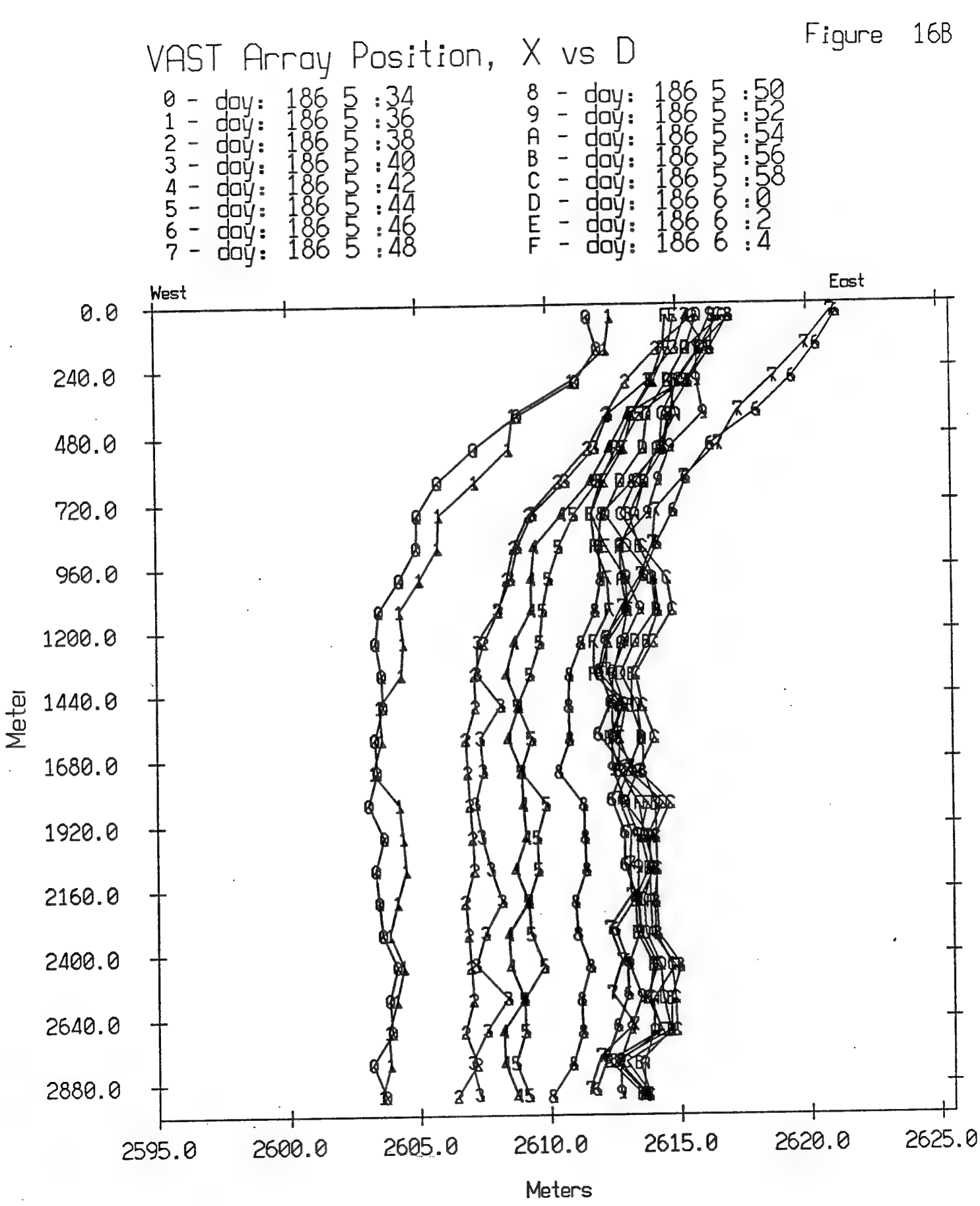
VAST Array Position, X vs D
0 - day: 186 5 :34
1 - day: 186 5 :36
2 - day: 186 5 :38
3 - day: 186 5 :40
4 - day: 186 5 :42
5 - day: 186 5 :44
6 - day: 186 5 :46
7 - day: 186 5 :48
8 - day: 186 5 :50
9 - day: 186 5 :52
A - day: 186 5 :54
B - day: 186 5 :56
C - day: 186 5 :58
D - day: 186 6 :0
E - day: 186 6 :2
F - day: 186 6 :4
West
East
0.0
240.0
480.0
720.0
960.0
1200.0
1440.0
1680.0
1920.0
2160.0
2400.0
2640.0
2880.0
Meter
2595.0
2600.0
2605.0
2610.0
2615.0
2620.0
2625.0
Meters

VAST Array Position, Y vs D

Figure 16C

0 - day: 186 5 :34
1 - day: 186 5 :36
2 - day: 186 5 :38
3 - day: 186 5 :40
4 - day: 186 5 :42
5 - day: 186 5 :44
6 - day: 186 5 :46
7 - day: 186 5 :48
8 - day: 186 5 :50
9 - day: 186 5 :52
A - day: 186 5 :54
B - day: 186 5 :56
C - day: 186 5 :58
D - day: 186 6 :0
E - day: 186 6 :2
F - day: 186 6 :4

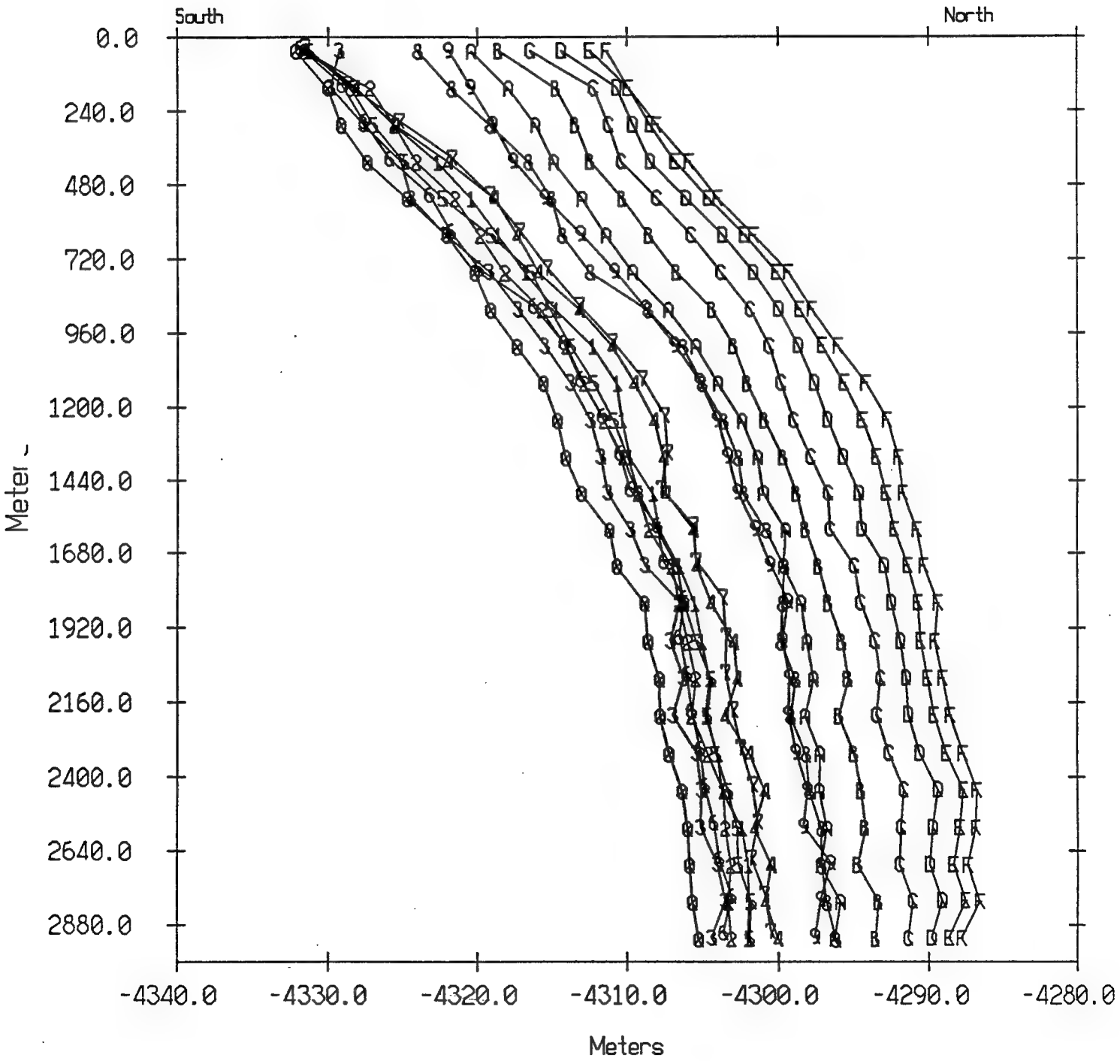

Figure 17 Slant range error decomposition

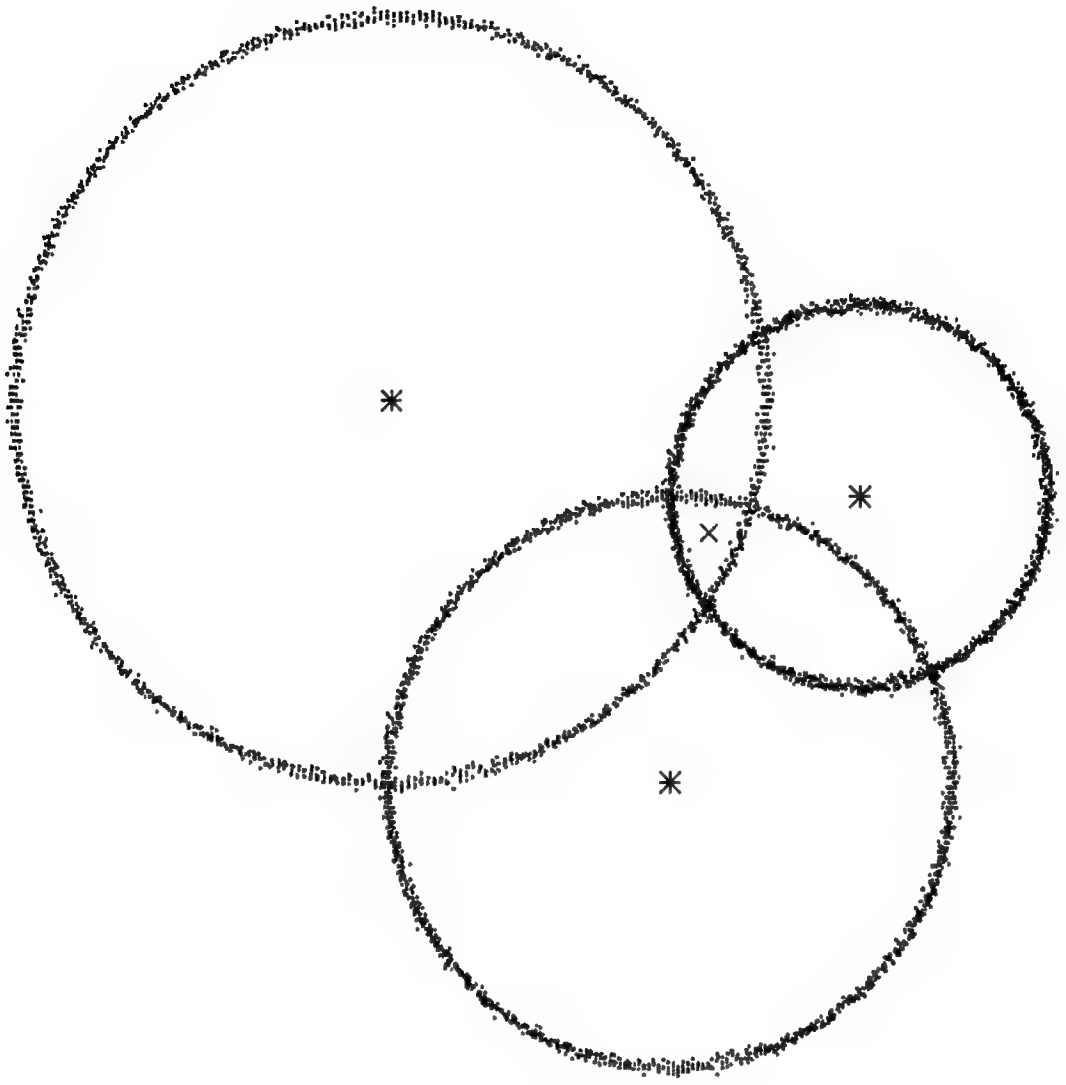

This is a two dimensional example of the error decomposition into a bias term and a random component. In this case the slant ranges are all too long (positive bias) which leads to the overlapping circles. In this two dimensional case the additive bias errors cancel if the transponders (*'s) are symetric. The width in the circles represents the random component and were in fact generated by adding Gaussian noise to the radii of the circles. The navigated solution (position with the minimum mean square error) is denoted by the x.

FIGURE 18. SUMMARY OF ERROR SOURCES

TRANSPONDER SURVEY ERRORS

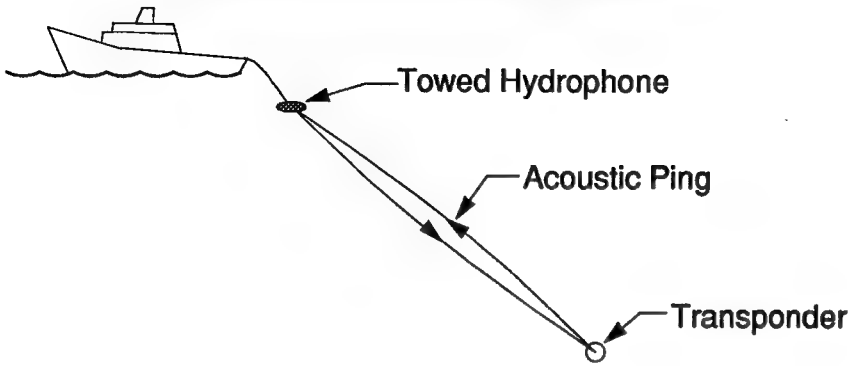

Random Errors

Source of Error	Estimated Error
Transponder Turn-Around-Time/2	0 -> 1 ms
Receiver Recognition Time/2 + Pen	-1 -> 4 ms
Digitizing Chart Recorder	-3 -> 3 ms
Total:	-4 -> 8 ms
	(worst case $\sigma \approx$ 4 m)

Bias Errors

Source of Error	Estimated Error
Sound Speed	4 ms
Refraction	2 ms

AEL ERRORS

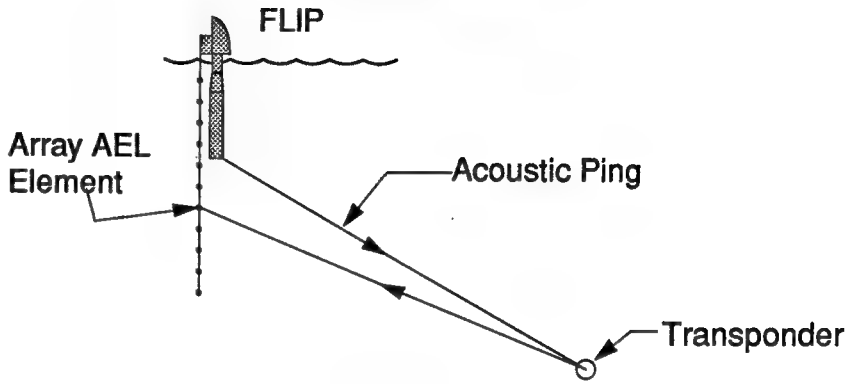

Random Errors

Source of Error	Estimated Error
Transponder Turn-Around-Time/2	0 -> 1 ms
Array Receiver Recognition Time	-2 -> 2 ms (Hardware)
	0 -> 1 ms (Software, fs ≠ 250)
Ship Receiver Recognition time/2	0 -> 1 ms
Flip Rotation	0 -> < 1 ms
Total	-2 -> 6 ms
	(worst case $\sigma \approx$ 3 m)

Bias Errors

Source of Error	Estimated Error
Sound Speed	4 ms
Refraction	1 - 2 ms (top -> bottom)
Hardware	< 5 ms

Figure 19A

How Slant Ranges + Noise Affect Transponder Position Error

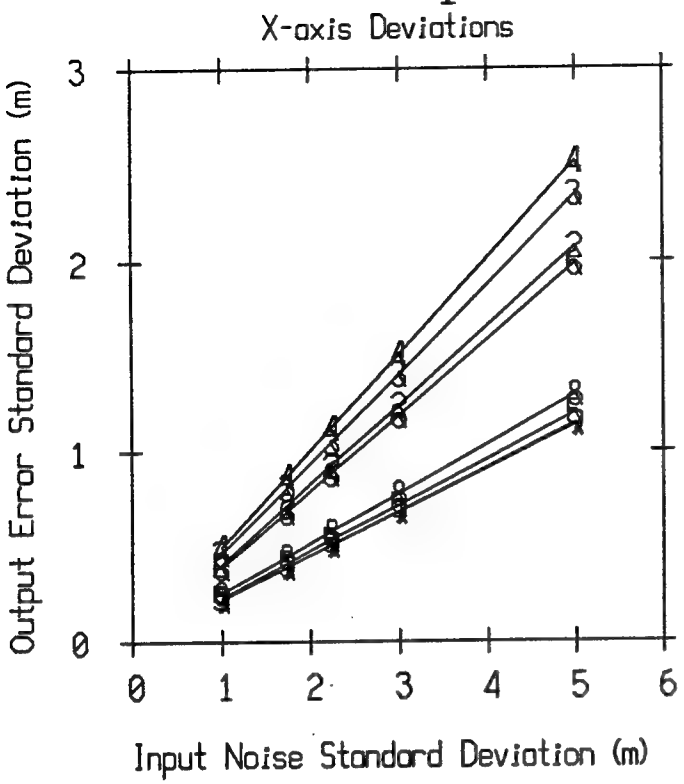

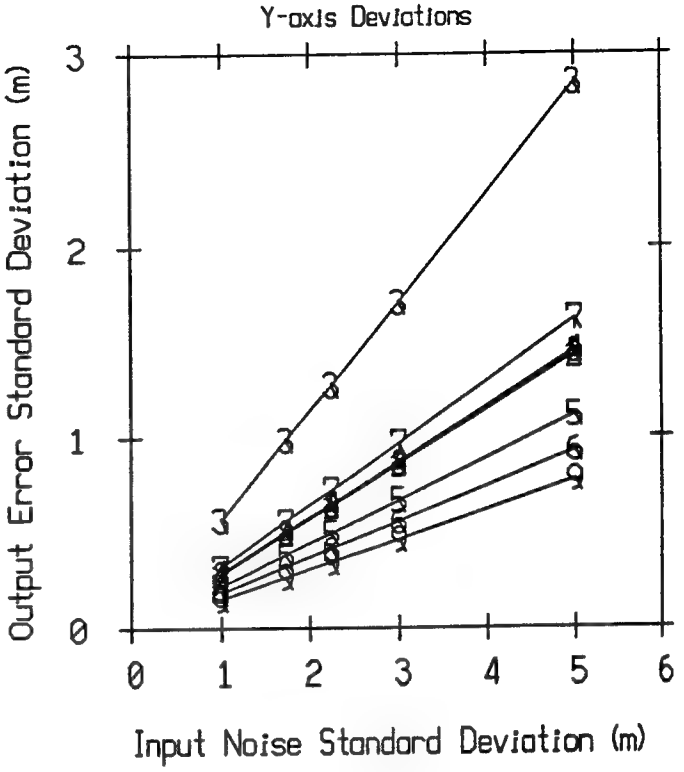

Point # represents transponder #

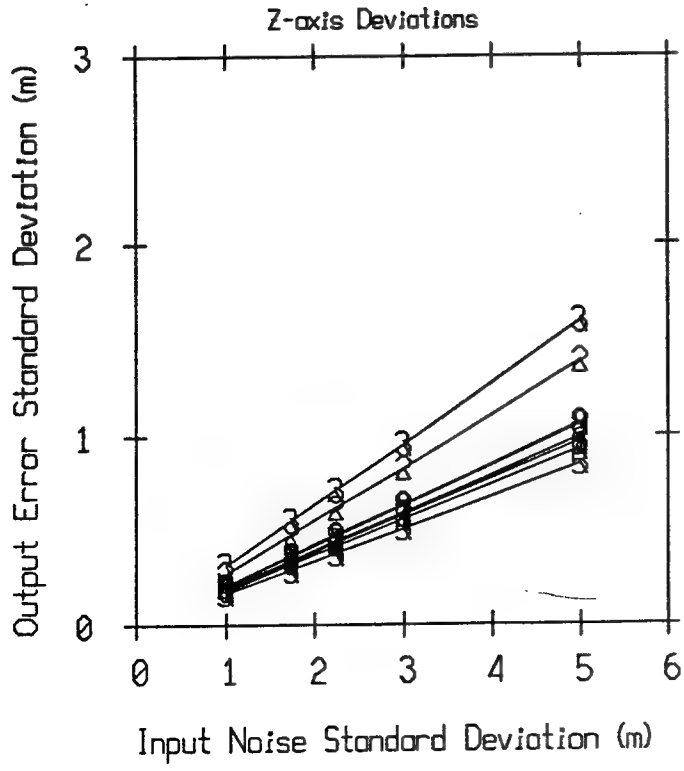

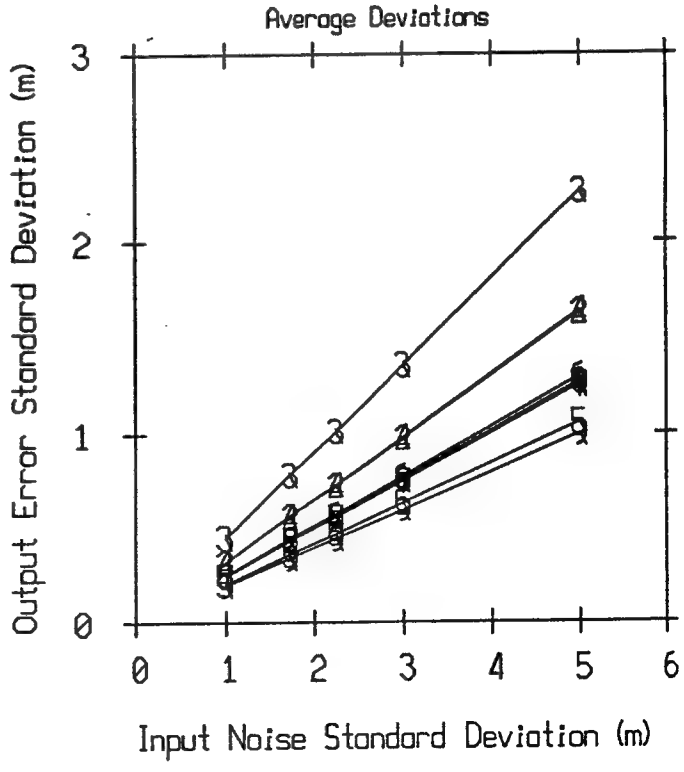

Figure 19B

How Random Transponder Positions Affect Array Position Error

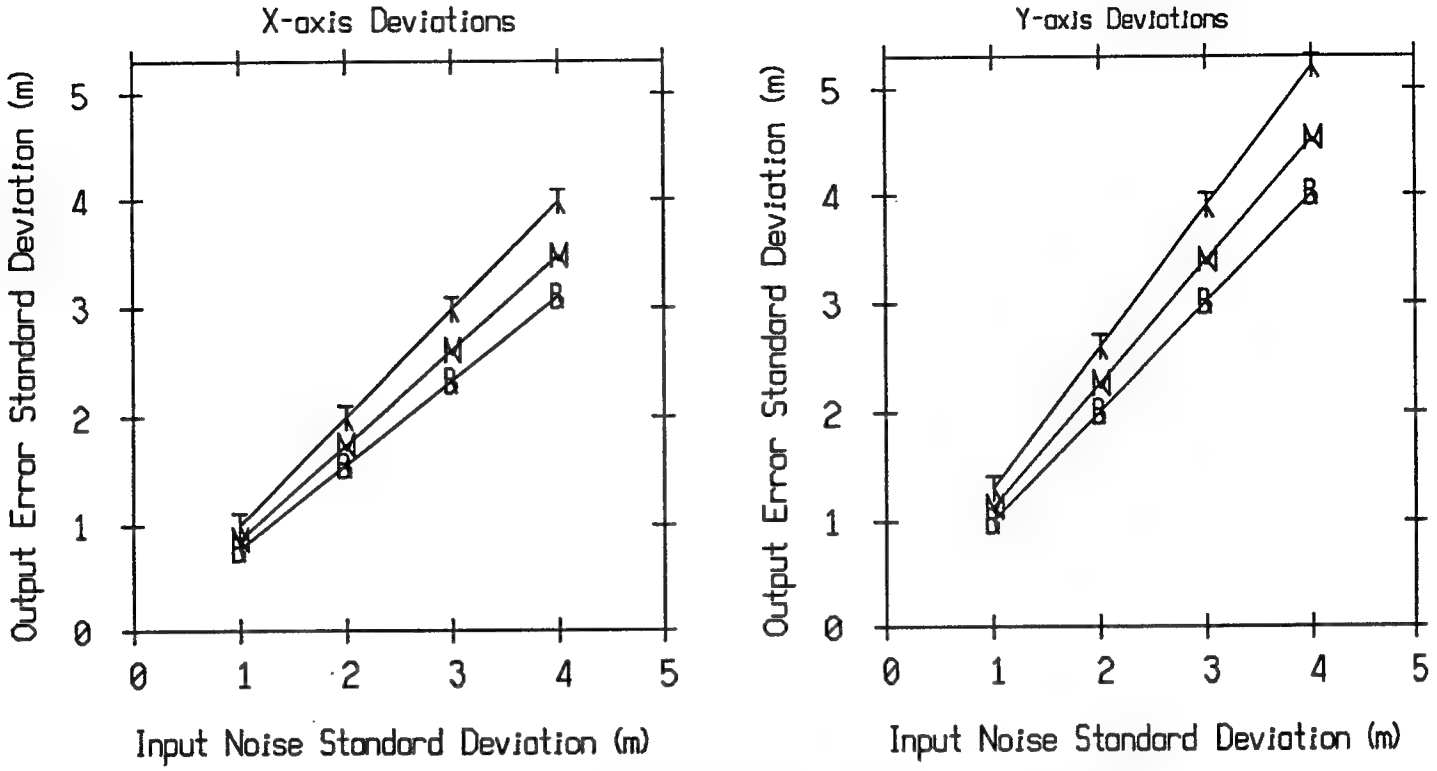

Point T represents Top Element
Point M represents Middle Element
Point B represents Bottom Element

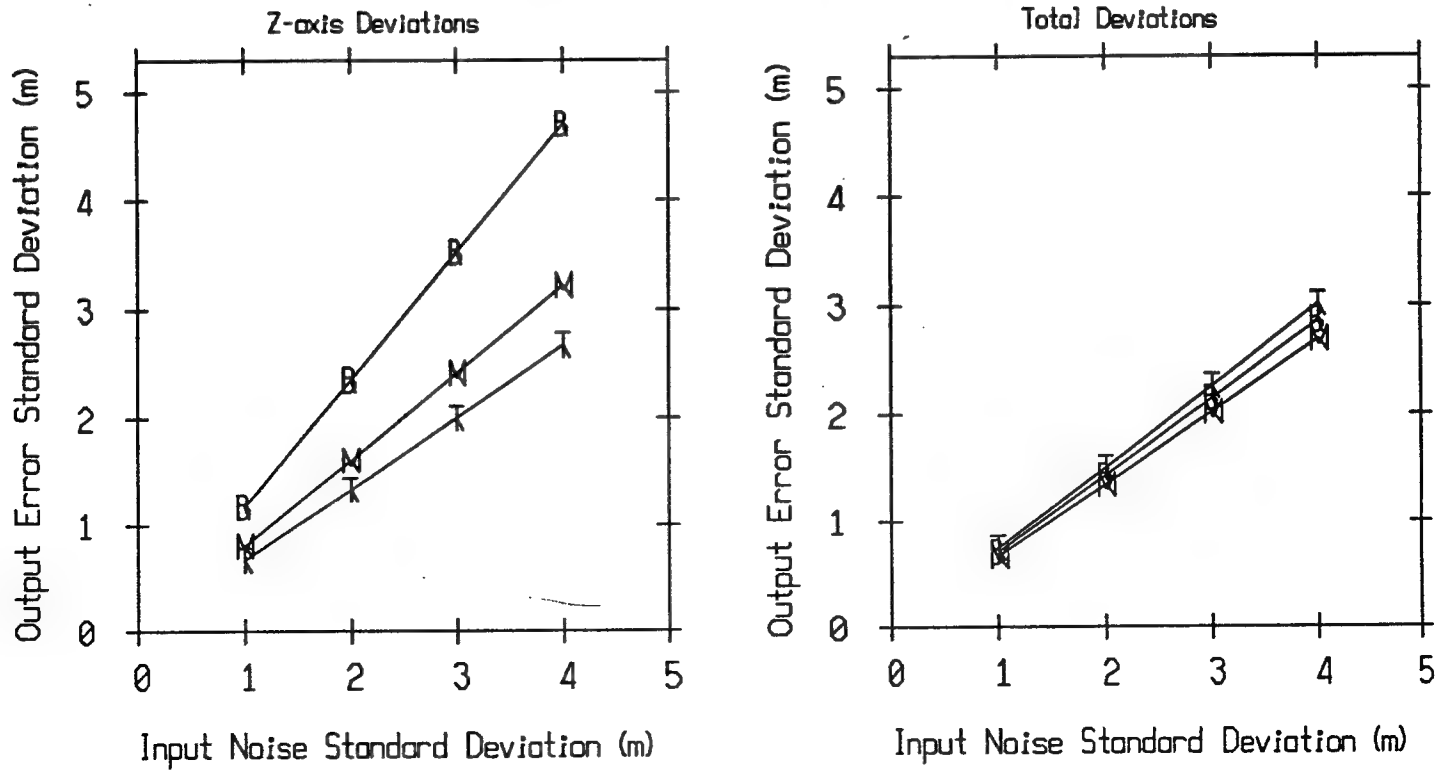

Figure 19C
How Random Slant Ranges Affect Array Position Error

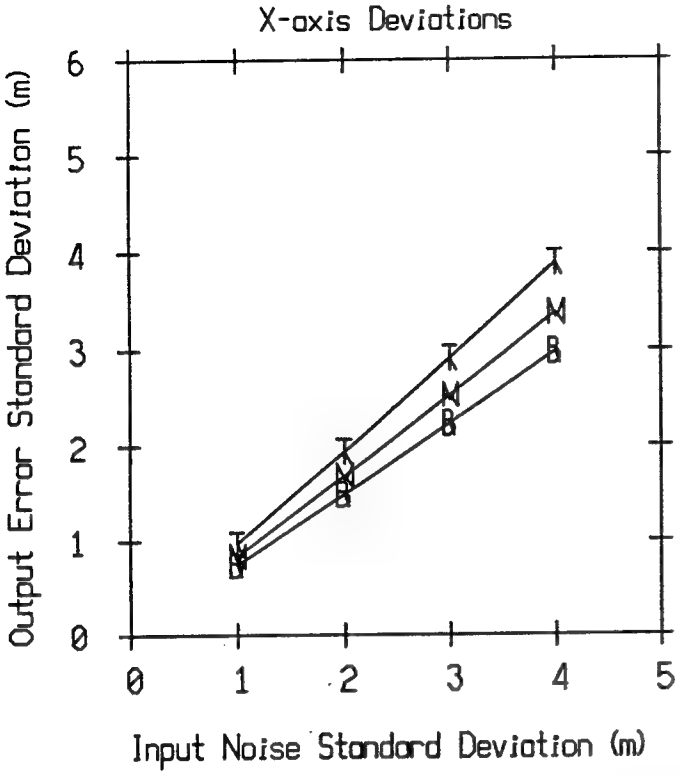

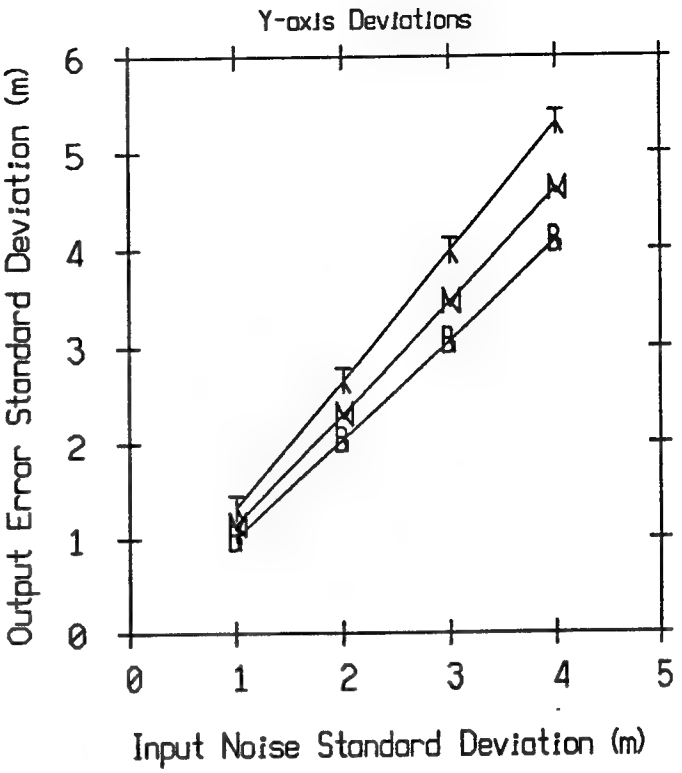

Point T represents Top Element
Point M represents Middle Element
Point B represents Bottom Element

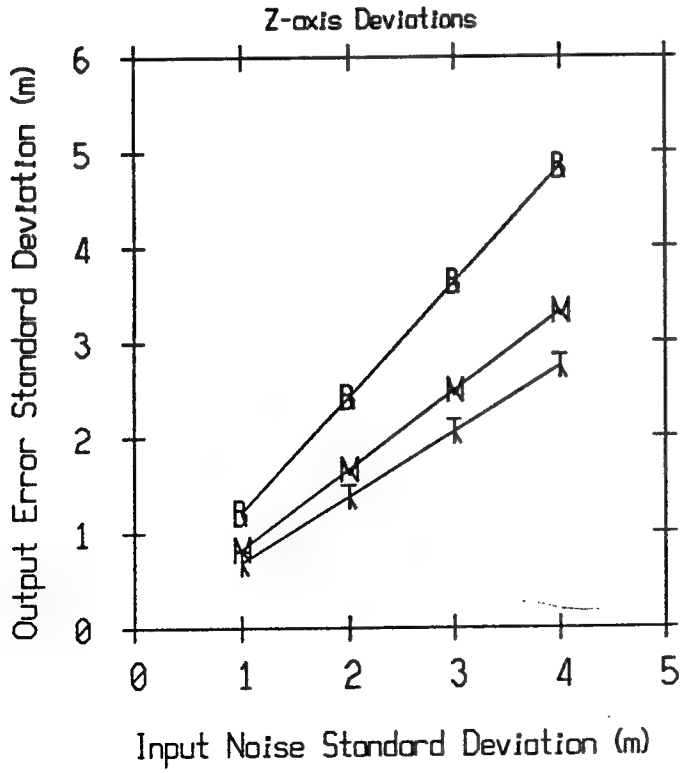

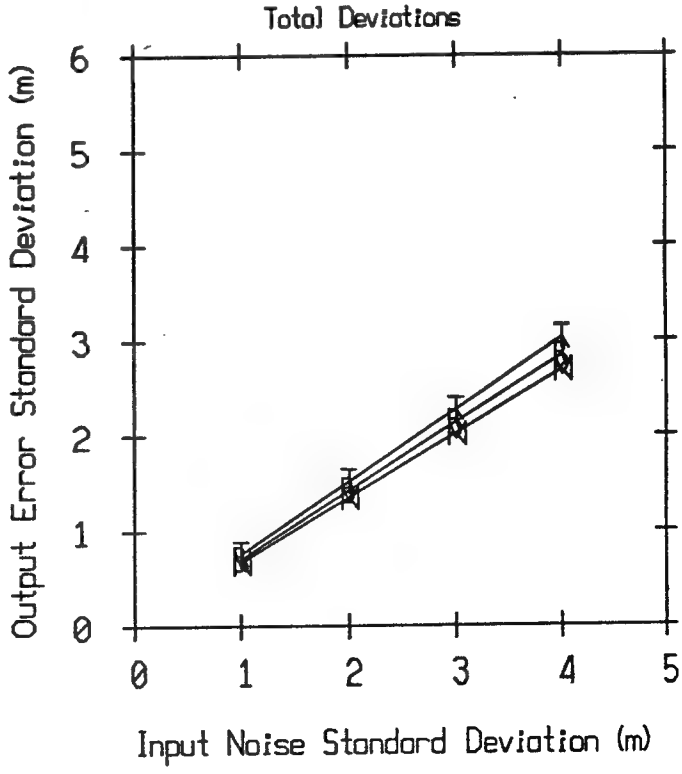

Figure 19D

How Radial Noise + Transponder Positions Affect Array Position Error

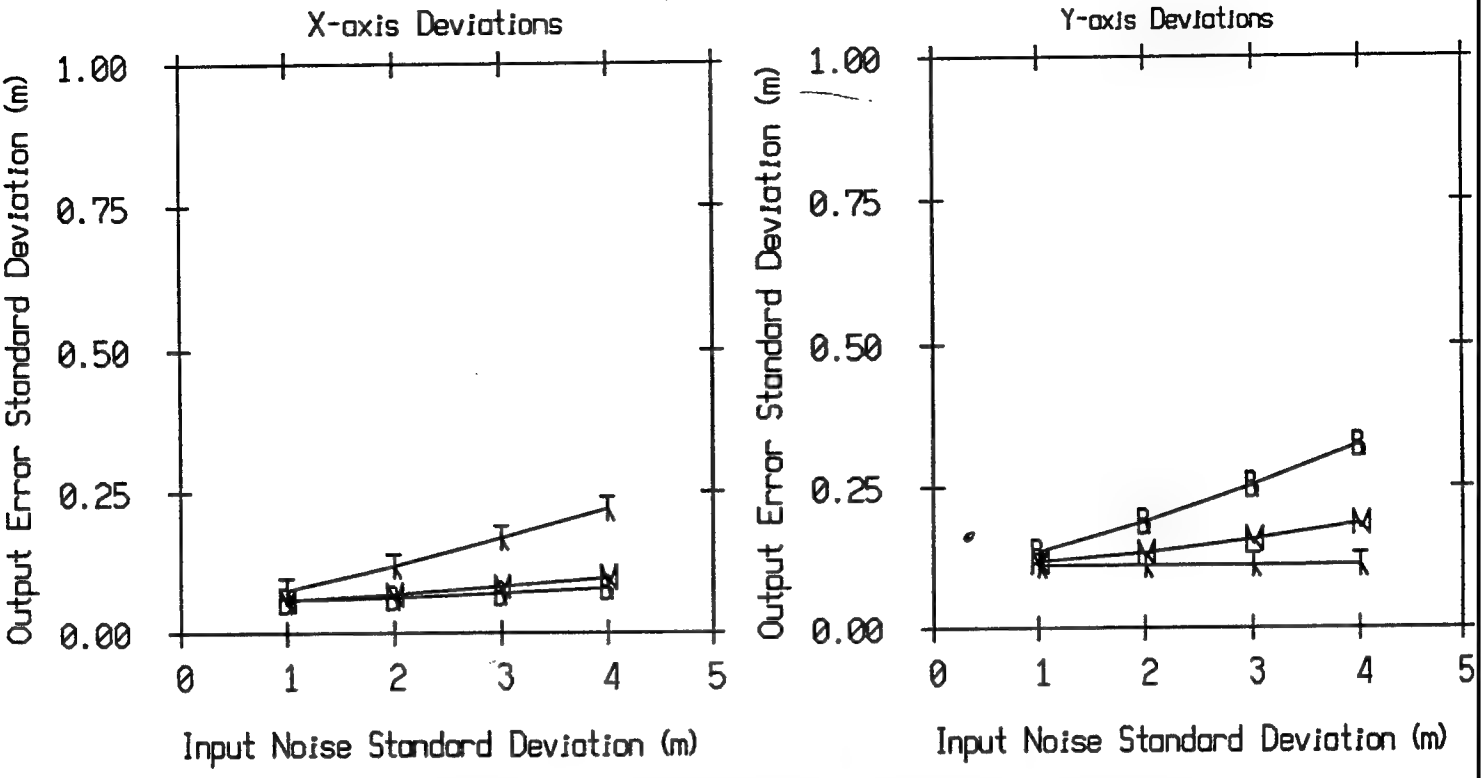

Point T represents Top Element
Point M represents Middle Element
Point B represents Bottom Element

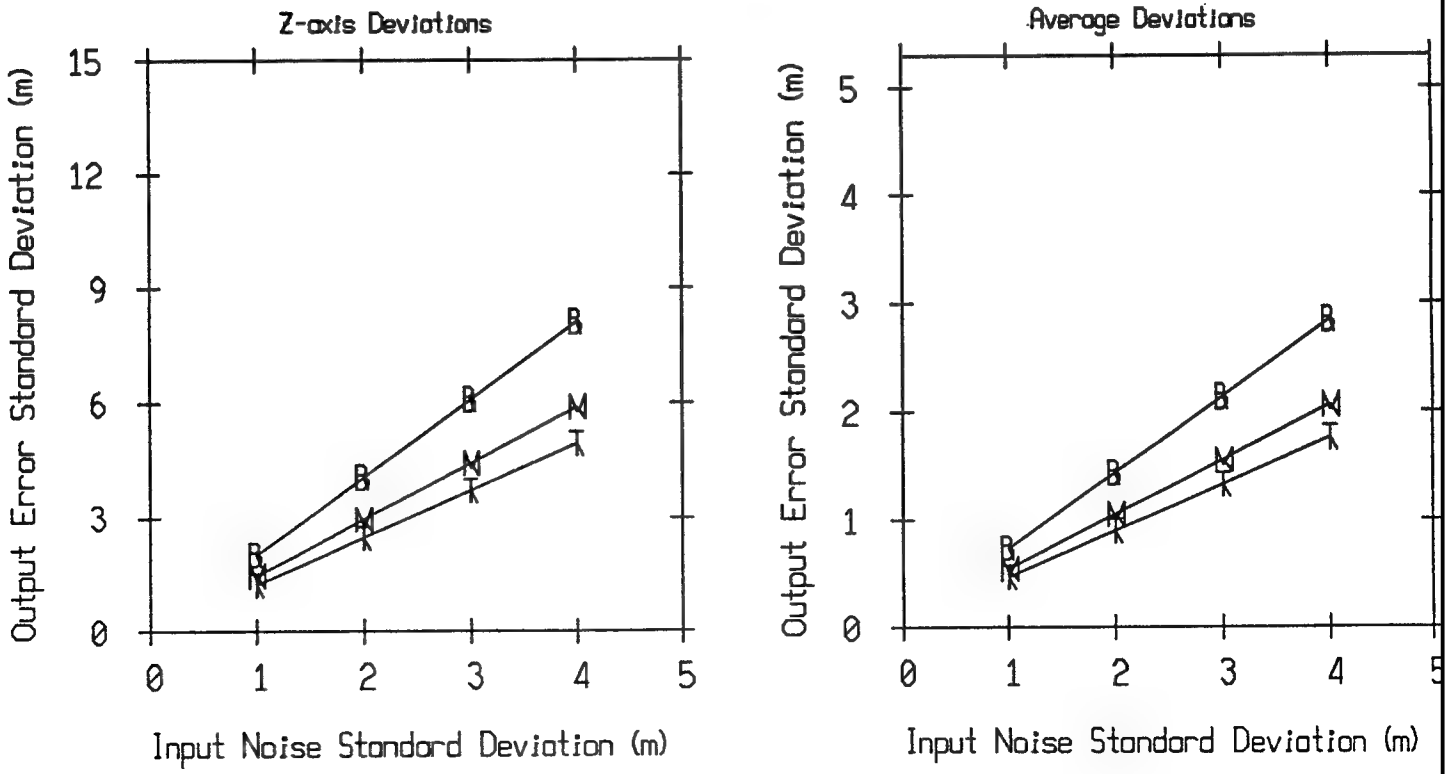

Figure 19E

How Slant Ranges + Noise [N(0,1)] Affect Transponder #3 Position Error

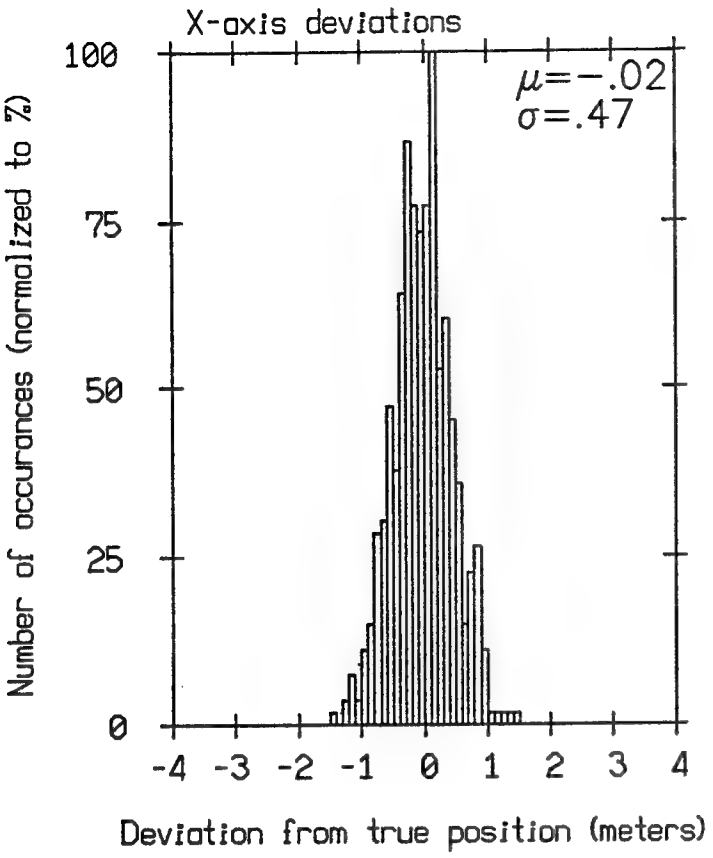

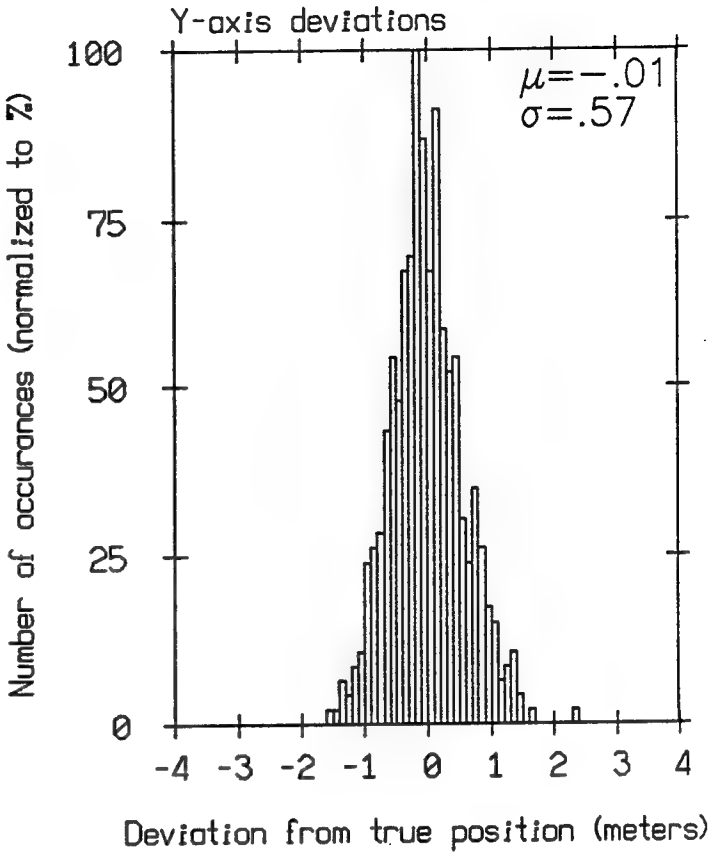

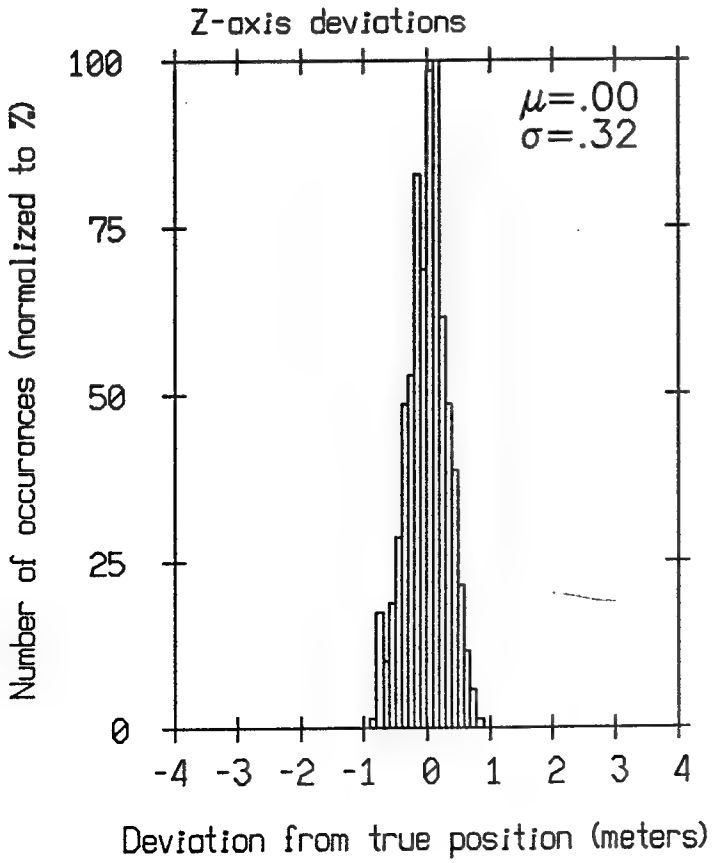

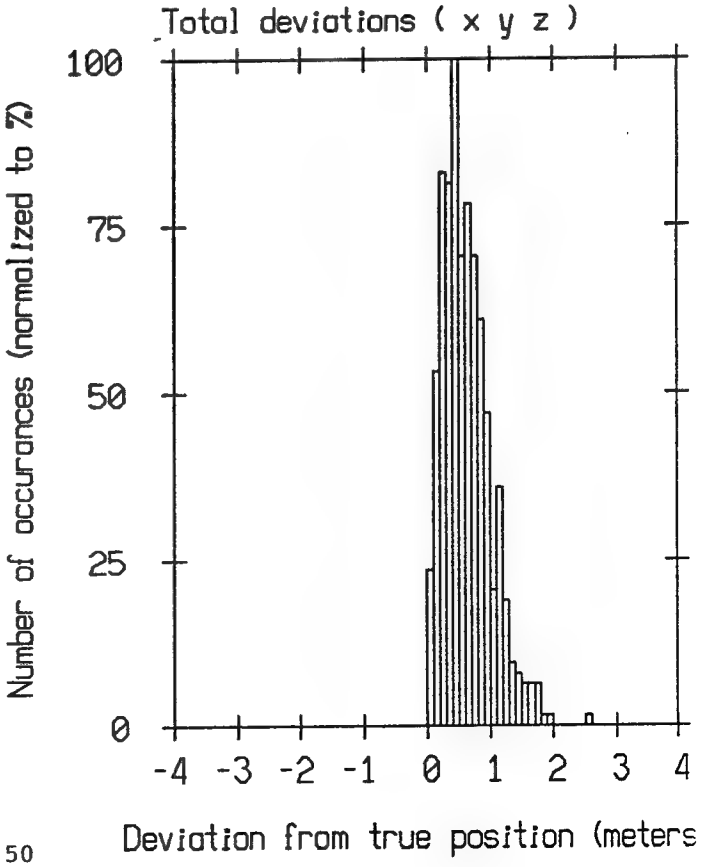

Figure 20.A.1 **Array/ Transponder Net Geometry**

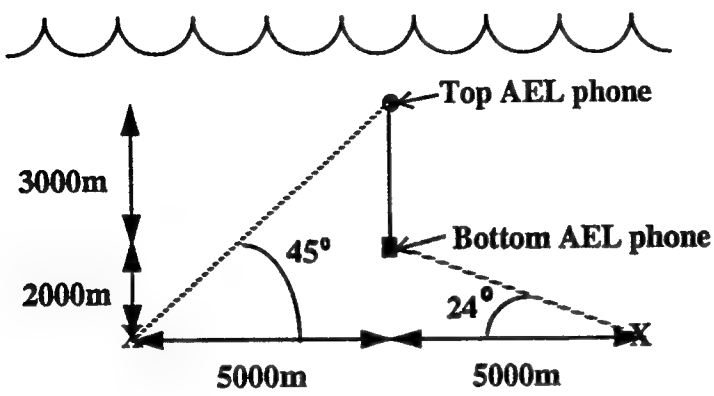

(X's denote transponders)

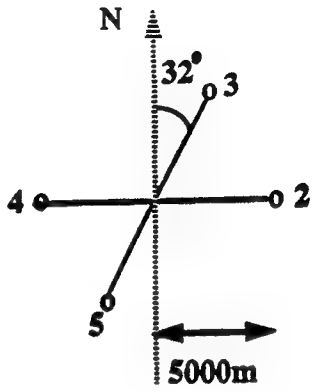

Plan View (o's denote transponders)

Figure 20.A.2 **E/W error in (2,4) yield SSE/NNW AEL error**

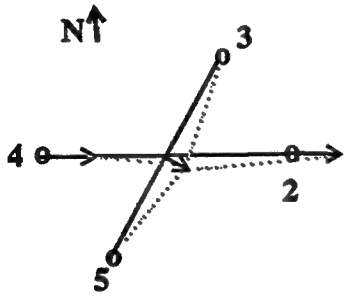

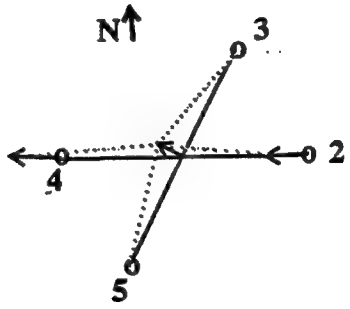

Figure 20.A.3 **E/W error in (3,5) yield N/S AEL error**

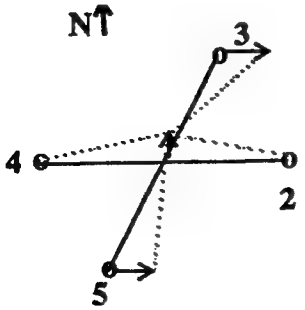

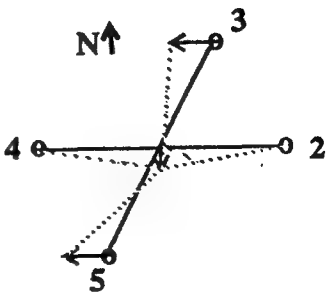

Figure 20.A.4 **N/S error in (2,4) yields neglibible AEL error**

Figure 20.A.5 **N/S error in (3,5) yields N/S AEL error**

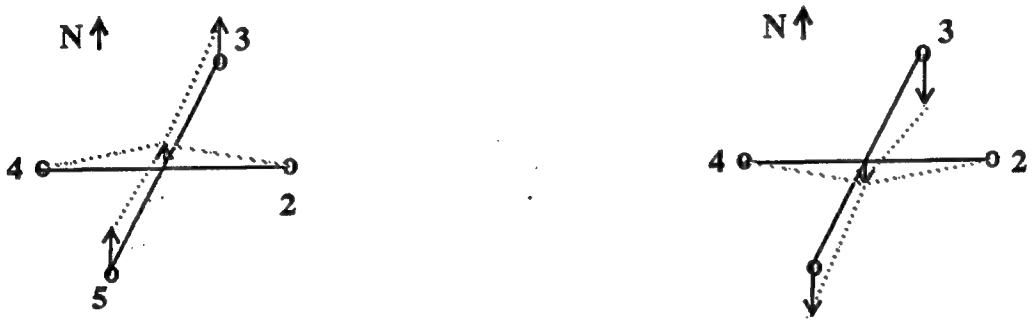

Figure 20.A.6

Inward/Outward transponder error raises/lowers depth of array 1-6m

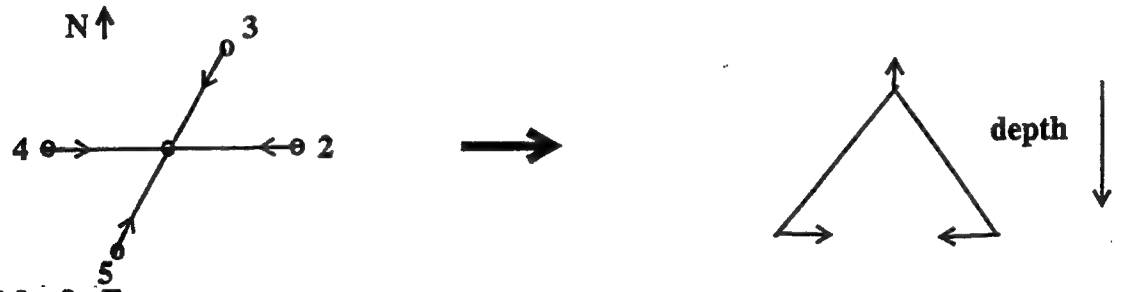

Figure 20.A.7

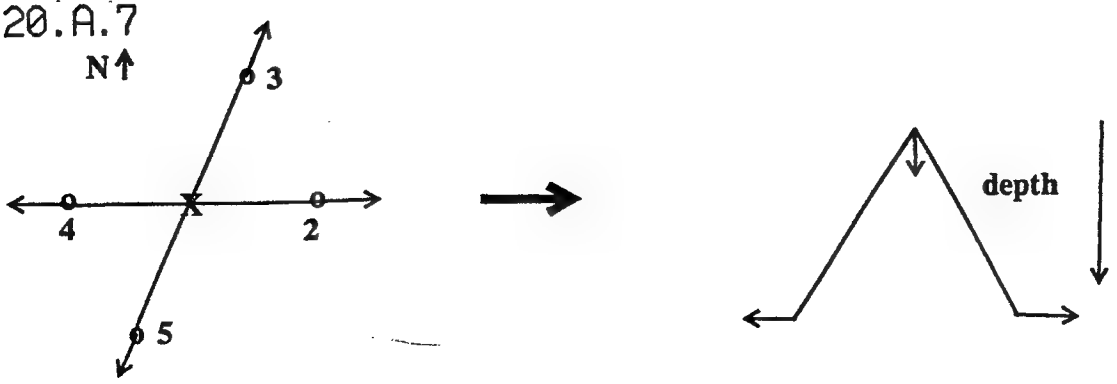

Upward/downward 10m transponder error yields 2.5m upward/downward AEL error
Further x-y ael error (~5m) will be perpendicular to the other axis in the direction of the downward transponder as follows:

Figure 20.A.8

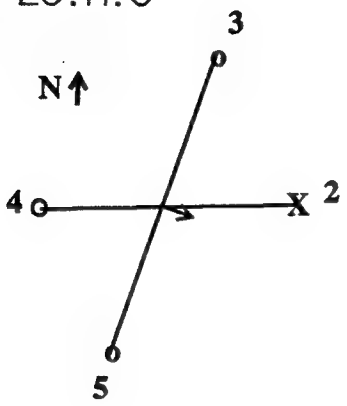

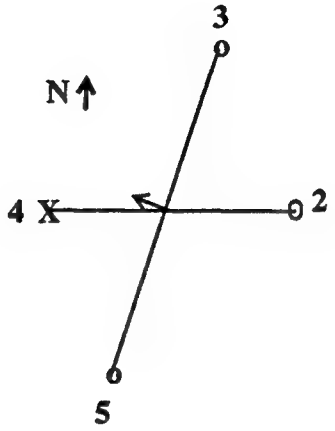

Figure 20.A.9

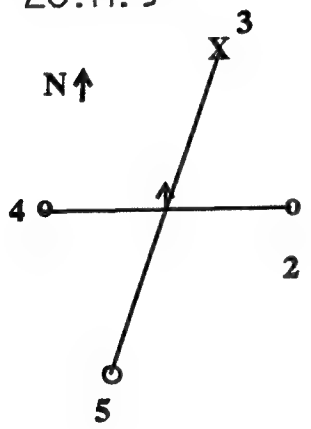

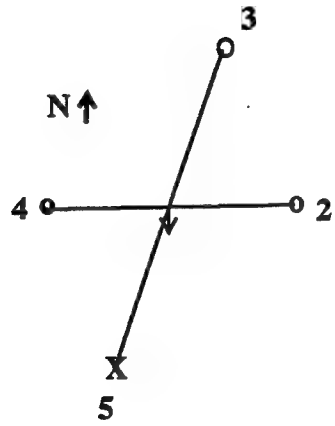

X denotes down

O denotes up

Figure 20.B.1

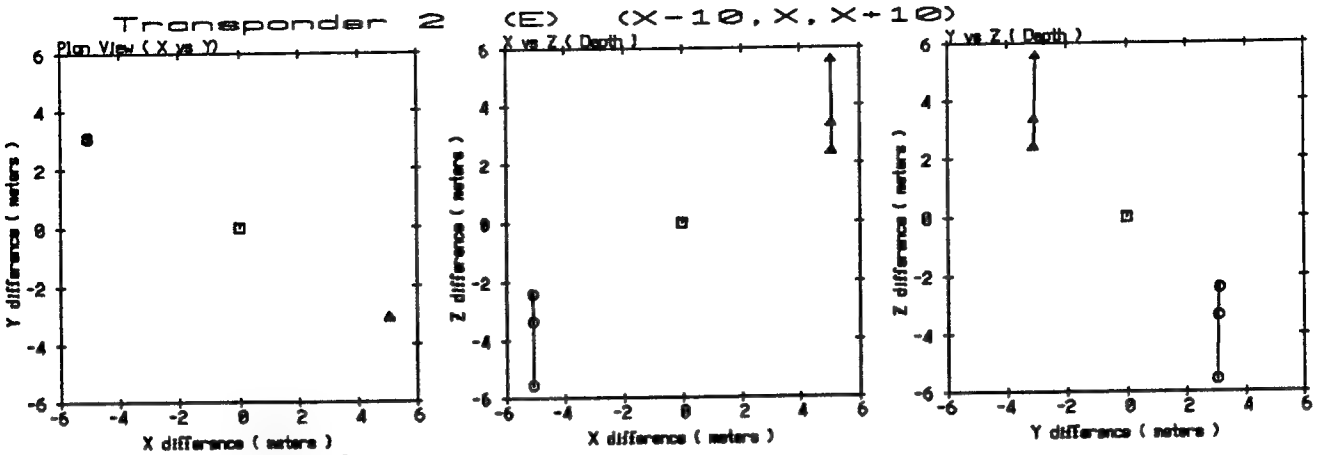

Figure 20.B.2

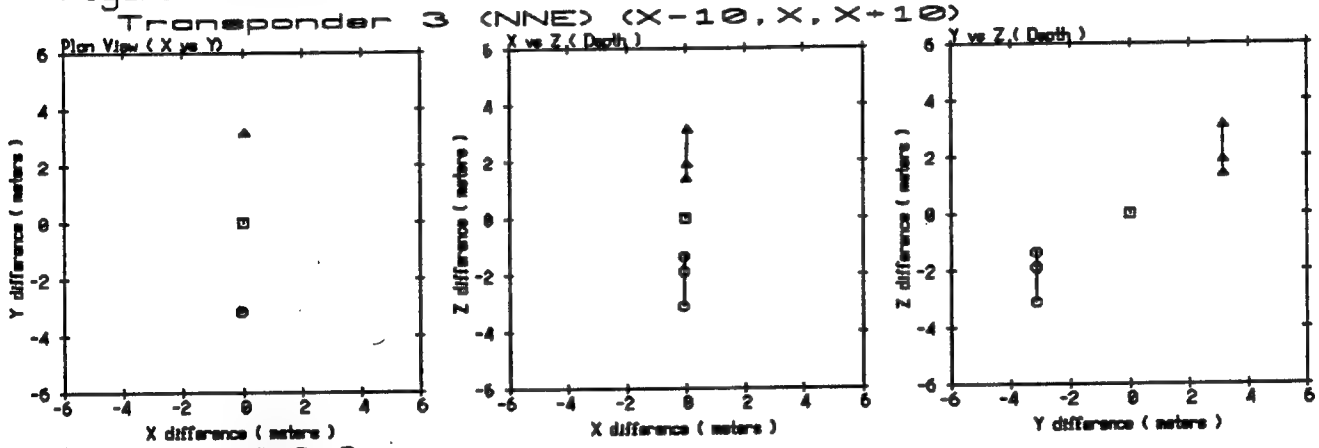

Figure 20.B.3

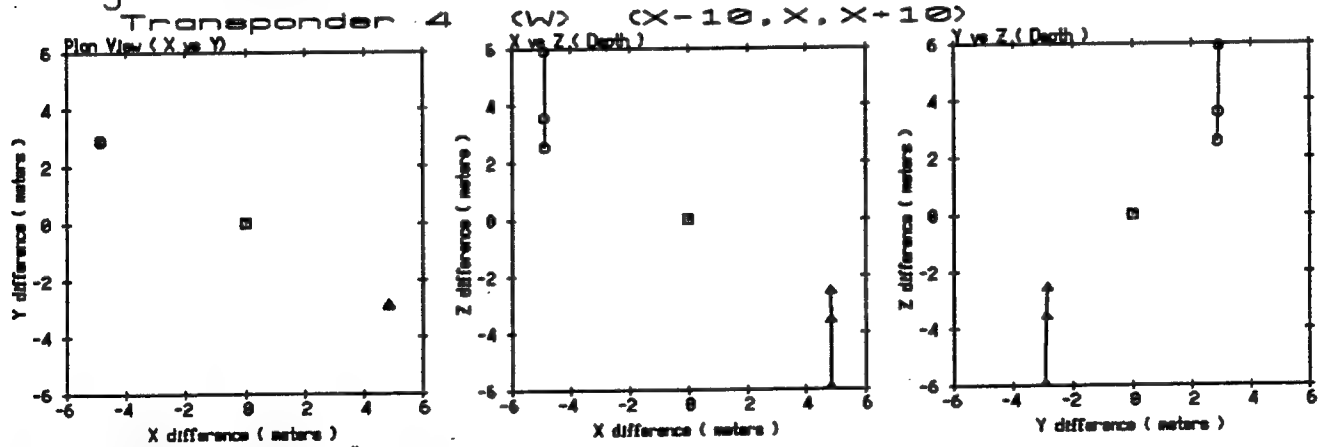

Figure 20.B.4

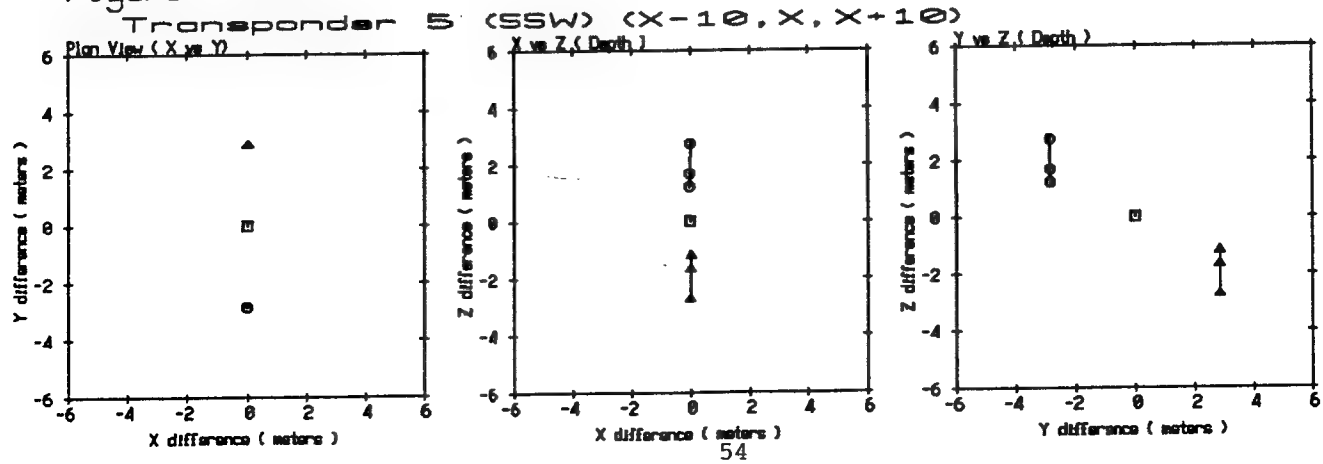

Figure 20.B.5

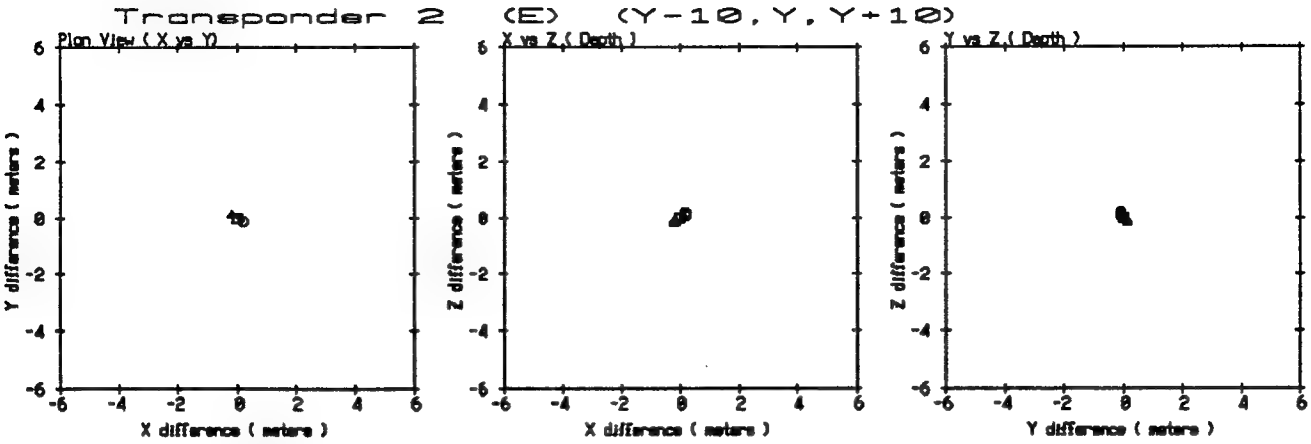

Figure 20.B.6

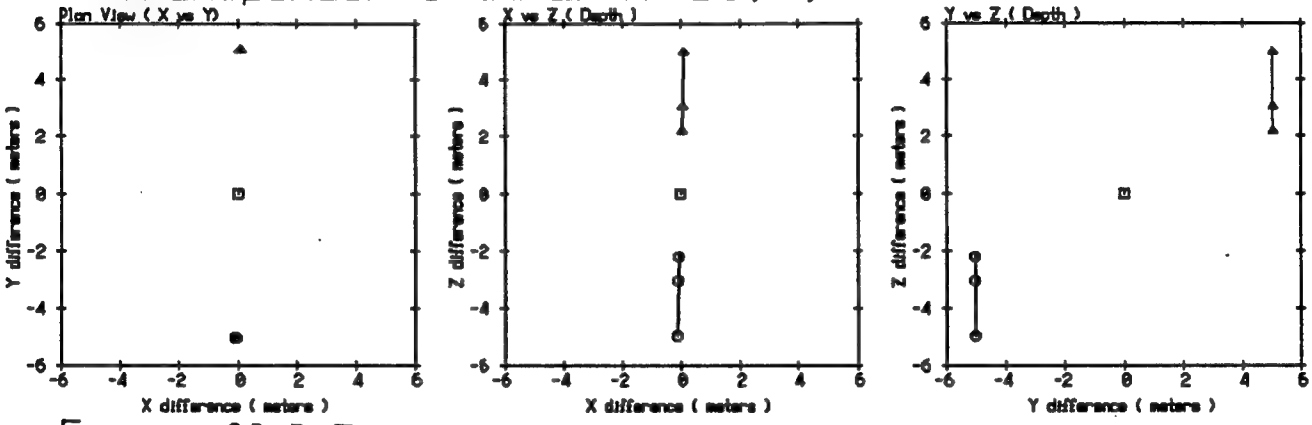

Figure 20.B.7

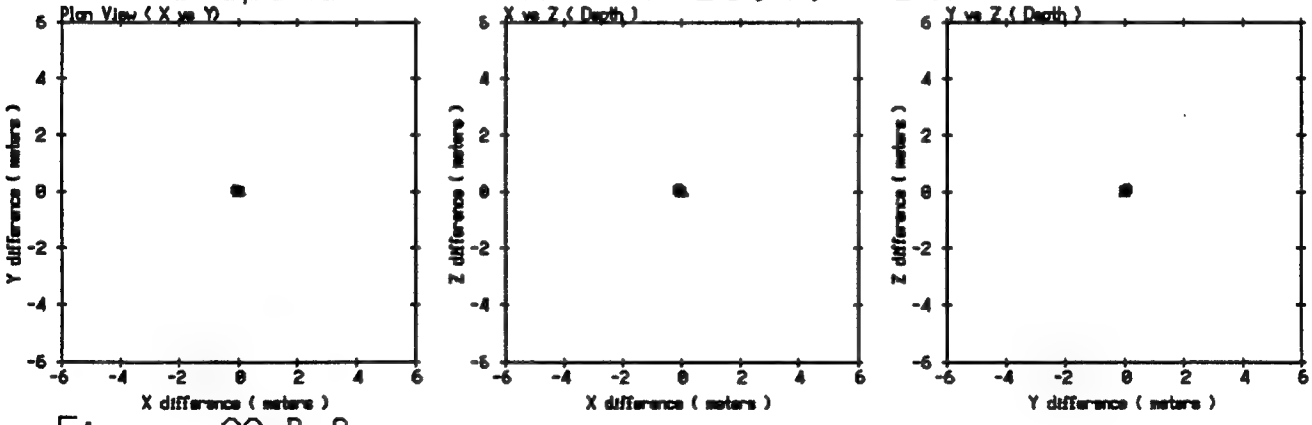

Figure 20.B.8

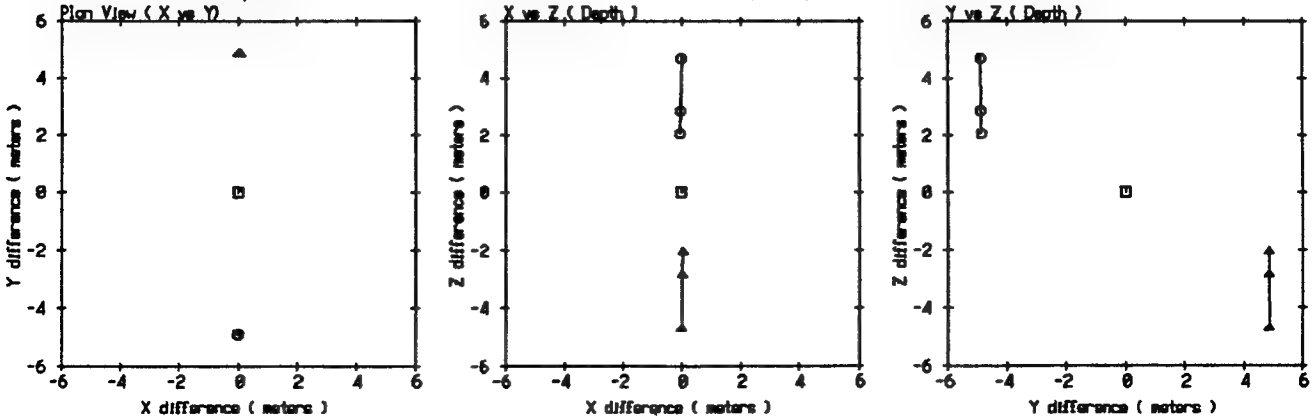

Figure 20.B.9

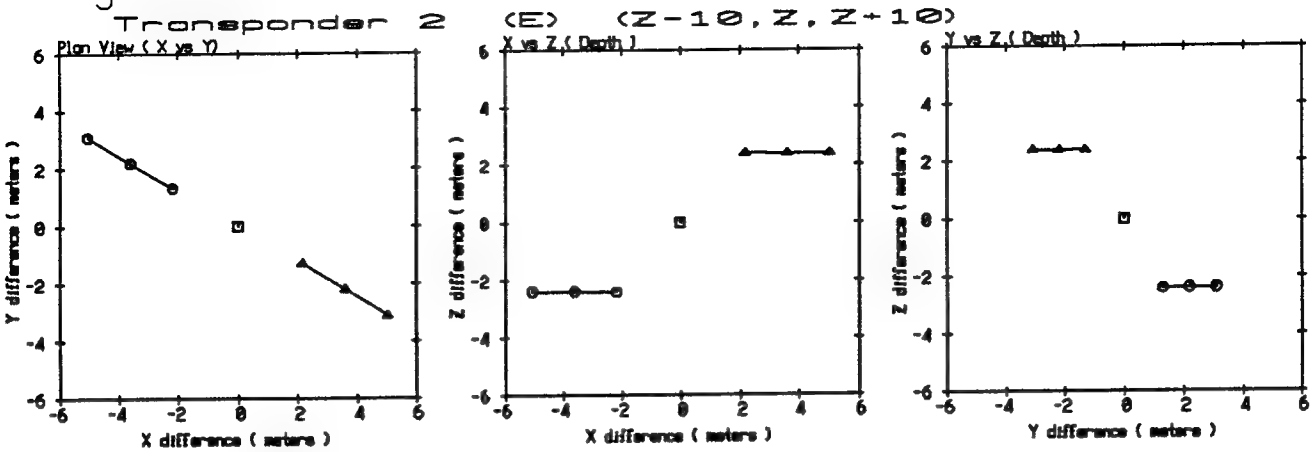

Figure 20.B.10

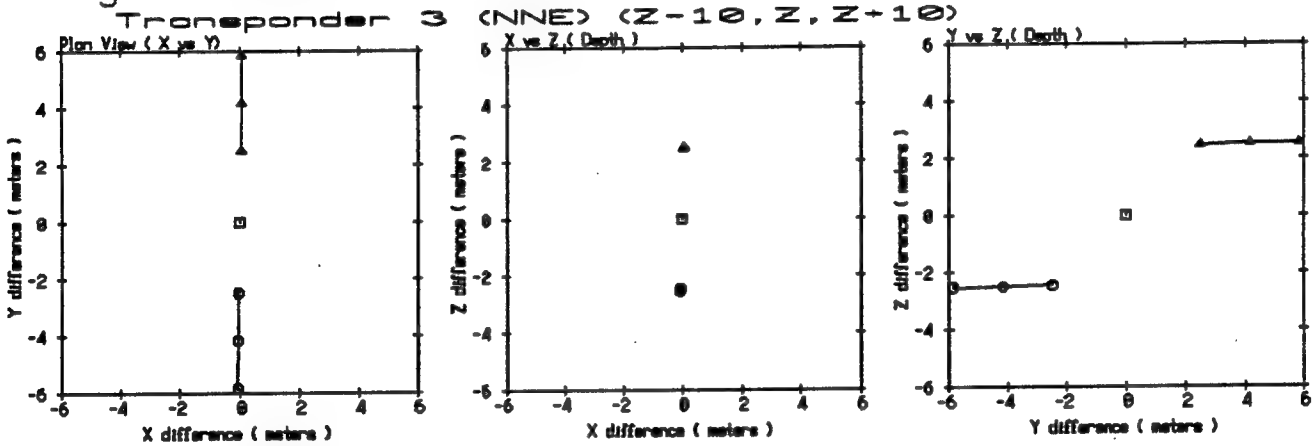

Figure 20.B.11

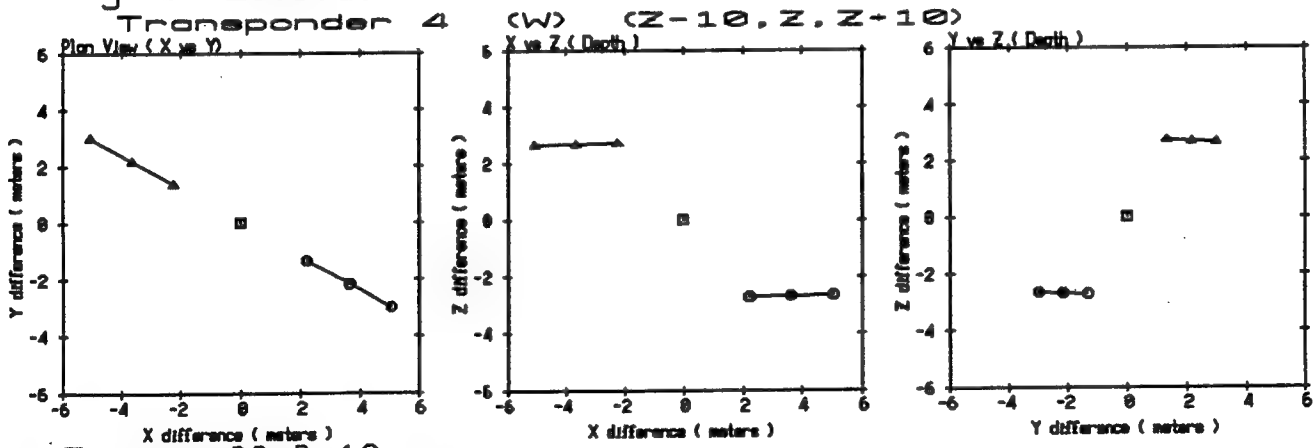

Figure 20.B.12

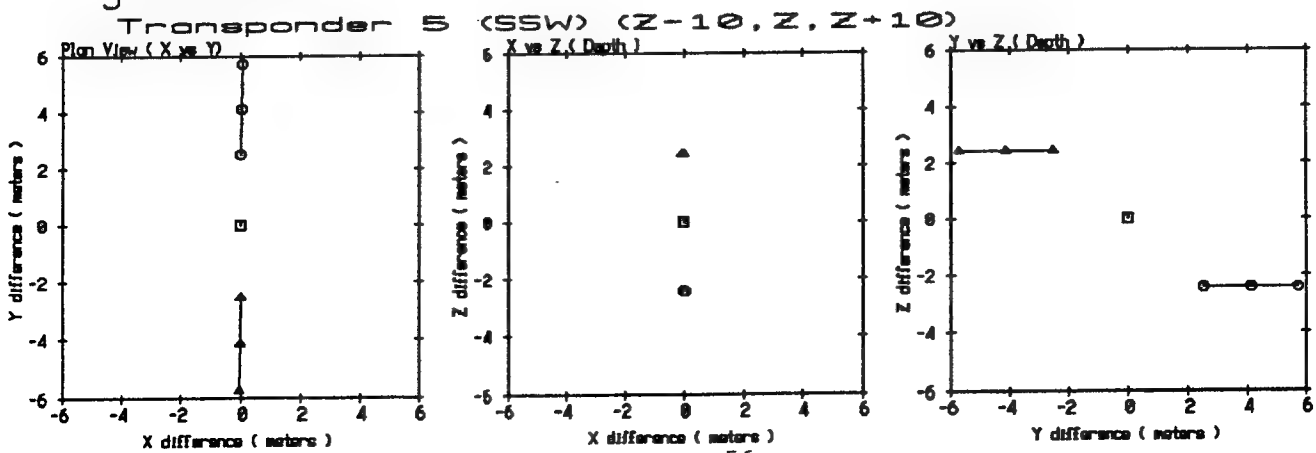

Figure 21A FLIP receiver travel times
Downward 12 KHz ping

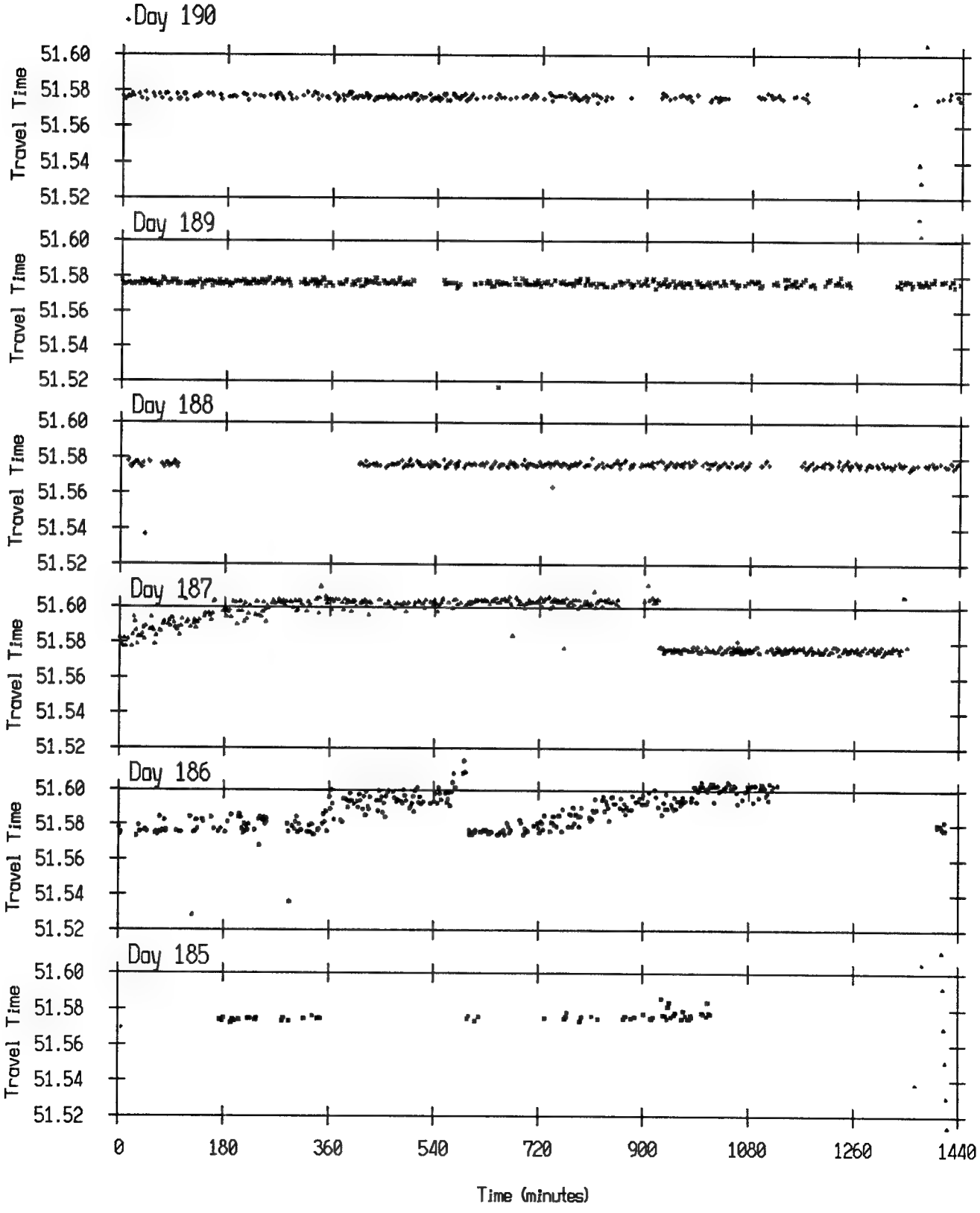

Figure 21B Detections for day 186

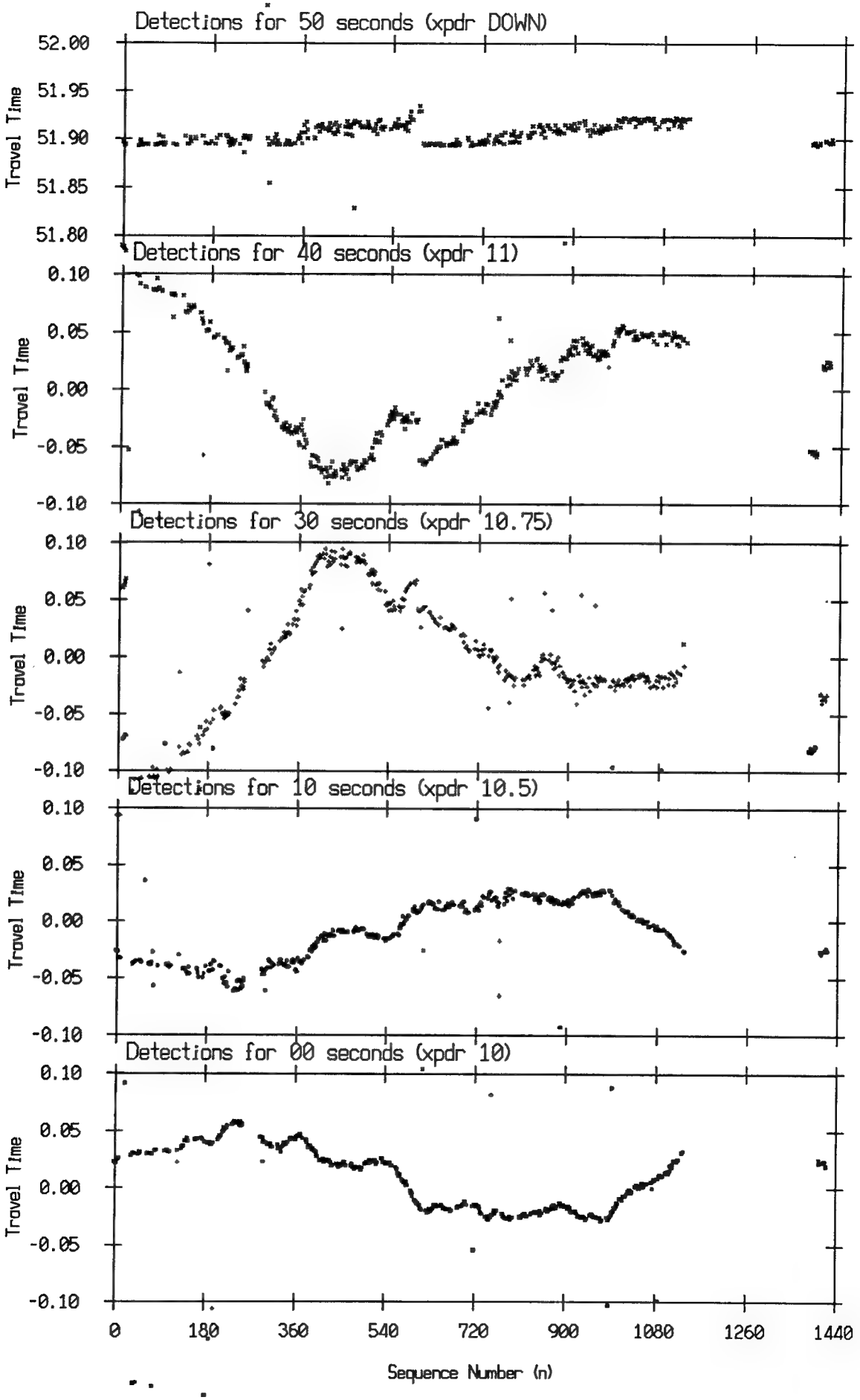

Figure 21C D Downward Data for Day 187

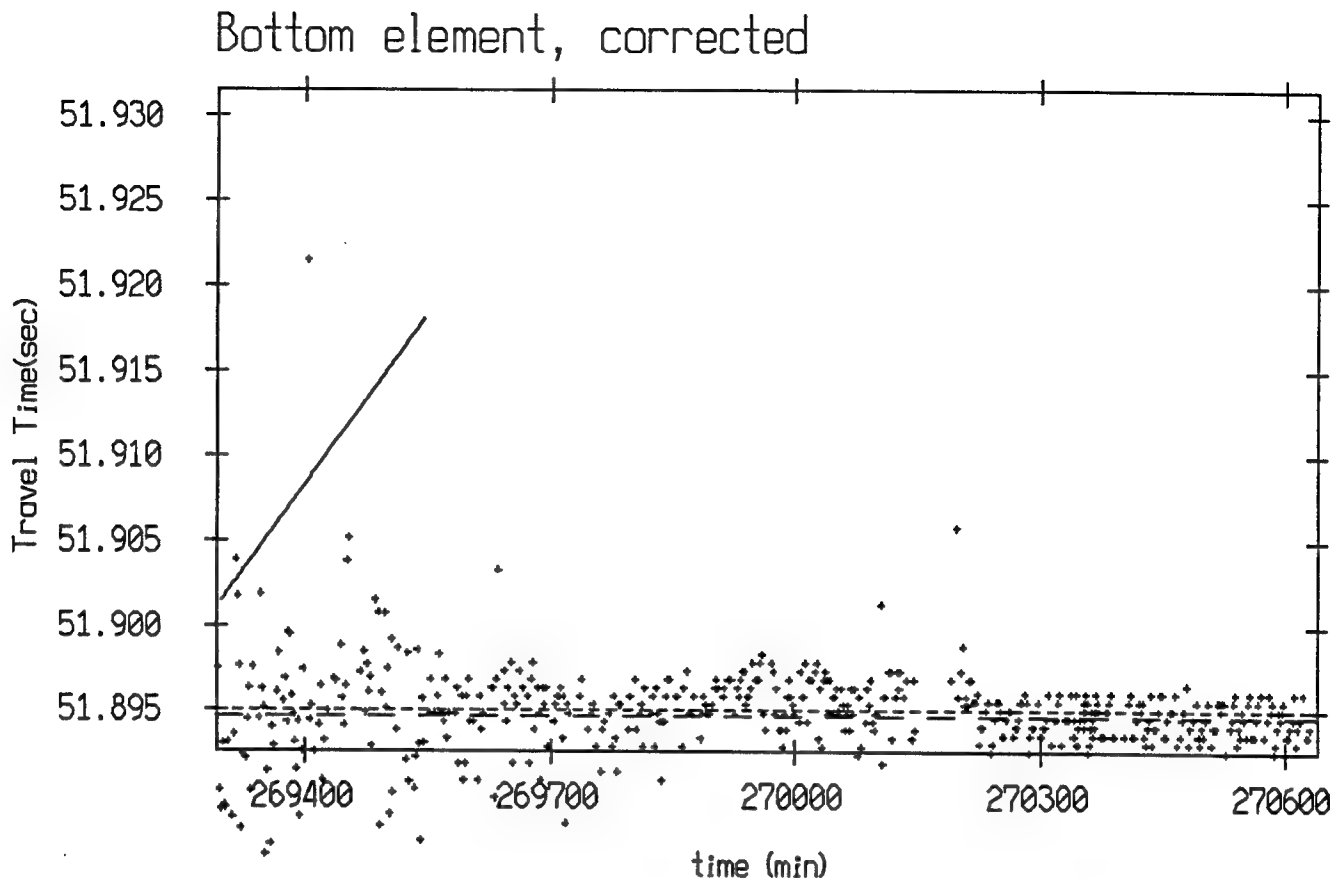

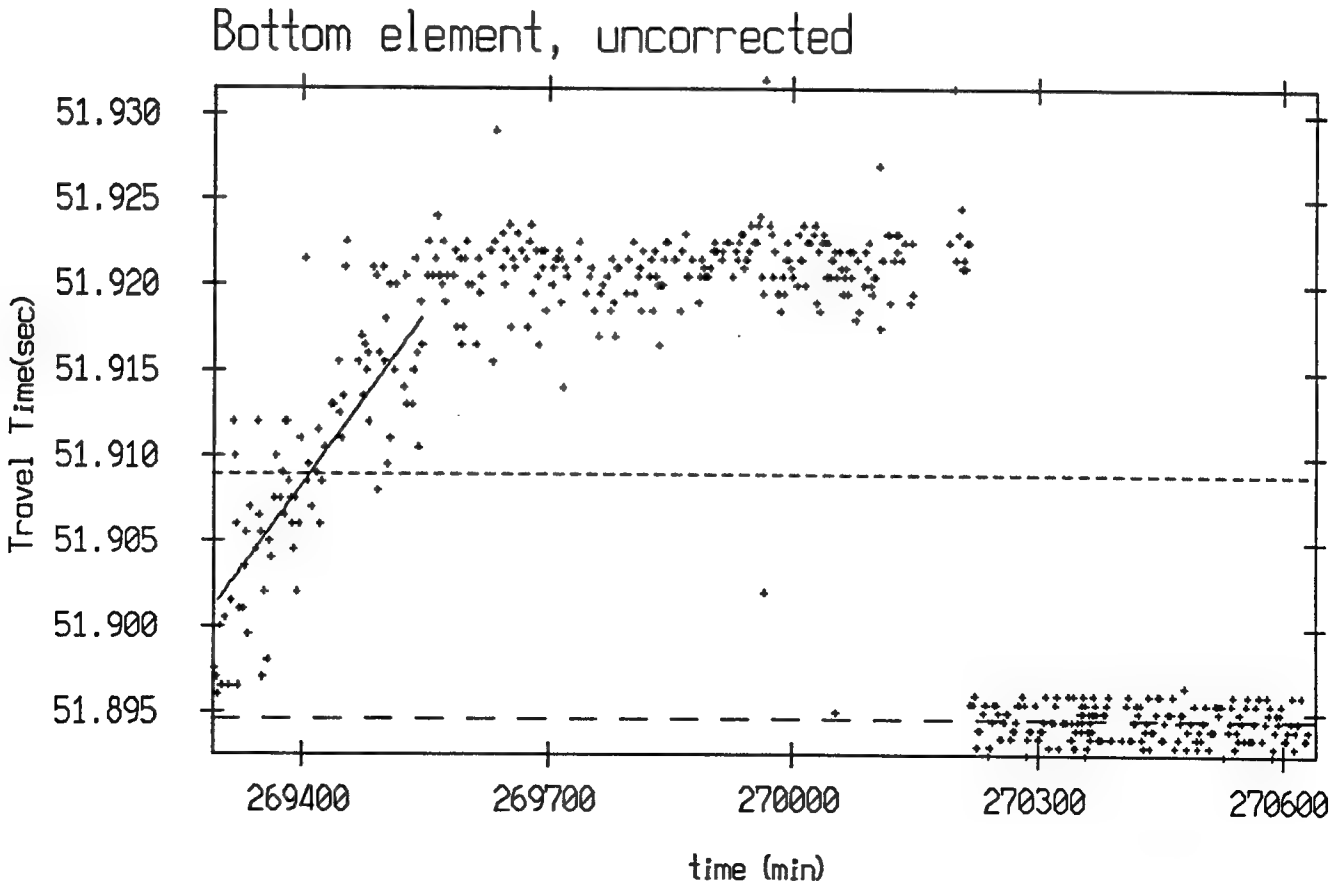

Figure 21E FLIP receiver travel times
Downward 12 KHz ping

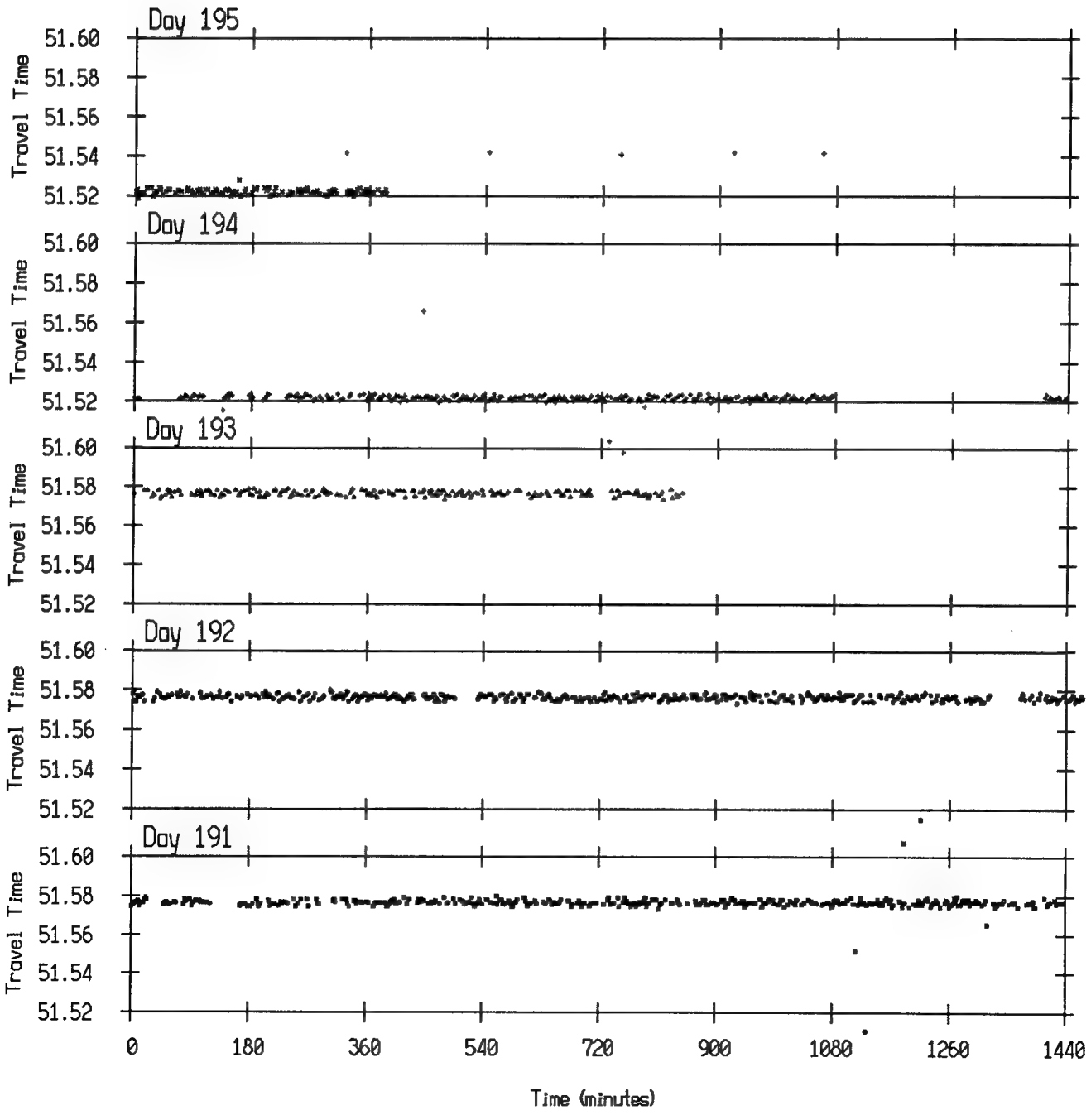

Figure 21F Detections for day 193

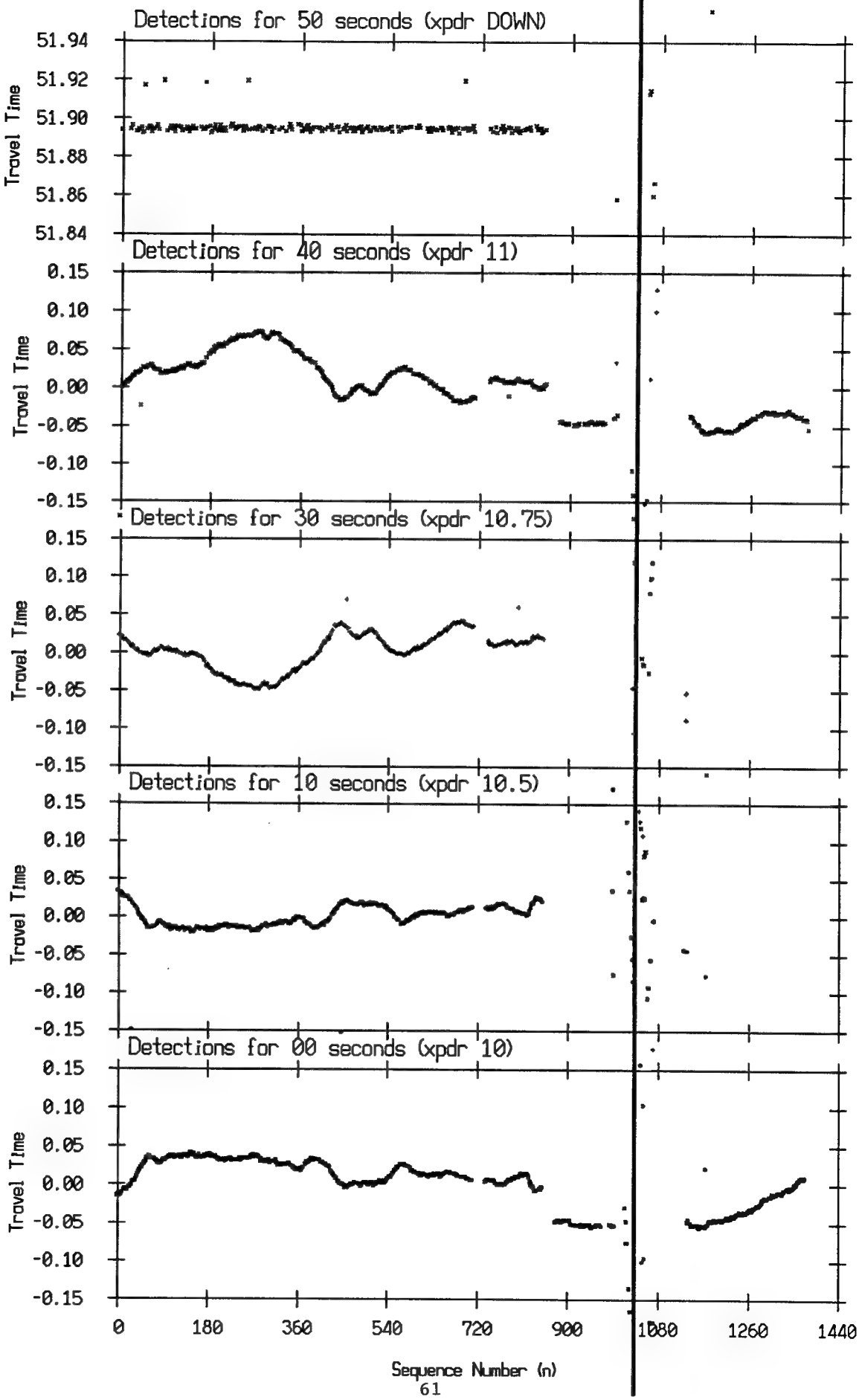

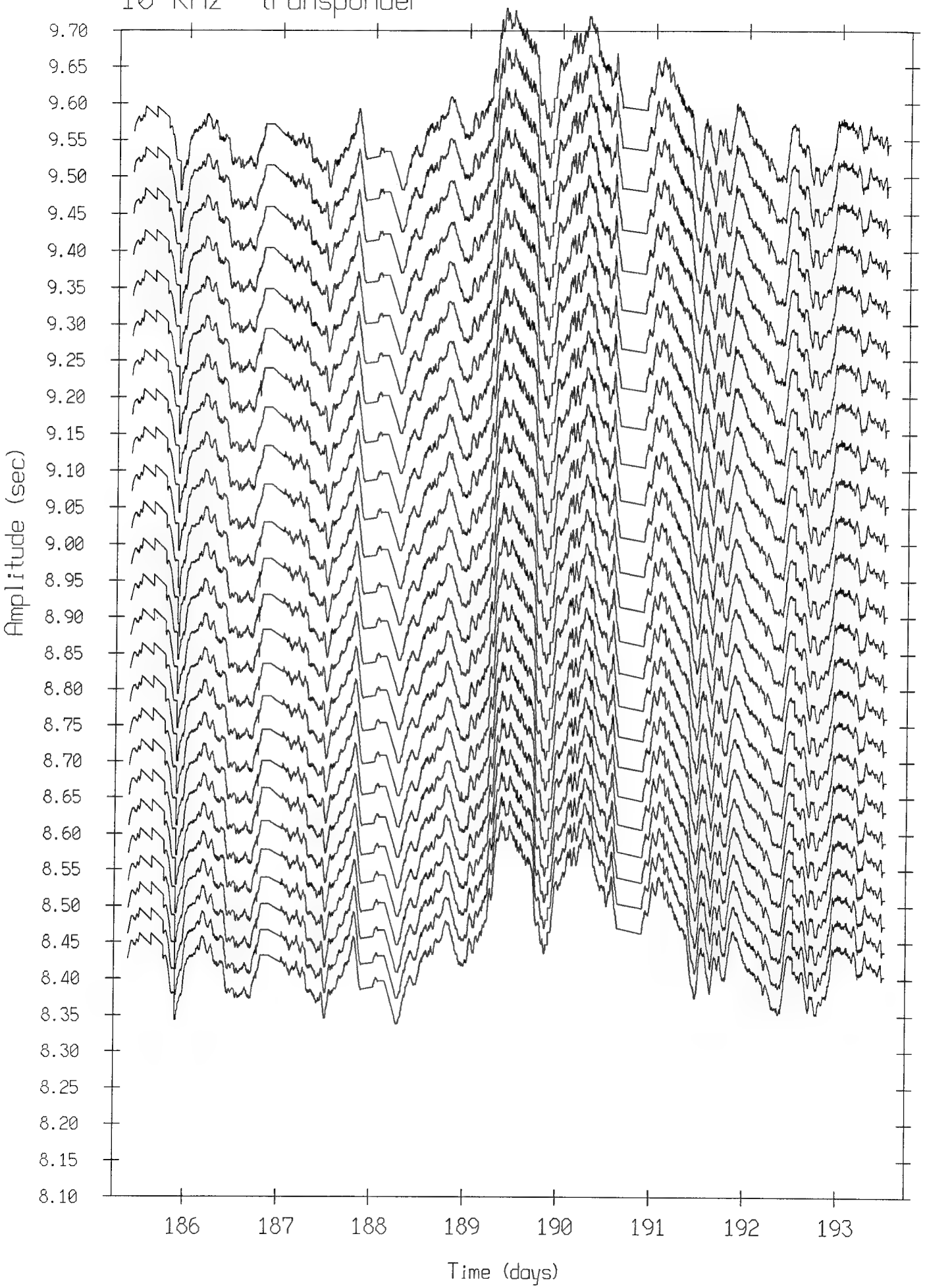
Figure 22A VAST MPL vertical array arrivals
10 KHz transponder
9.70
9.65
9.60
9.55
9.50
9.45
9.40
9.35
9.30
9.25
9.20
9.15
9.10
9.05
9.00
8.95
8.90
8.85
8.80
8.75
8.70
8.65
8.60
8.55
8.50
8.45
8.40
8.35
8.30
8.25
8.20
8.15
8.10
Amplitude (sec)
186
187
188
189
190
191
192
193
Time (days)

Figure 22B VAST MPL vertical array arrivals
105 KHz transponder

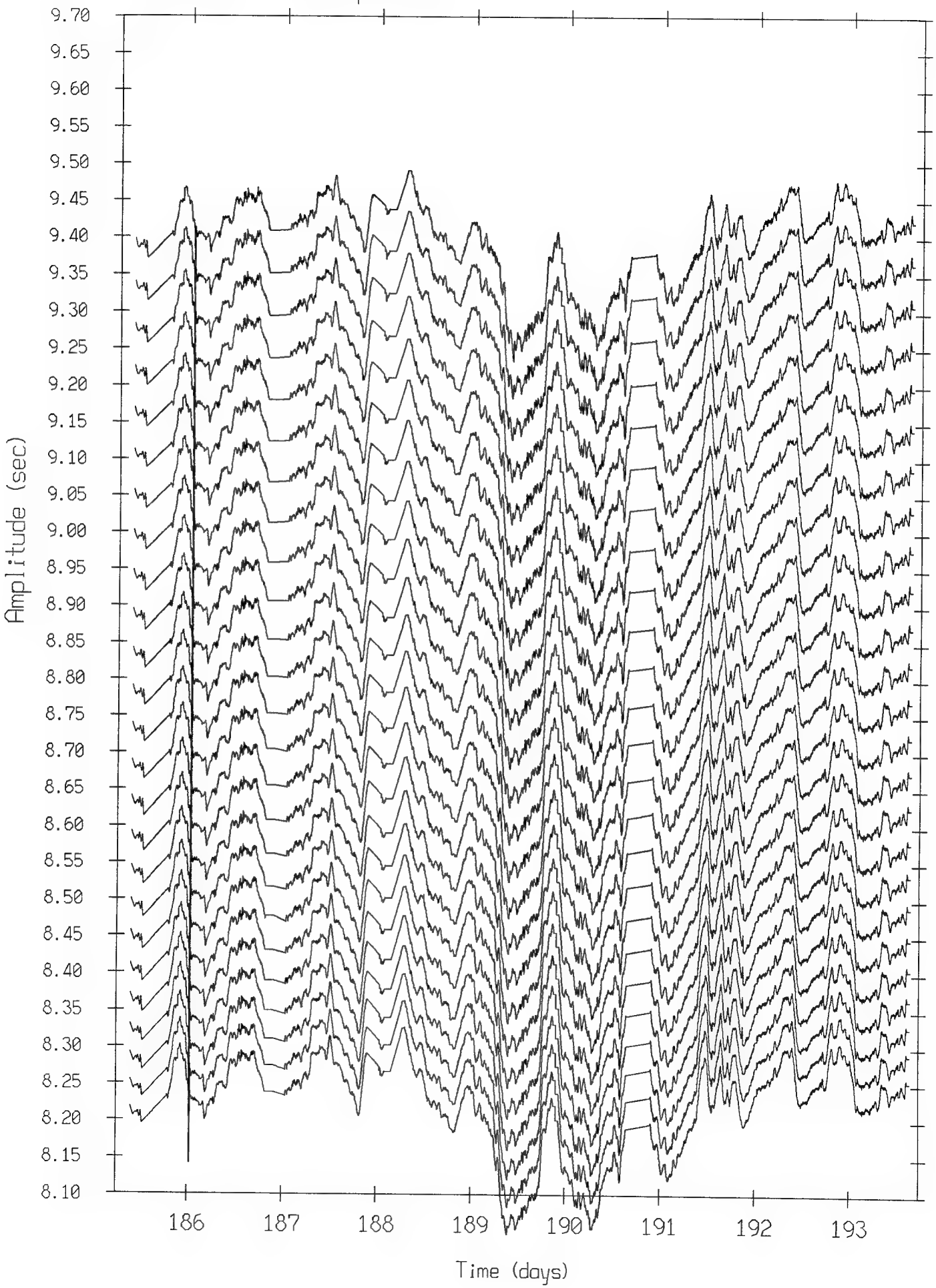

Figure 22C VAST MPL vertical array arrivals
1075 KHz transponder

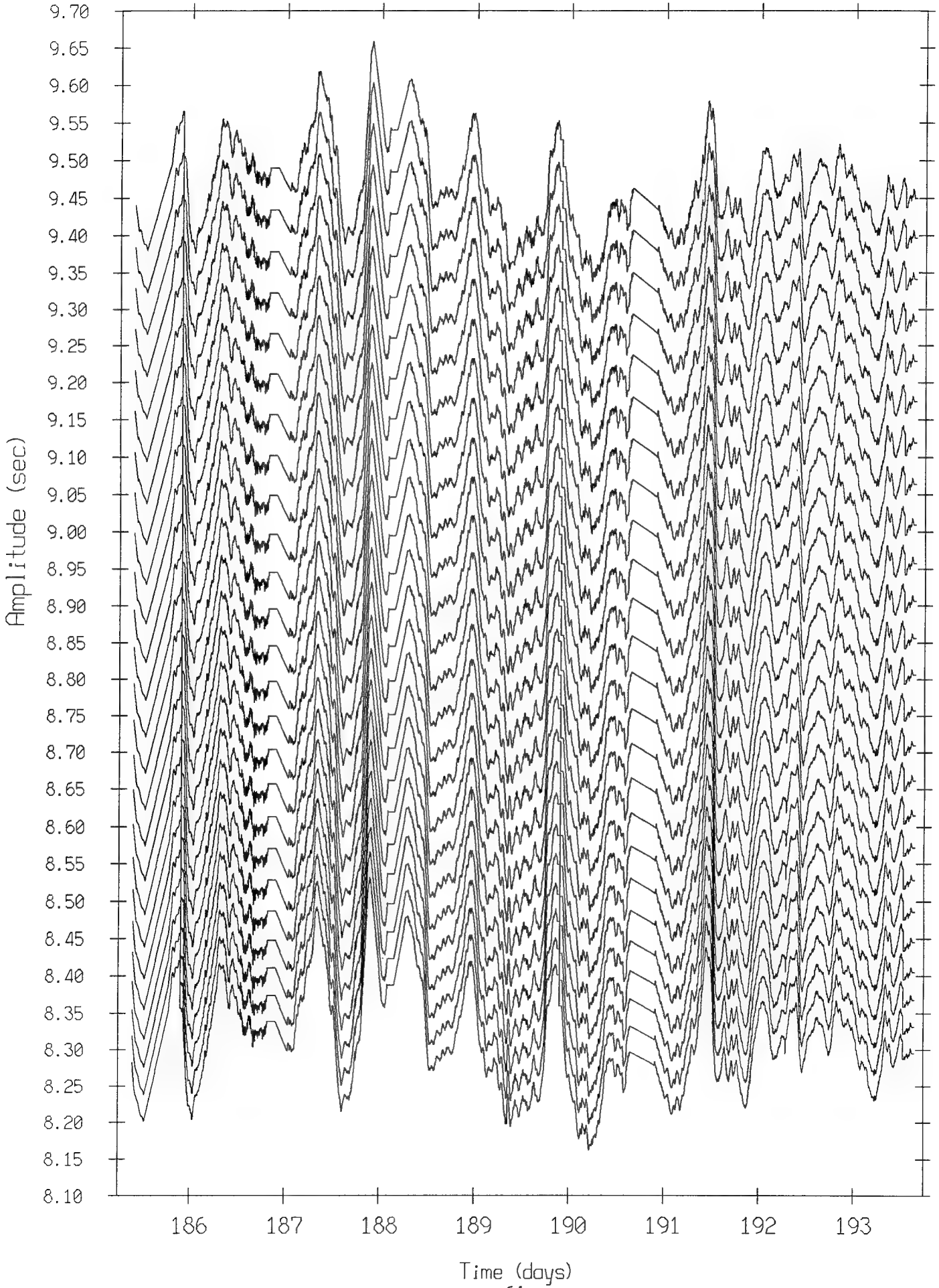

Figure 22D VAST MPL vertical array arrivals
11 KHz transponder

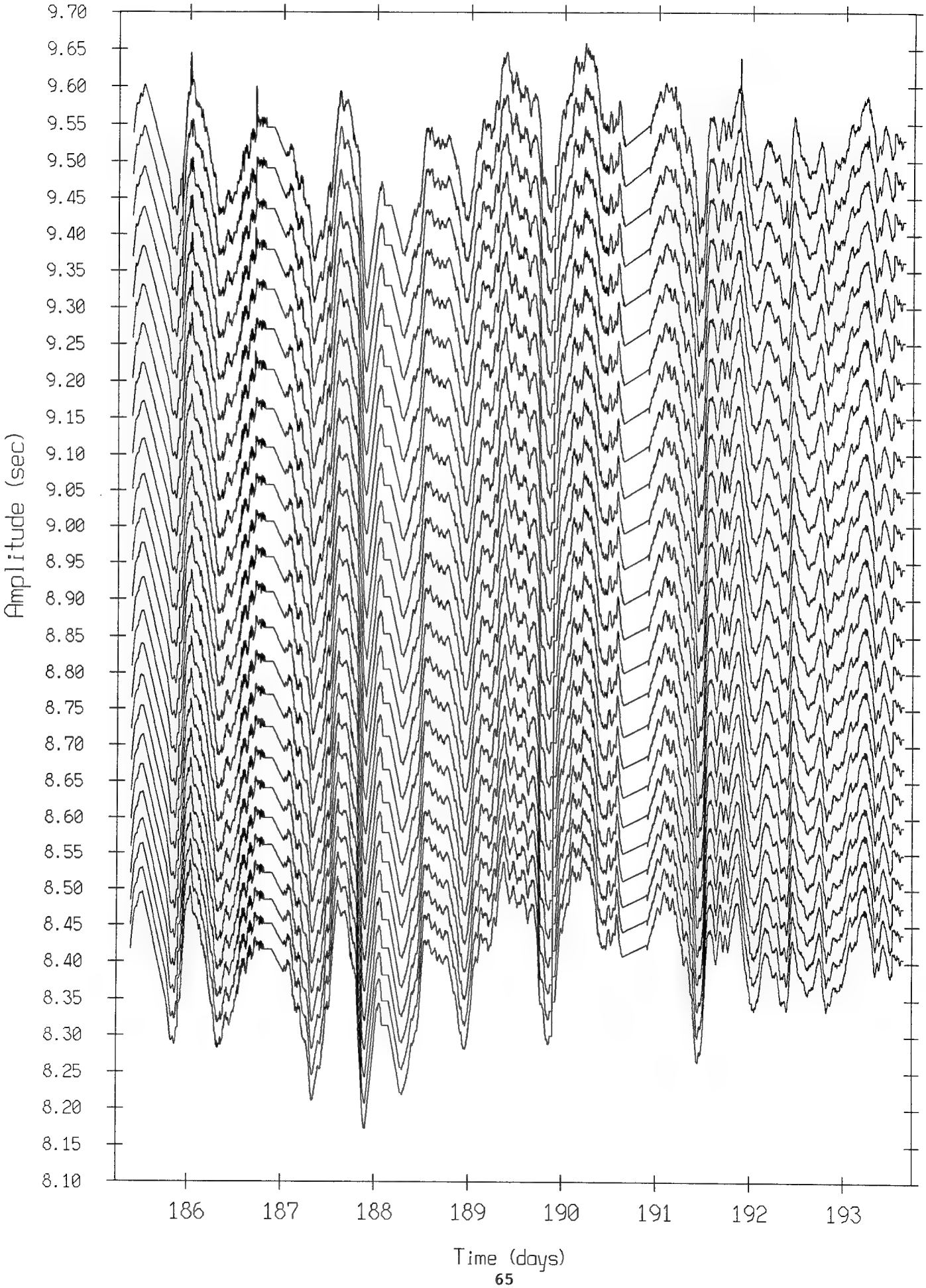

Figure 23A VAST MPL vertical array
Standard deviations of 10 Khz transponder arrivals

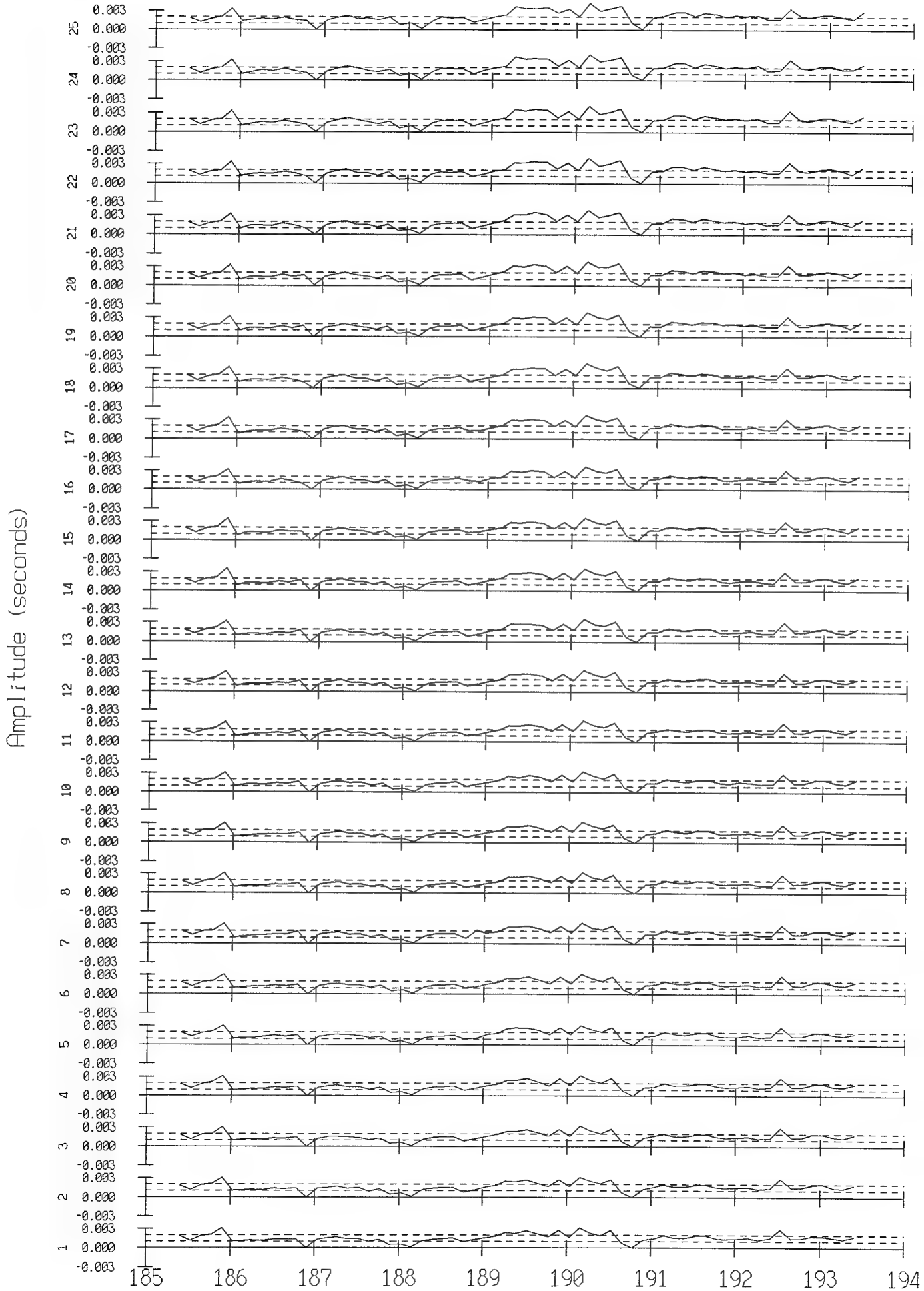

Figure 23B VAST MPL vertical array
Standard deviations of 105 Khz transponder arrivals

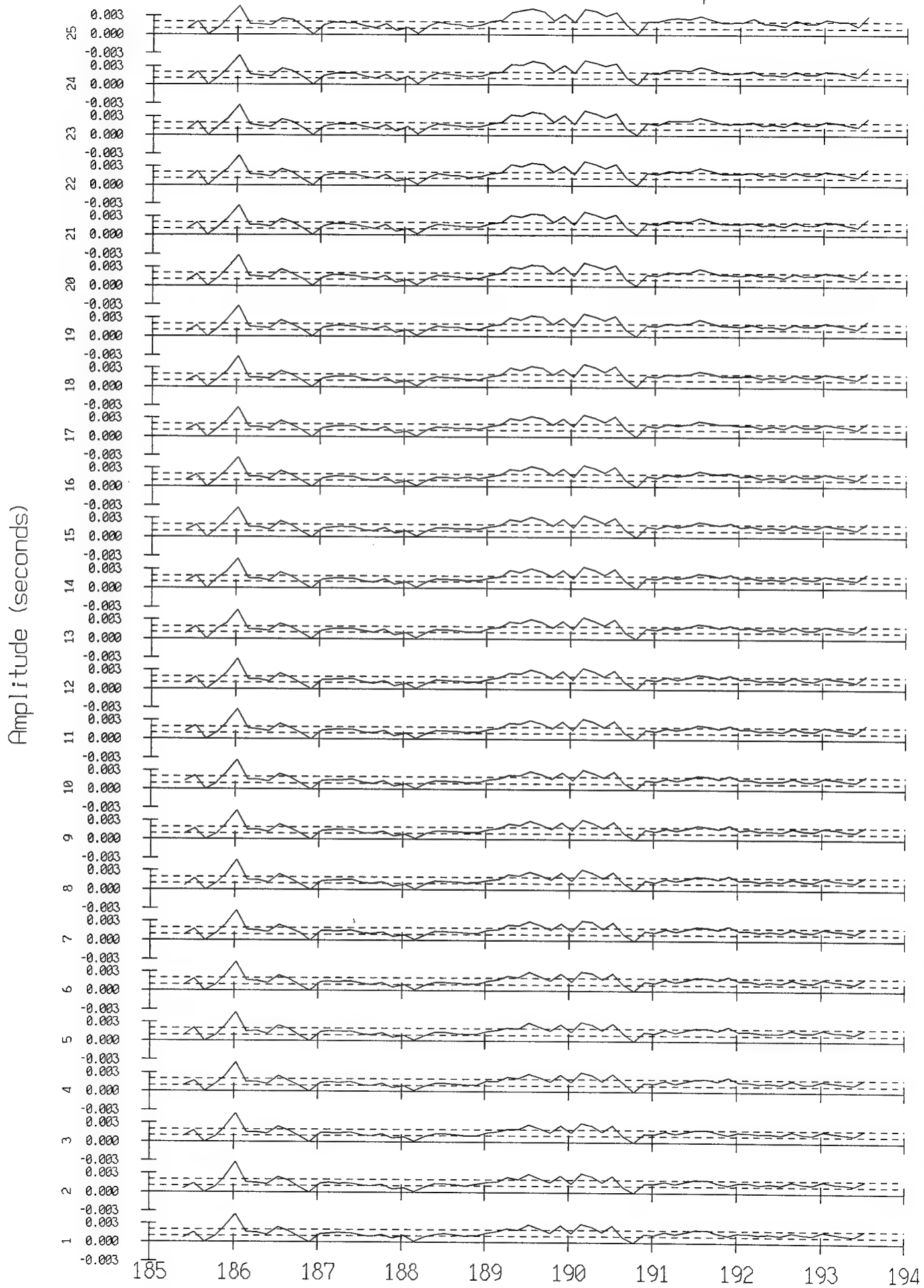

Figure 23C VAST MPL vertical array
Standard deviations of 1075 Khz transponder arrivals

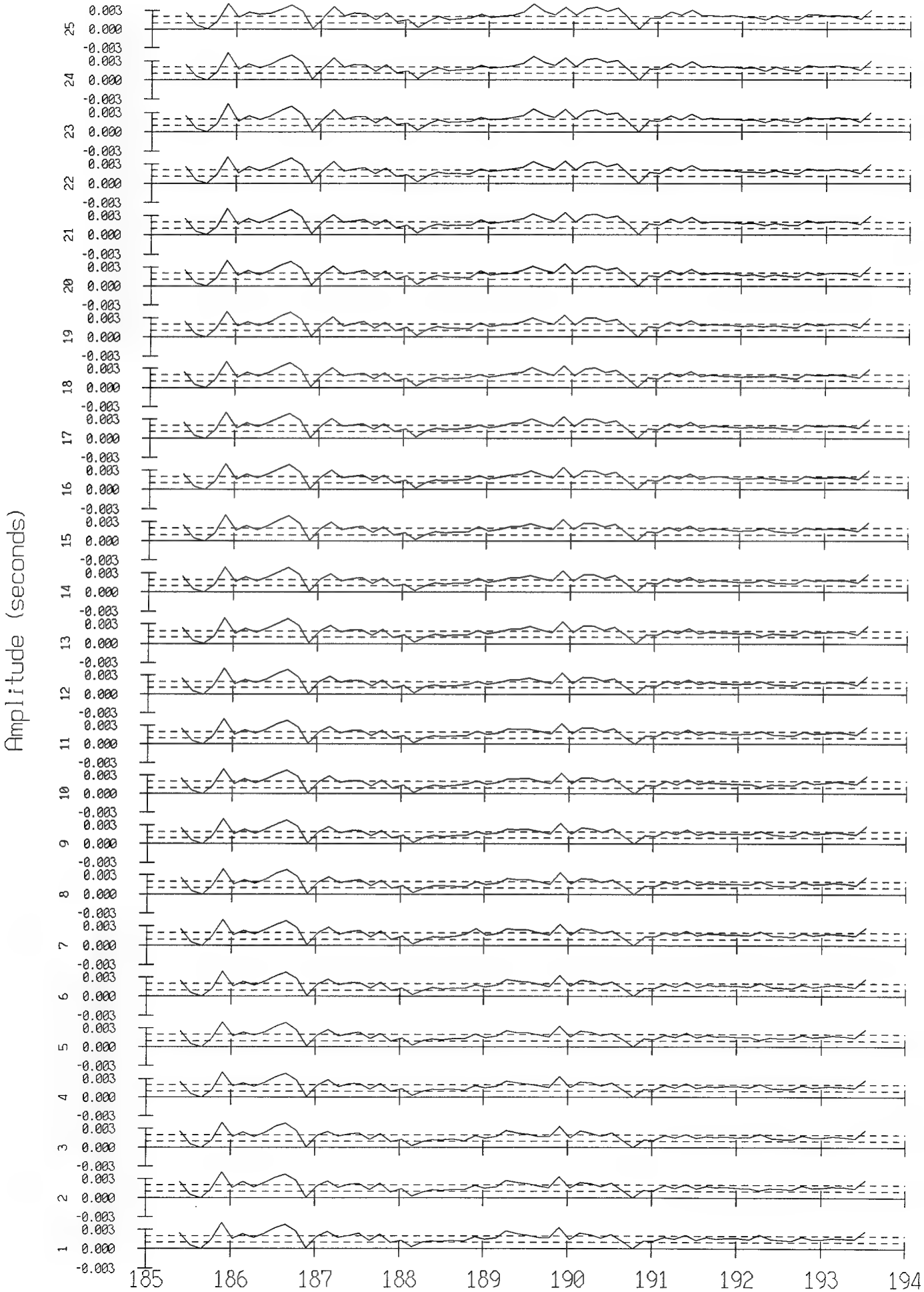

Figure 23D VAST MPL vertical array
Standard deviations of 11 Khz transponder arrivals

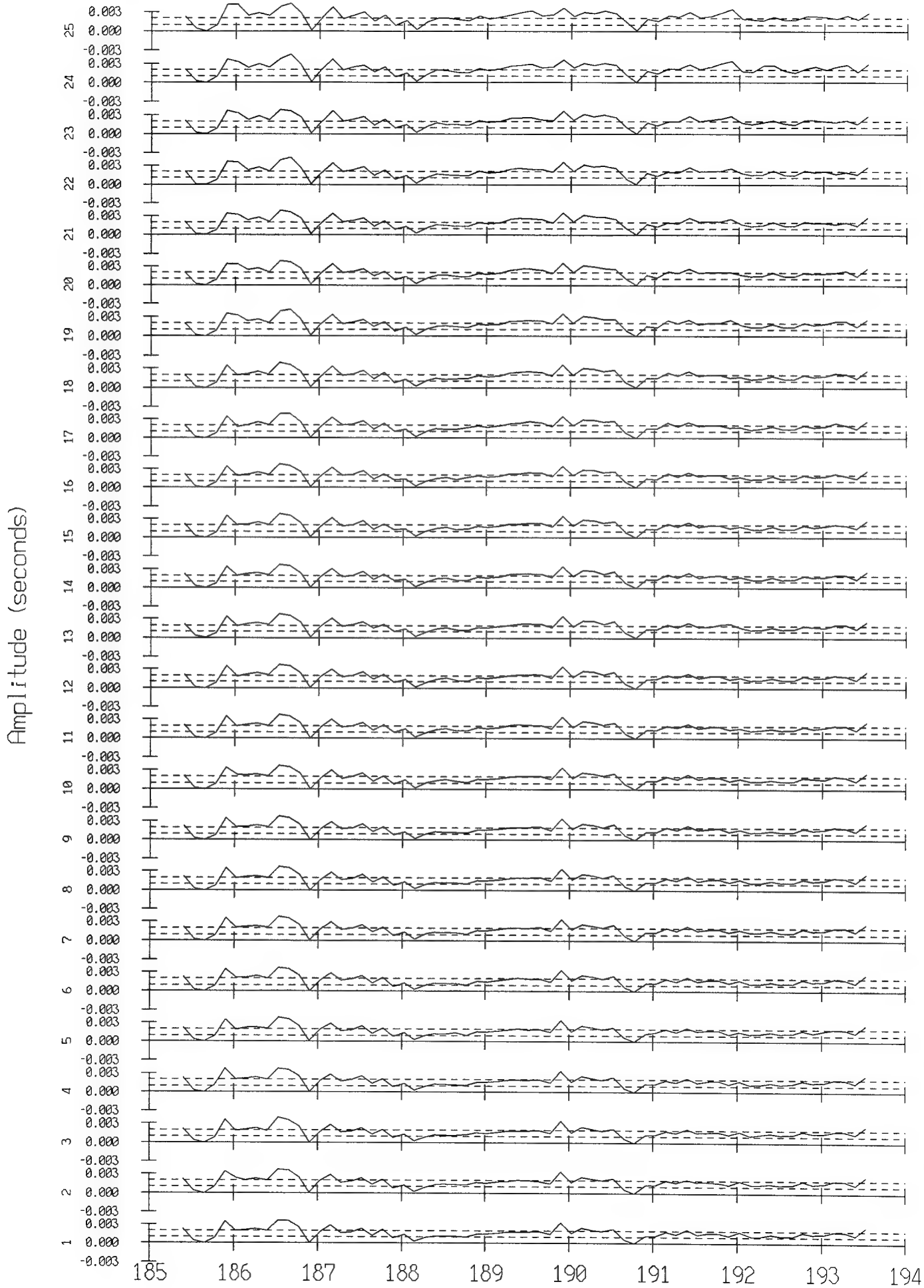

Figure 24 Blowup of a trace's standard deviations

The following plot suggests an upper bound of ~1-2 RMS for the random error. Note this is an upper bound as some of this error is attributable ot fine scale array motion. Also note the larger deviations during days 189-190 occur during rough weather/high wind conditions (see figures 29A,B,C).

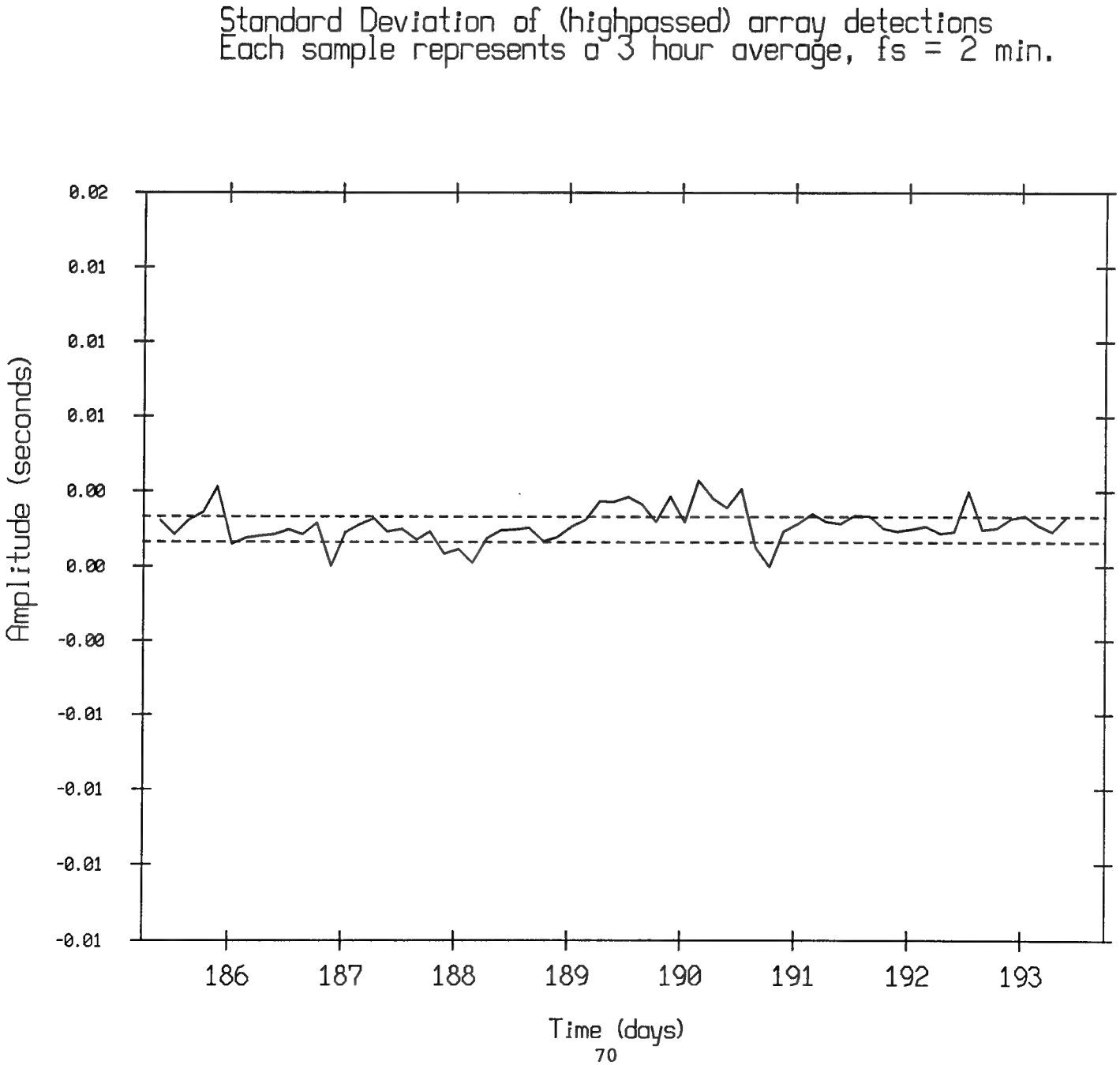

Figure 25

Transfer Function Magnitude, |H(f)|
55-coefficient high-pass FIR filter
(used to create figures 23A-D, 24, and 26A-D)

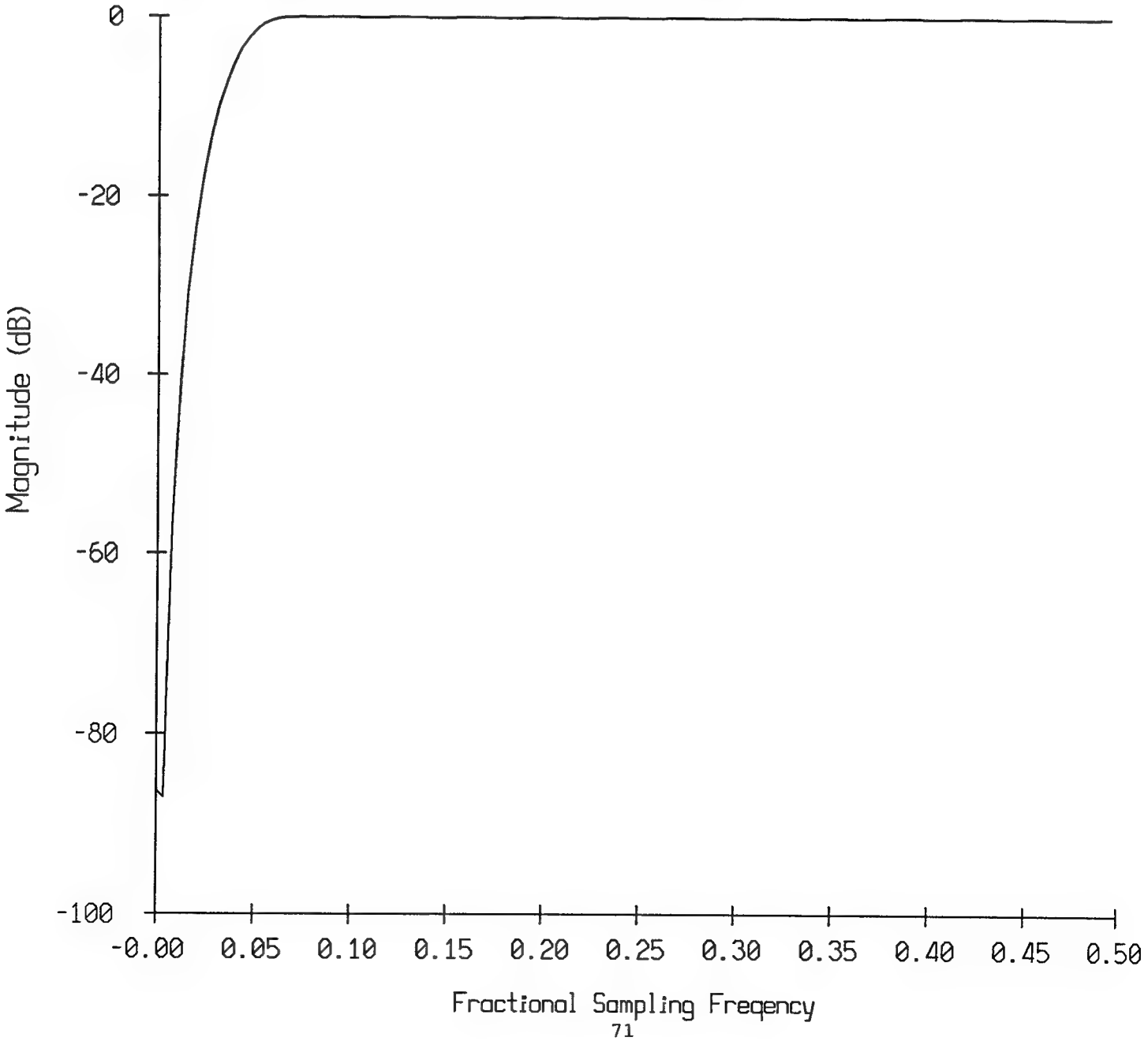

Figure 26A Standard Deviation of (hightpassed) AEL
x axis

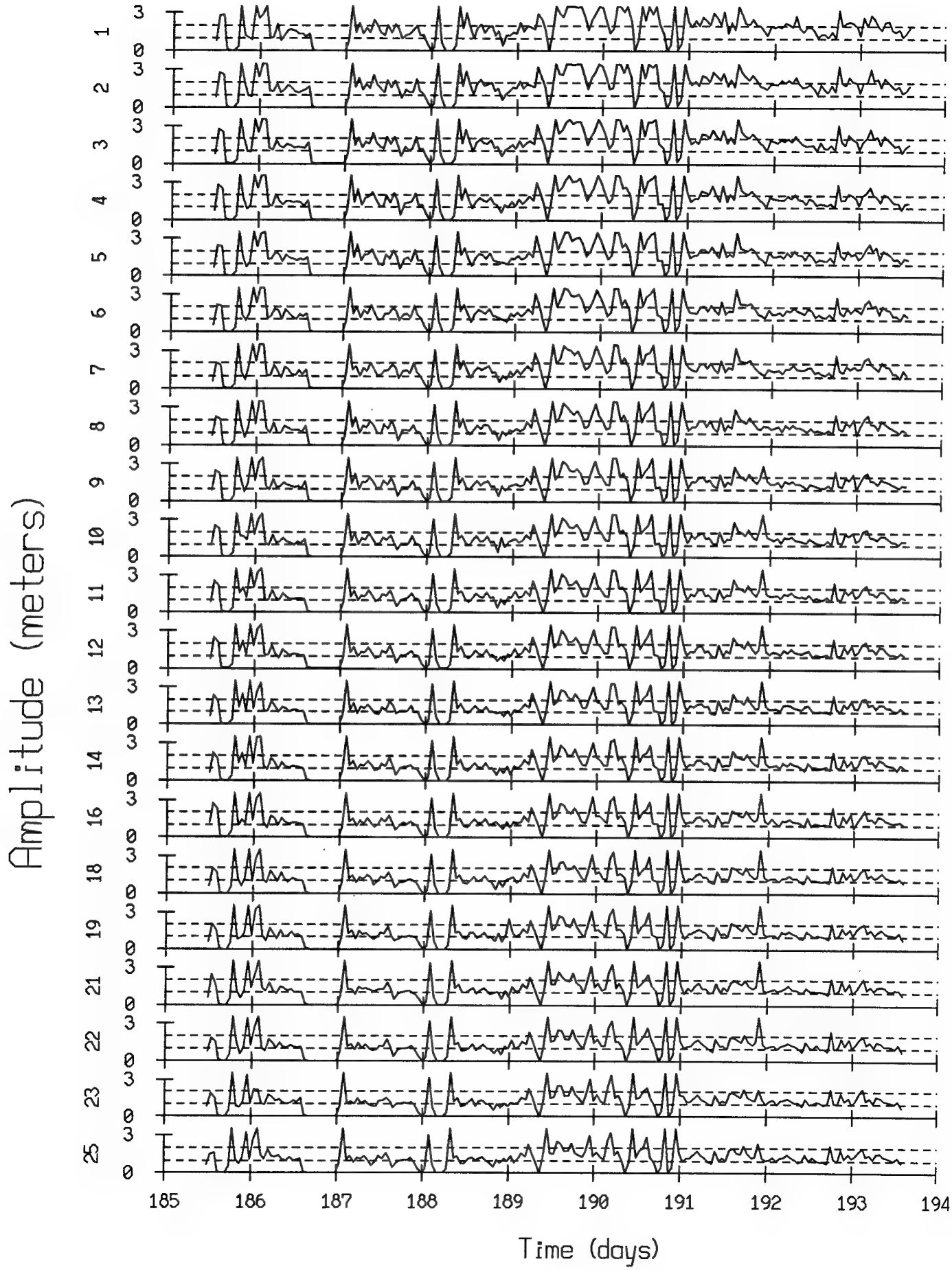

Figure 26B Standard Deviation of (hightpassed) AEL y axis

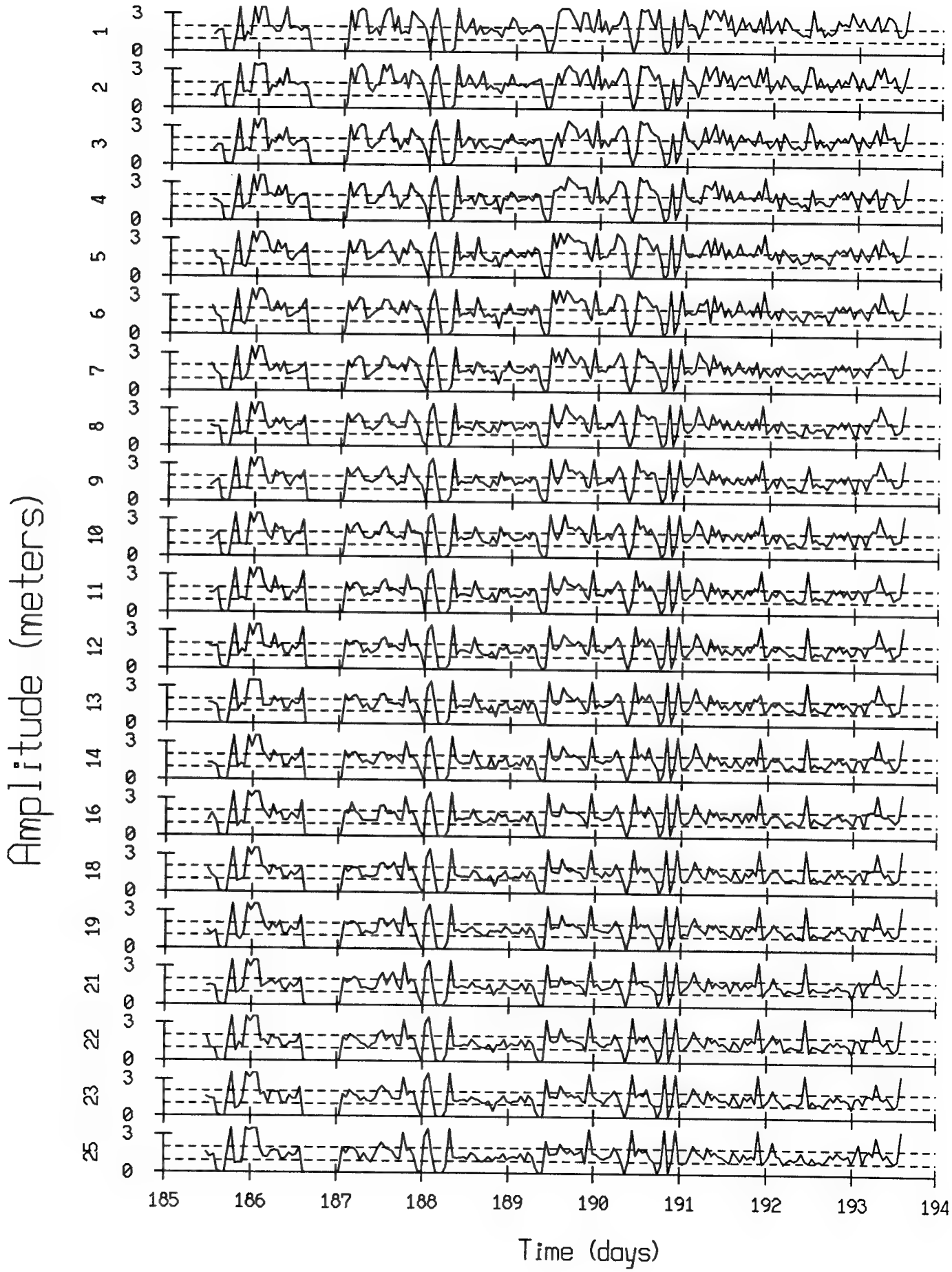

Figure 26C Standard Deviation of (hightpassed) AEL
z axis

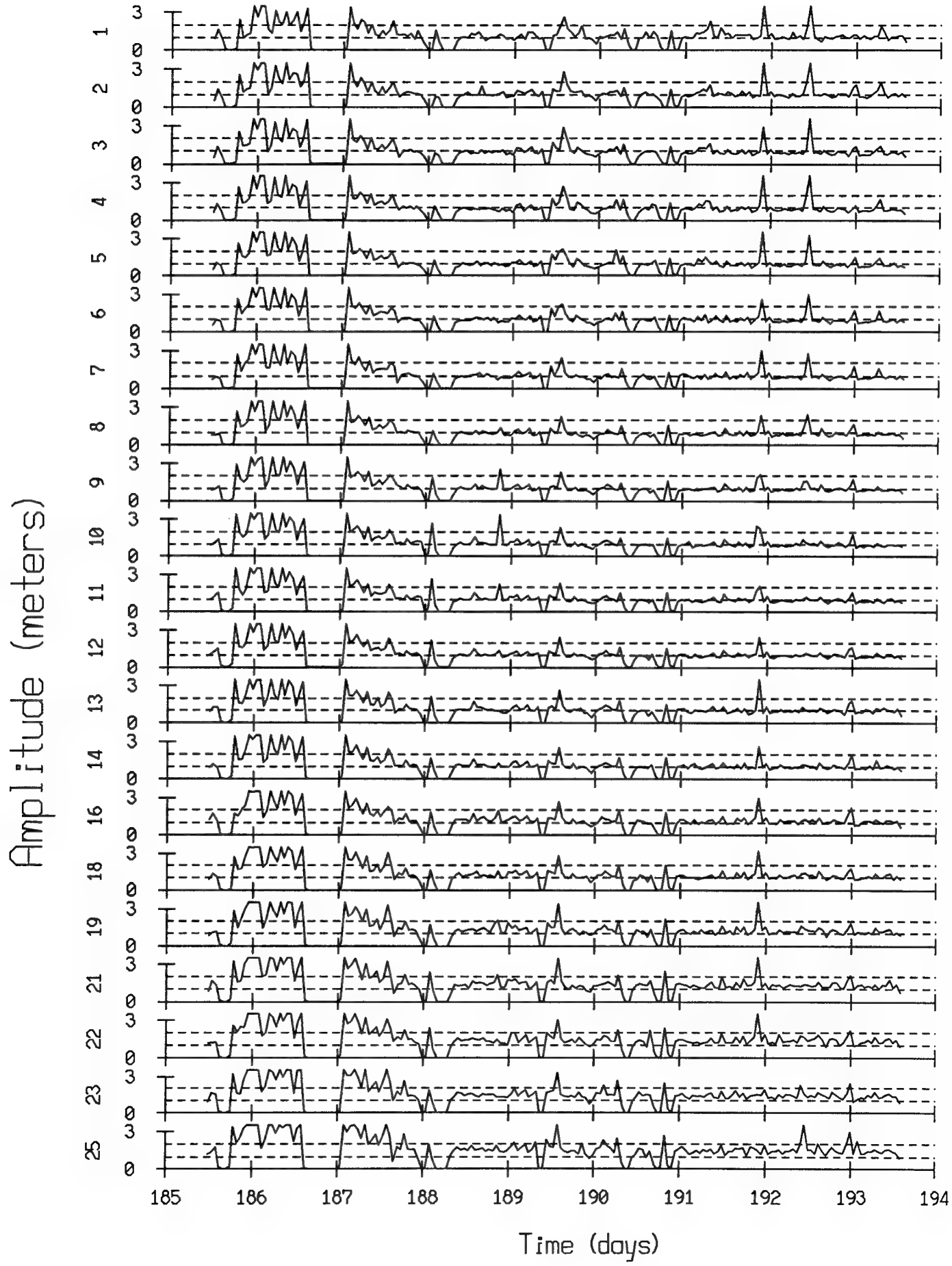

Figure 27A

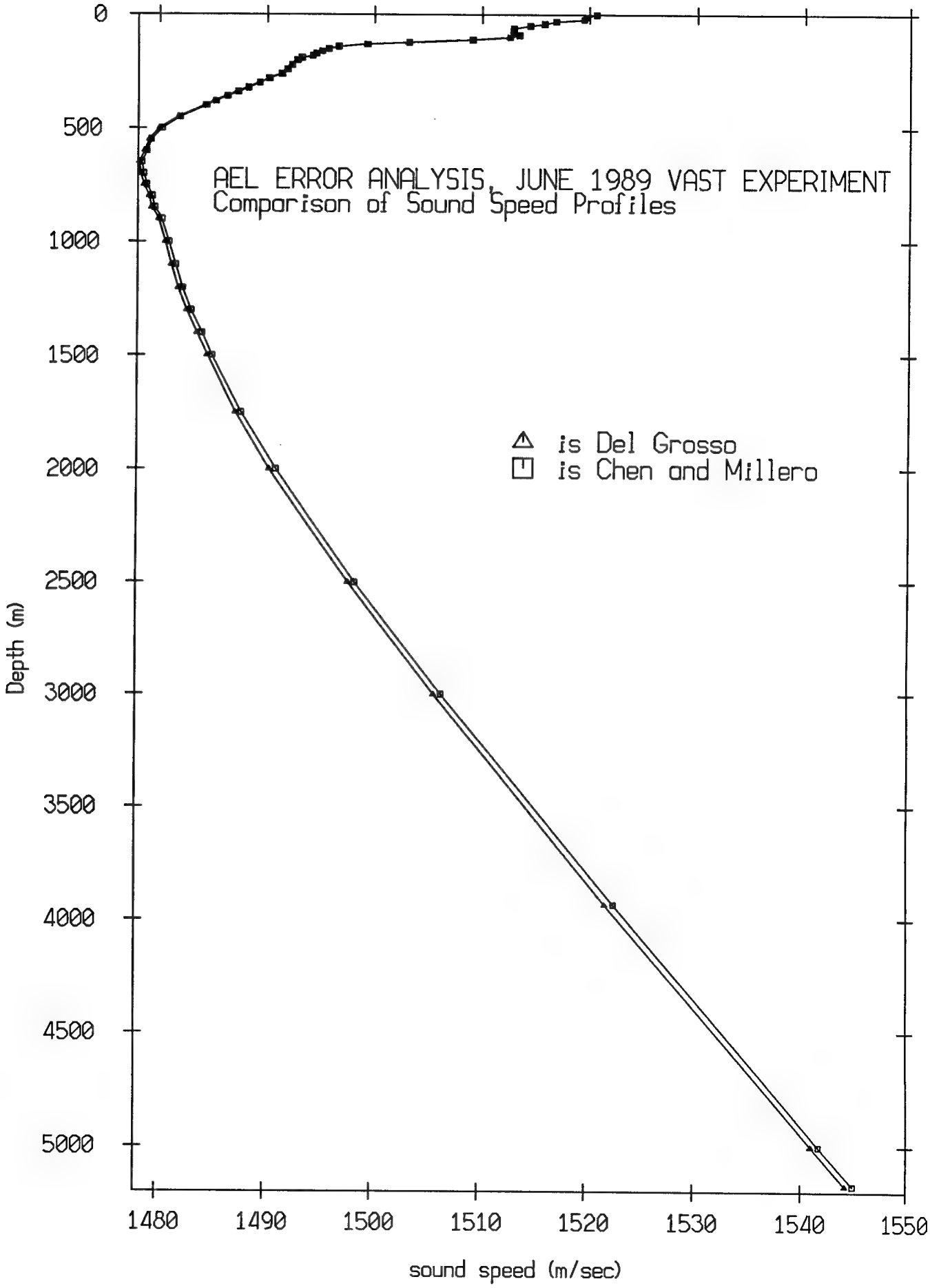
AEL ERROR ANALYSIS, JUNE 1989 VAST EXPERIMENT
Comparison of Sound Speed Profiles
is Del Grosso
is Chen and Millero
Depth (m)
0
500
1000
1500
2000
2500
3000
3500
4000
4500
5000
1480
1490
1500
1510
1520
1530
1540
1550
sound speed (m/sec)

Figure 27B

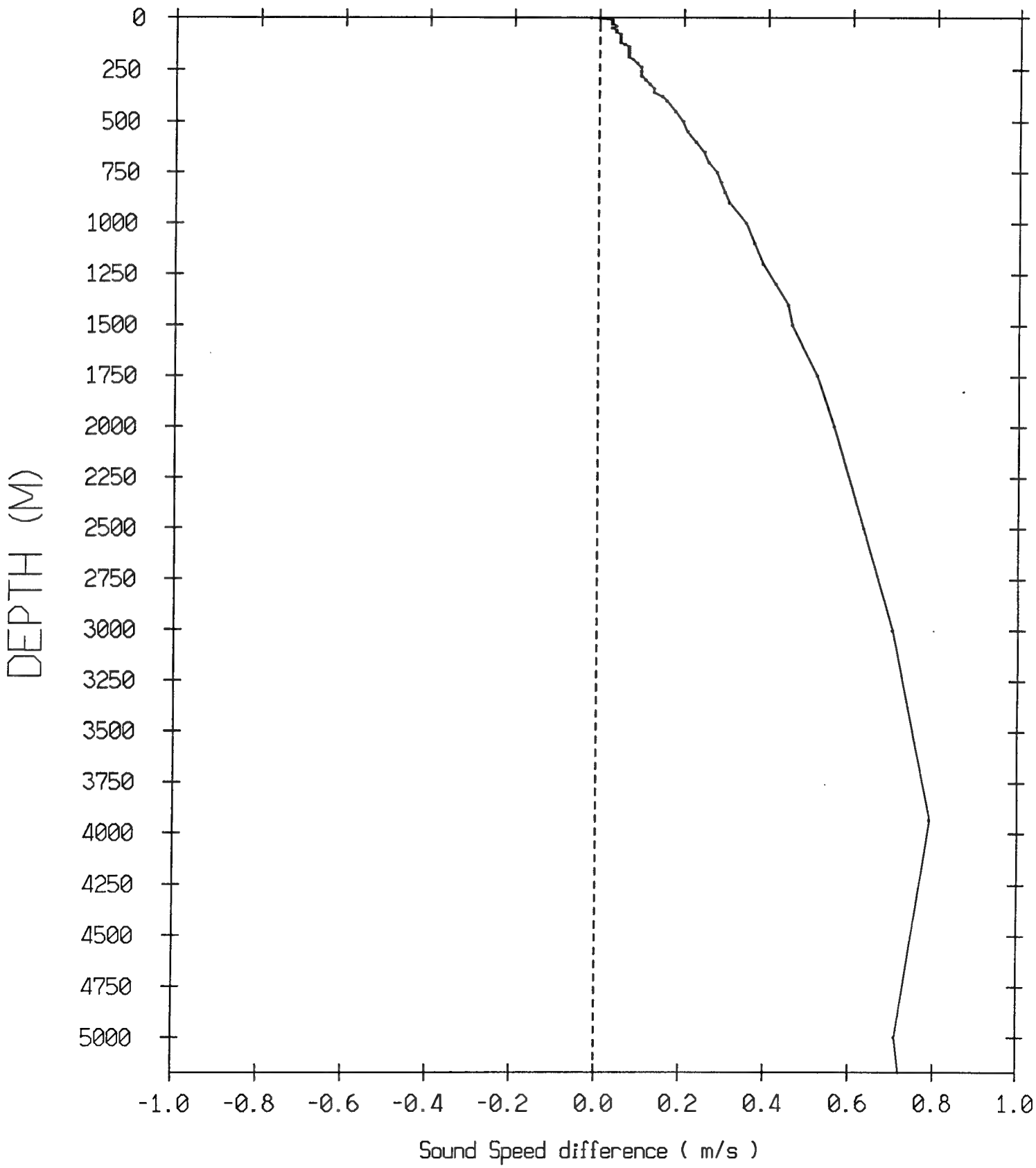
J195 CTD (Chen Millero - Del Grosso)
DEPTH (M)
0
250
500
750
1000
1250
1500
1750
2000
2250
2500
2750
3000
3250
3500
3750
4000
4250
4500
4750
5000
-1.0
-0.8
-0.6
-0.4
-0.2
0.0
0.2
0.4
0.6
0.8
1.0
Sound Speed difference (m/s)

Figure 27C

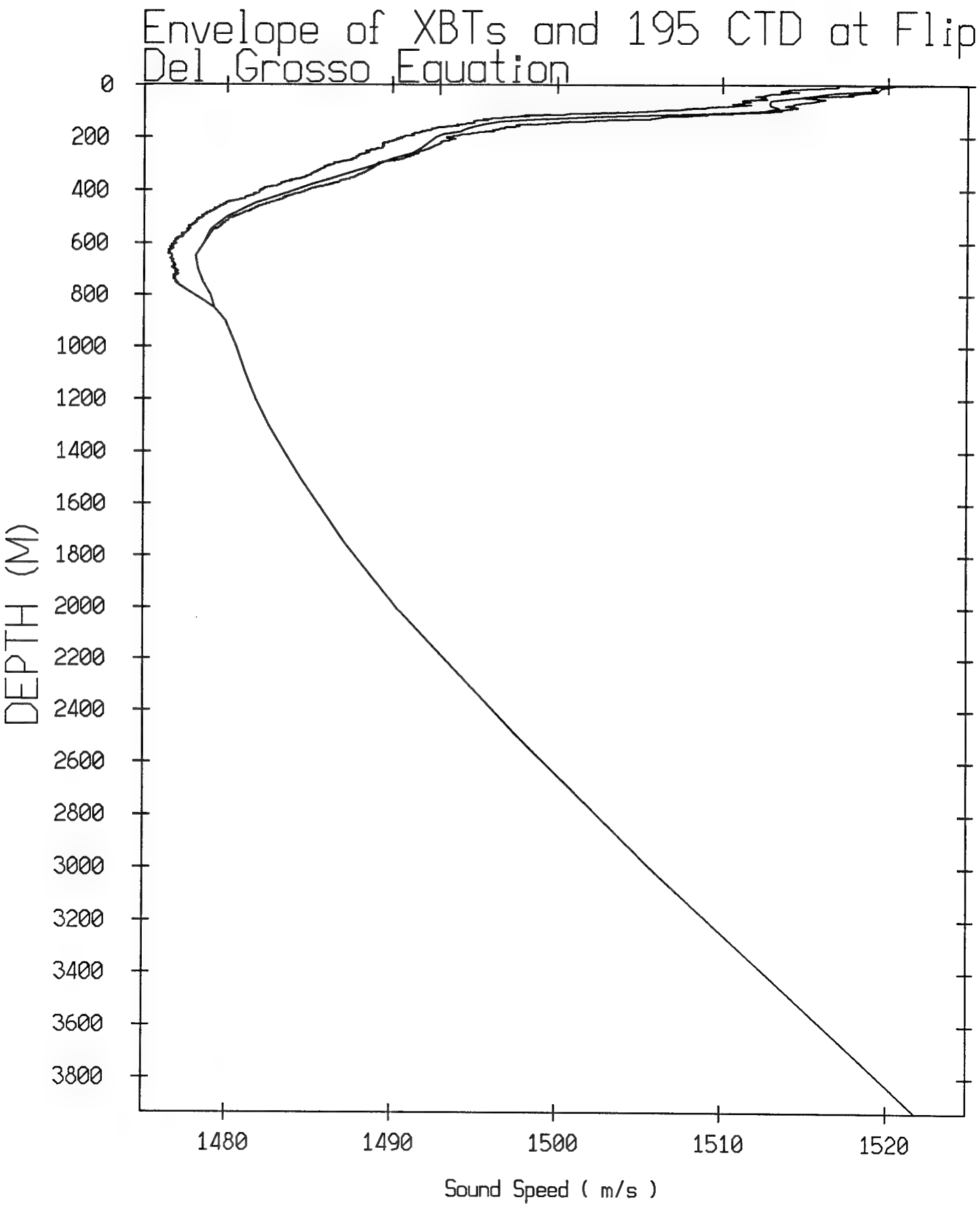
Envelope of XBTs and 195 CTD at Flip
Del Grosso Equation
0
200
400
600
800
1000
1200
1400
1600
1800
2000
2200
2400
2600
2800
3000
3200
3400
3600
3800
DEPTH (M)
1480
1490
1500
1510
1520
Sound Speed (m/s)

Figure 27D

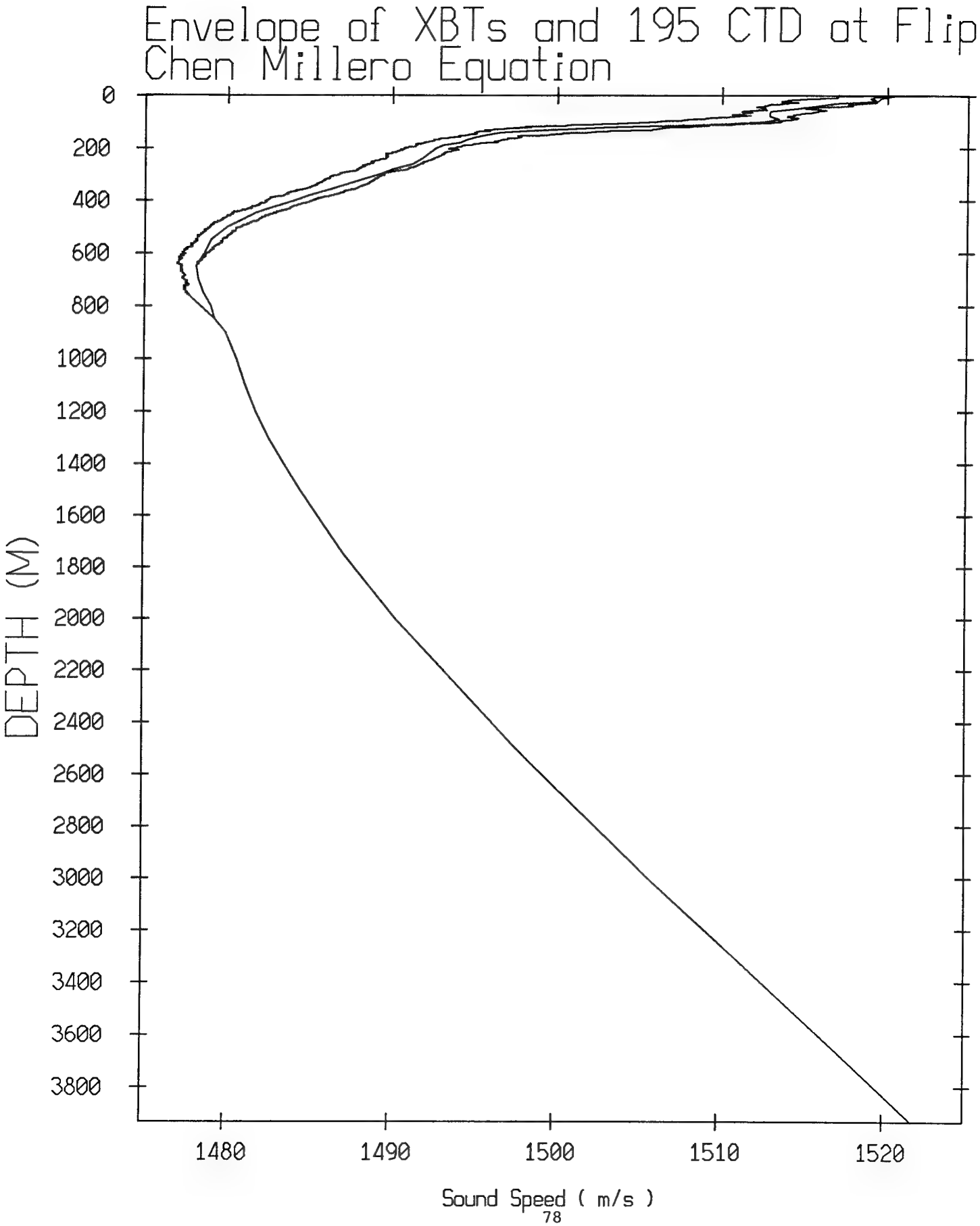
Envelope of XBTs and 195 CTD at Flip
Chen Millero Equation
DEPTH (M)
0
200
400
600
800
1000
1200
1400
1600
1800
2000
2200
2400
2600
2800
3000
3200
3400
3600
3800
1480
1490
1500
1510
1520
Sound Speed (m/s)

Figure 27E

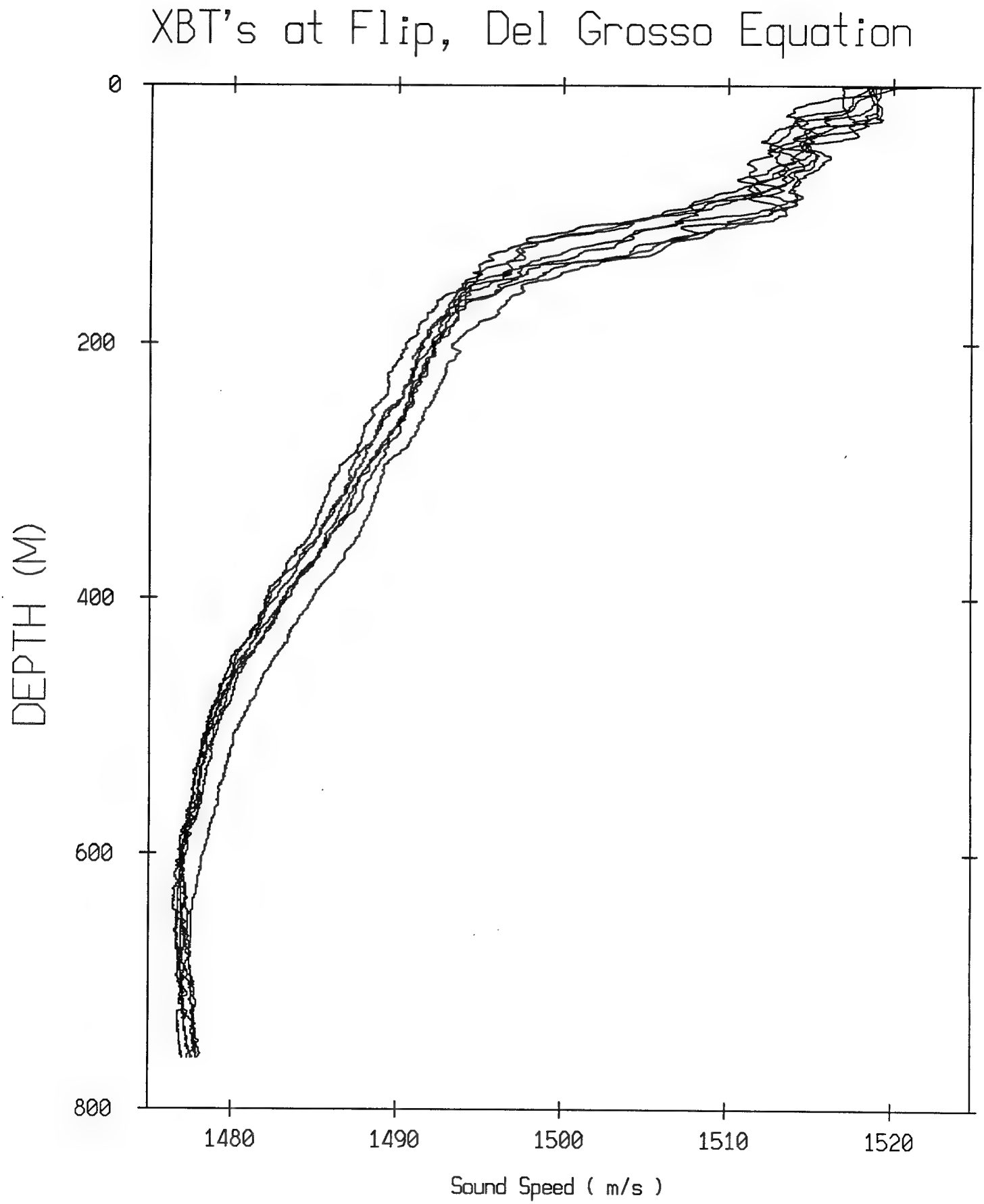
XBT's at Flip, Del Grosso Equation
0
200
400
600
800
DEPTH (M)
1480
1490
1500
1510
1520
Sound Speed (m/s)

Figure 27F

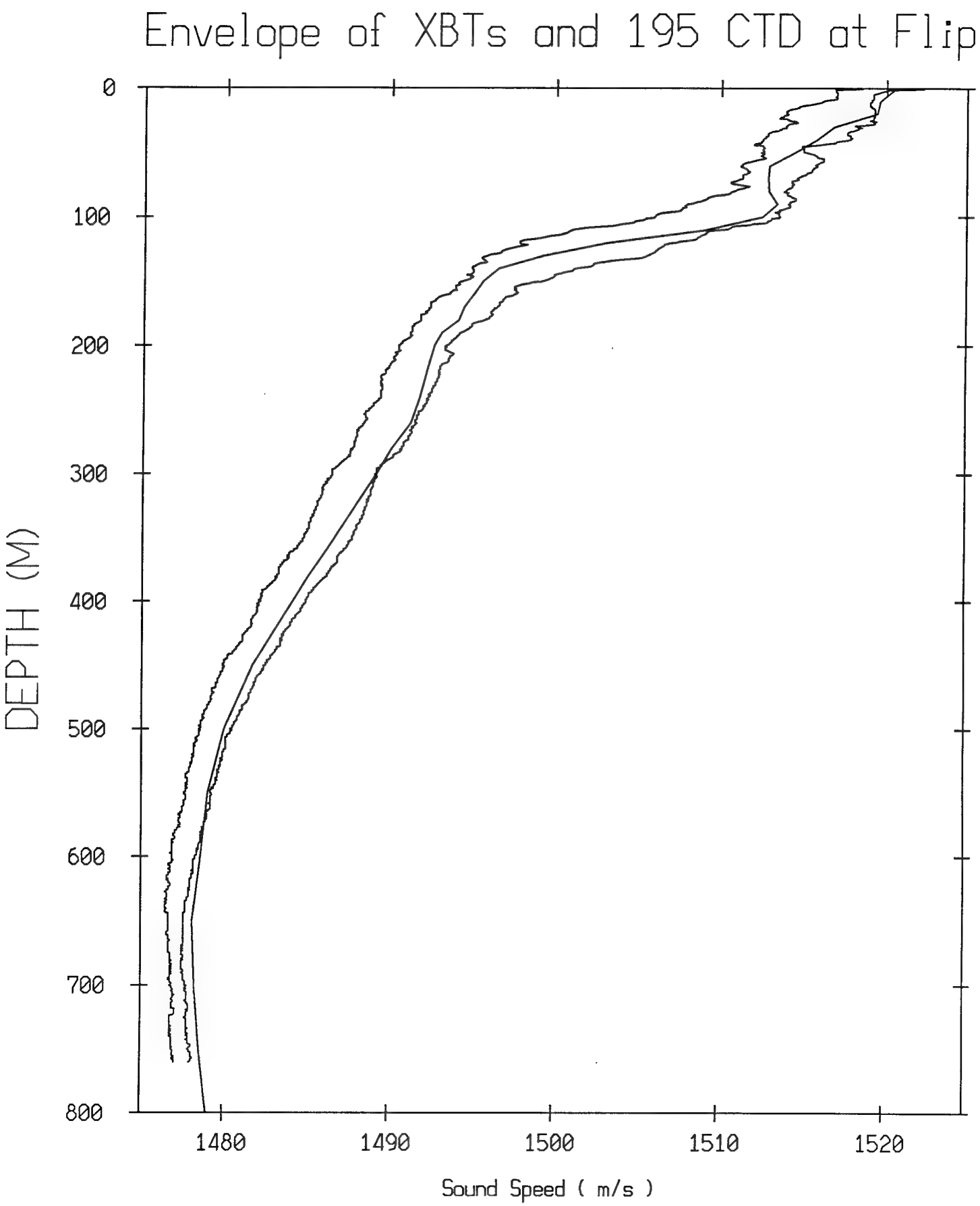
Envelope of XBTs and 195 CTD at Flip
0
100
200
300
400
500
600
700
800
DEPTH (M)
1480
1490
1500
1510
1520
Sound Speed (m/s)

Figure 28A

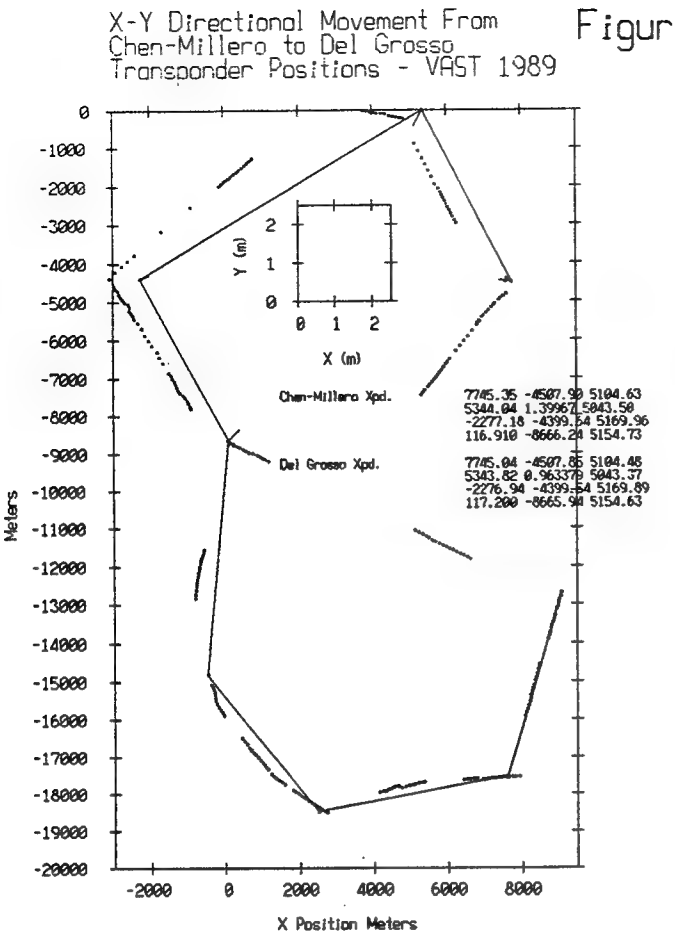
X-Y Directional Movement From
Chen-Millero to Del Grosso
Transponder Positions - VAST 1989
Y (m)
X (m)
Chen-Millero Xpd.
7745.35 -4507.99 5104.63
5344.04 1.39967 5043.50
-2277.18 -4399.64 5169.96
116.910 -8666.24 5154.73
Del Grosso Xpd.
7745.04 -4507.85 5104.48
5343.82 0.963379 5043.37
-2276.94 -4399.64 5169.89
117.200 -8665.94 5154.63
Meters
X Position Meters

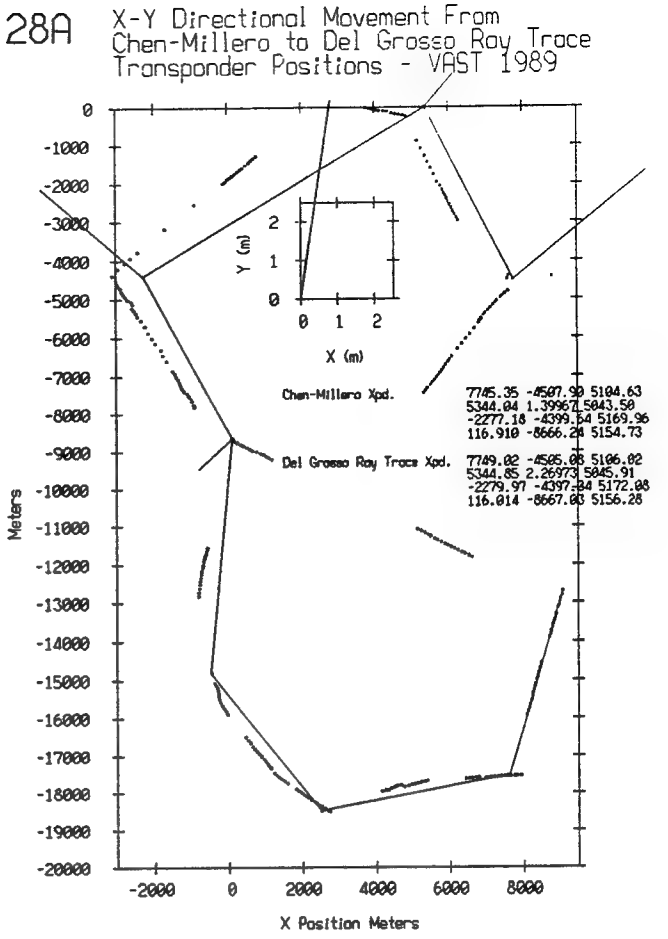
X-Y Directional Movement From
Chen-Millero to Del Grosso Ray Trace
Transponder Positions - VAST 1989
Y (m)
X (m)
Chen-Millero Xpd.
7745.35 -4507.99 5104.63
5344.04 1.39967 5043.50
-2277.18 -4399.64 5169.96
116.910 -8666.24 5154.73
Del Grosso Ray Trace Xpd.
7749.02 -4505.08 5106.02
5344.85 2.26973 5045.91
-2279.97 -4397.84 5172.08
116.014 -8667.03 5156.28
Meters
X Position Meters

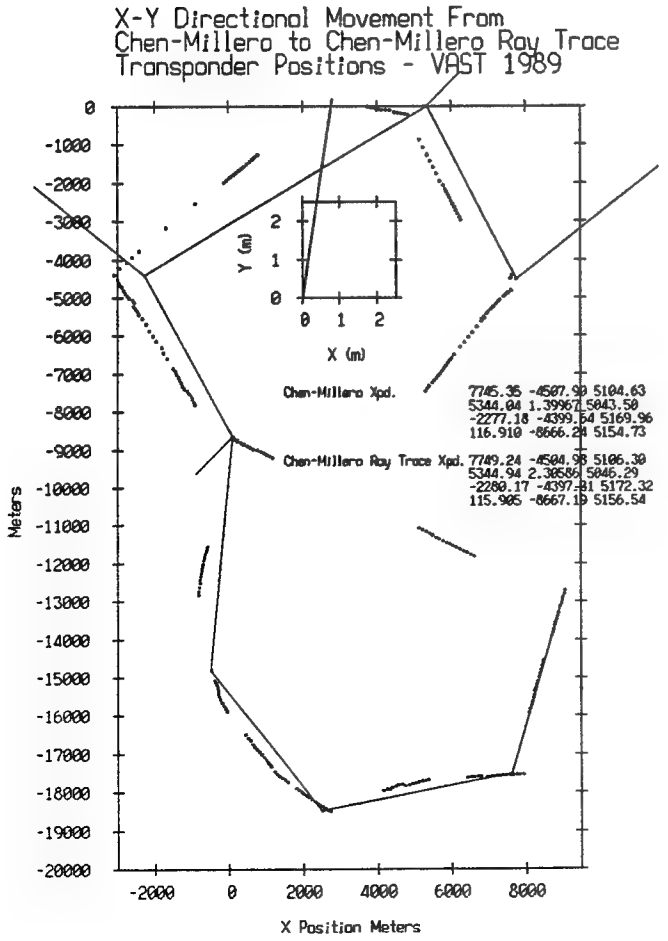
X-Y Directional Movement From
Chen-Millero to Chen-Millero Ray Trace
Transponder Positions - VAST 1989
Y (m)
X (m)
Chen-Millero Xpd.
7745.35 -4507.99 5104.63
5344.04 1.39967 5043.50
-2277.18 -4399.64 5169.96
116.910 -8666.24 5154.73
Chen-Millero Ray Trace Xpd.
7749.24 -4504.98 5106.30
5344.94 2.38586 5046.29
-2280.17 -4397.81 5172.32
115.905 -8667.19 5156.54
Meters
X Position Meters

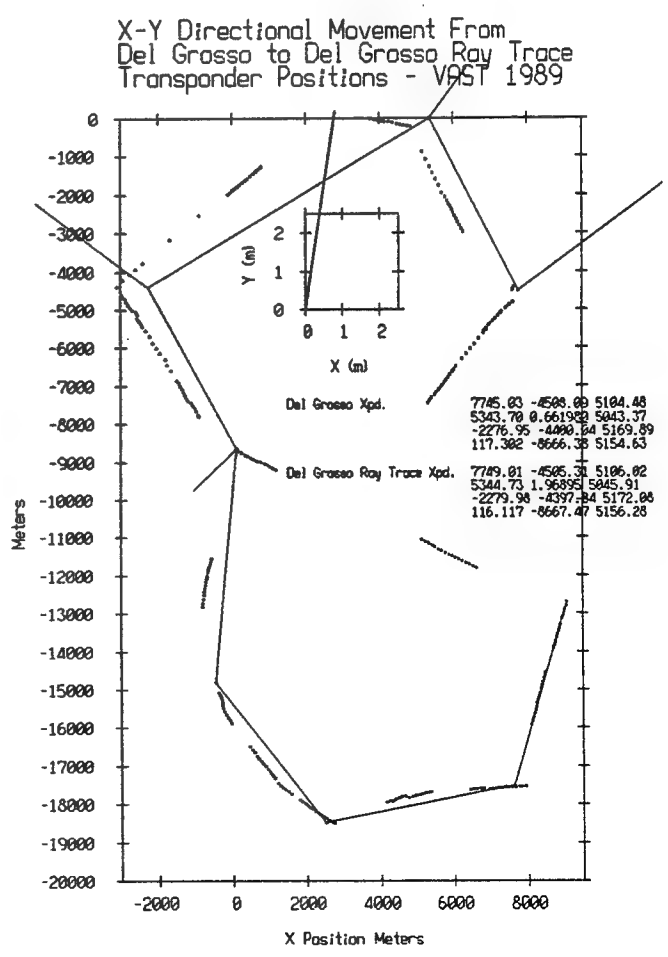
X-Y Directional Movement From
Del Grosso to Del Grosso Ray Trace
Transponder Positions - VAST 1989
Y (m)
X (m)
Del Grosso Xpd.
7745.03 -4508.00 5104.48
5343.70 0.661938 5043.37
-2276.95 -4400.64 5169.89
117.302 -8666.38 5154.63
Del Grosso Ray Trace Xpd.
7749.01 -4505.31 5106.02
5344.73 1.96895 5045.91
-2279.98 -4397.84 5172.08
116.117 -8667.47 5156.28
Meters
X Position Meters

X-Z Directional Movement From
Chen-Millero to Del Grosso
Transponder Positions - VAST 1989

Figure 28B

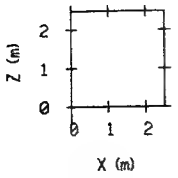

Chen-Millero Xpd.
7745.35 -4507.90 5104.63
5344.04 1.39967 5043.50
-2277.18 -4399.64 5169.96
116.910 -8666.24 5154.73

Del Grosso Xpd.
7745.04 -4507.85 5104.48
5343.82 0.963379 5043.37
-2276.94 -4399.54 5169.89
117.200 -8665.94 5154.63

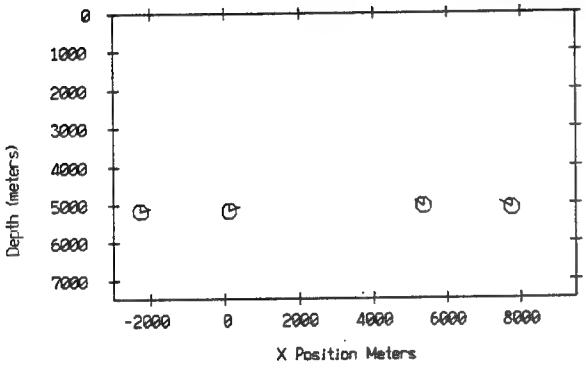

X-Z Directional Movement From
Chen-Millero to Del Grosso Ray Trace
Transponder Positions - VAST 1989

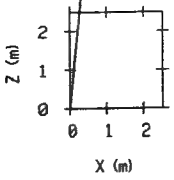

Chen-Millero Xpd.
7745.35 -4507.90 5104.63
5344.04 1.39967 5043.50
-2277.18 -4399.64 5169.96
116.910 -8666.24 5154.73

Del Grosso Ray Trace Xpd.
7749.02 -4505.08 5106.02
5344.85 2.26973 5045.91
-2279.97 -4397.34 5172.08
116.014 -8667.03 5156.28

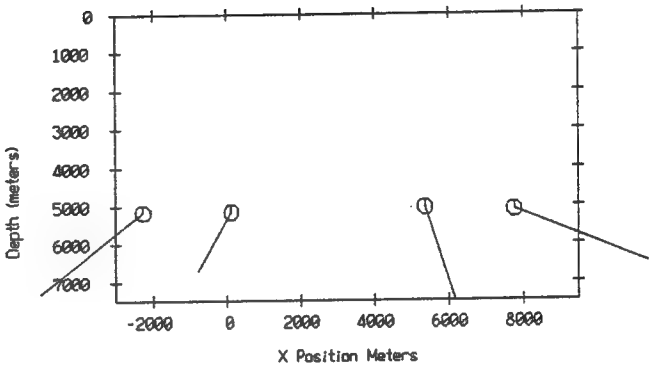

X-Z Directional Movement From
Chen-Millero to Chen-Millero Ray Trace
Transponder Positions - VAST 1989

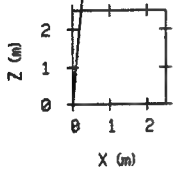

Chen-Millero Xpd.
7745.35 -4507.90 5104.63
5344.04 1.39967 5043.50
-2277.18 -4399.64 5169.96
116.910 -8666.24 5154.73

Chen-Millero Ray Trace Xpd.
7749.24 -4504.98 5106.30
5344.94 2.39586 5046.29
-2280.17 -4397.31 5172.32
115.905 -8667.19 5156.54

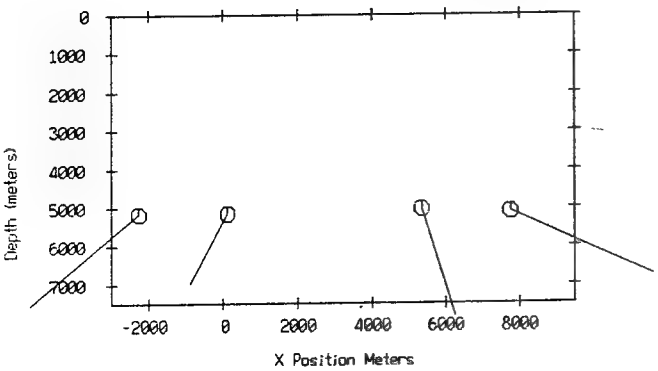

X-Z Directional Movement From
Del Grosso to Del Grosso Ray Trace
Transponder Positions - VAST 1989

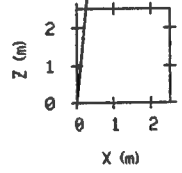

Del Grosso Xpd.
7745.03 -4508.09 5104.48
5343.70 0.661980 5043.37
-2276.95 -4400.04 5169.89
117.382 -8666.38 5154.63

Del Grosso Ray Trace Xpd.
7749.01 -4505.31 5106.02
5344.73 1.96895 5045.91
-2279.98 -4397.84 5172.08
116.117 -8667.47 5156.28

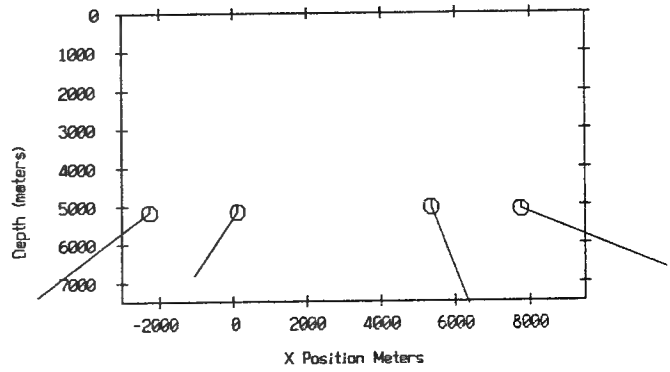

Figure 28C

Y-Z Directional Movement From
Chen-Millero to Del Grosso
Transponder Positions - VAST 1989

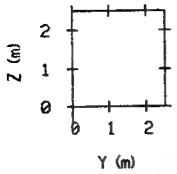

Chen-Millero Xpd.
7745.35 -4507.90 5104.63
5344.04 1.39967 5043.50
-2277.18 -4399.64 5169.96
116.910 -8666.24 5154.73

Del Grosso Xpd.
7745.04 -4507.85 5104.48
5343.82 0.963379 5043.37
-2276.94 -4399.54 5169.89
117.200 -8665.94 5154.63

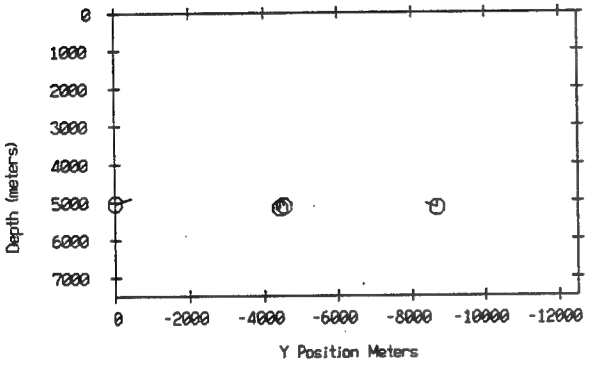

Y-Z Directional Movement From
Chen-Millero to Del Grosso Ray Trace
Transponder Positions - VAST 1989

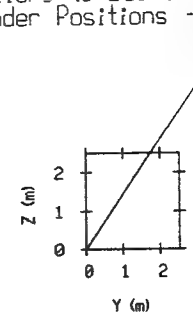

Chen-Millero Xpd.
7745.35 -4507.90 5104.63
5344.04 1.39967 5043.50
-2277.18 -4399.64 5169.96
116.910 -8666.24 5154.73

Del Grosso Ray Trace Xpd.
7749.02 -4505.08 5106.02
5344.85 2.26973 5045.91
-2279.97 -4397.34 5172.08
116.814 -8667.03 5156.28

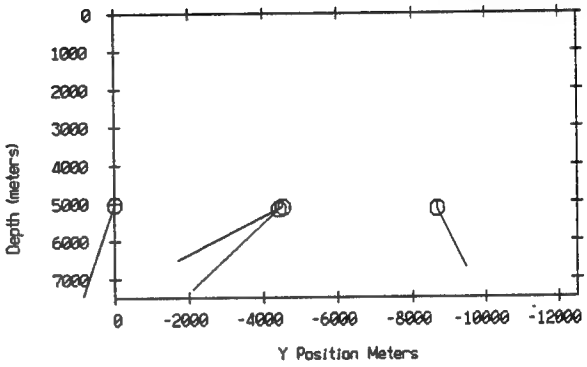

Y-Z Directional Movement From
Chen-Millero to Chen-Millero Ray Trace
Transponder Positions - VAST 1989

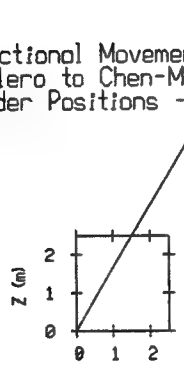

Chen-Millero Xpd.
7745.35 -4507.90 5104.63
5344.04 1.39967 5043.50
-2277.18 -4399.64 5169.96
116.910 -8666.24 5154.73

Chen-Millero Ray Trace Xpd.
7749.24 -4504.98 5106.30
5344.94 2.30586 5045.29
-2280.17 -4397.31 5172.32
115.905 -8667.19 5156.54

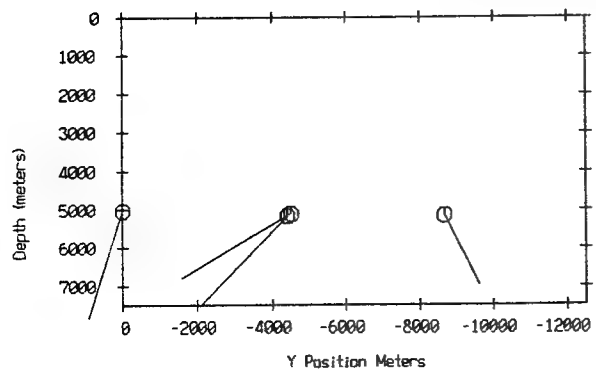

Y-Z Directional Movement From
Del Grosso to Del Grosso Ray Trace
Transponder Positions - VAST 1989

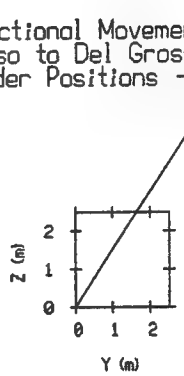

Del Grosso Xpd.
7745.03 -4508.09 5104.48
5343.70 0.661980 5043.37
-2276.95 -4400.04 5169.89
117.302 -8666.38 5154.63

Del Grosso Ray Trace Xpd.
7749.01 -4505.31 5106.02
5344.73 1.96895 5045.91
-2279.98 -4397.84 5172.08
116.117 -8667.47 5156.28

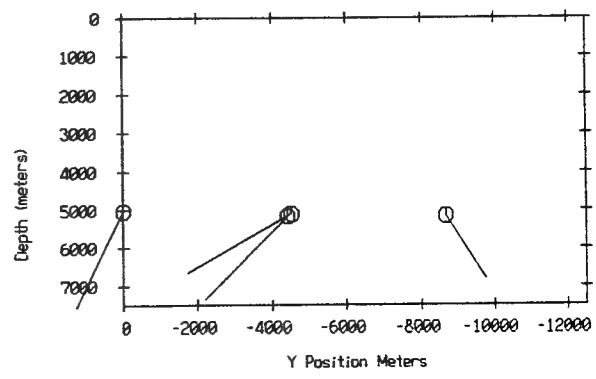

Figure 29A

Wind Speed Vs. Time
Day 185 -> Day 195

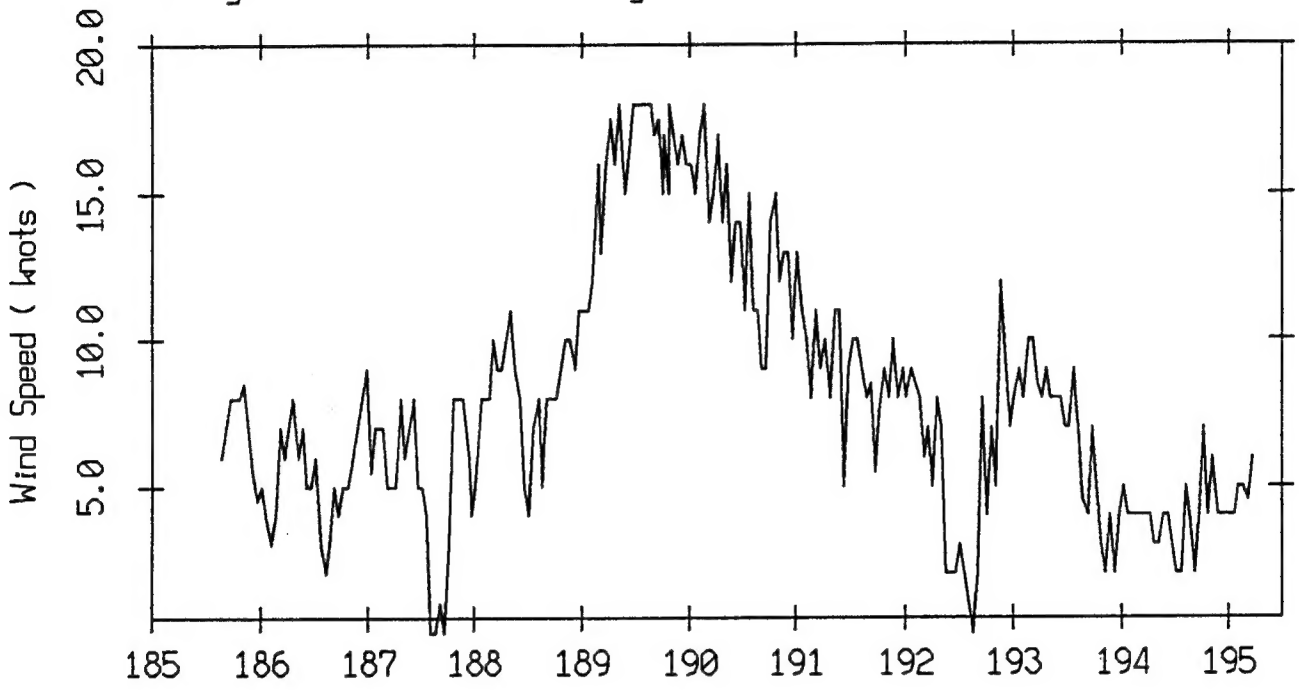

Figure 29B

Heading Vs. Time
Day 185 -> Day 195

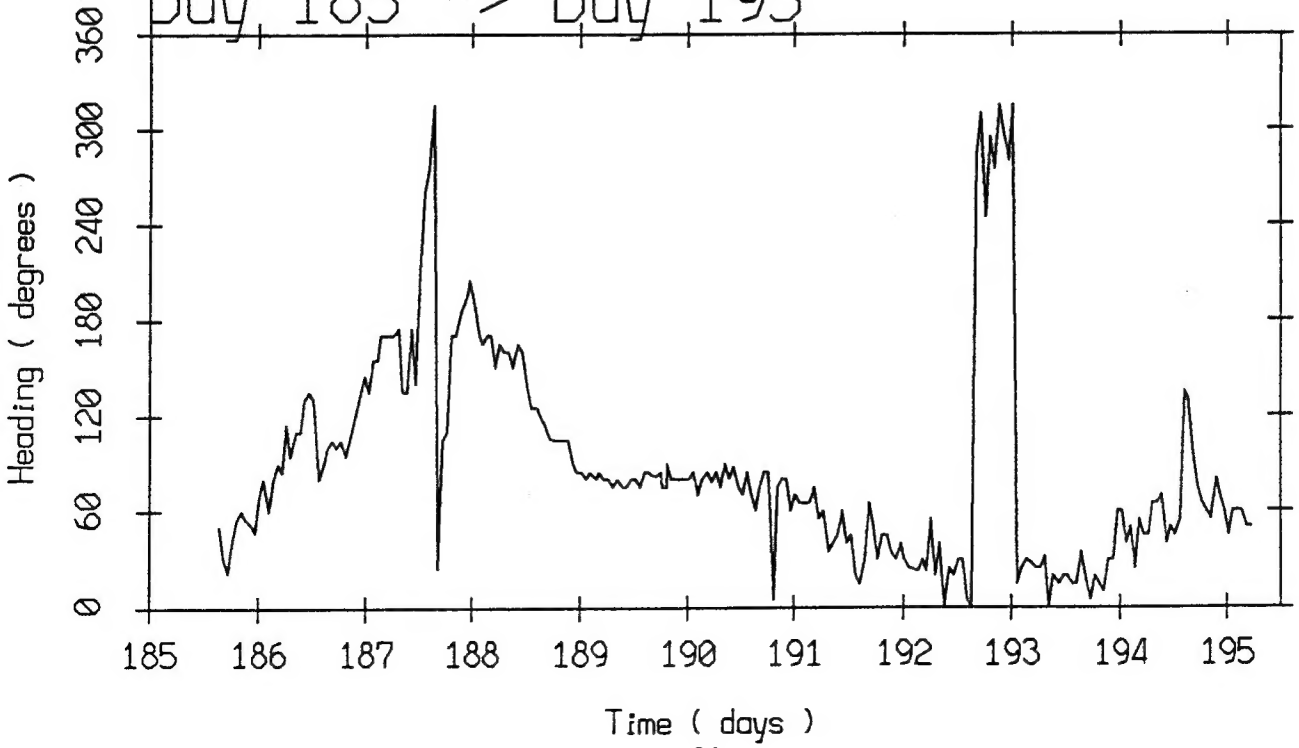

Figure 29C
Wind Speed Vs. Time
Day 185 -> Day 195

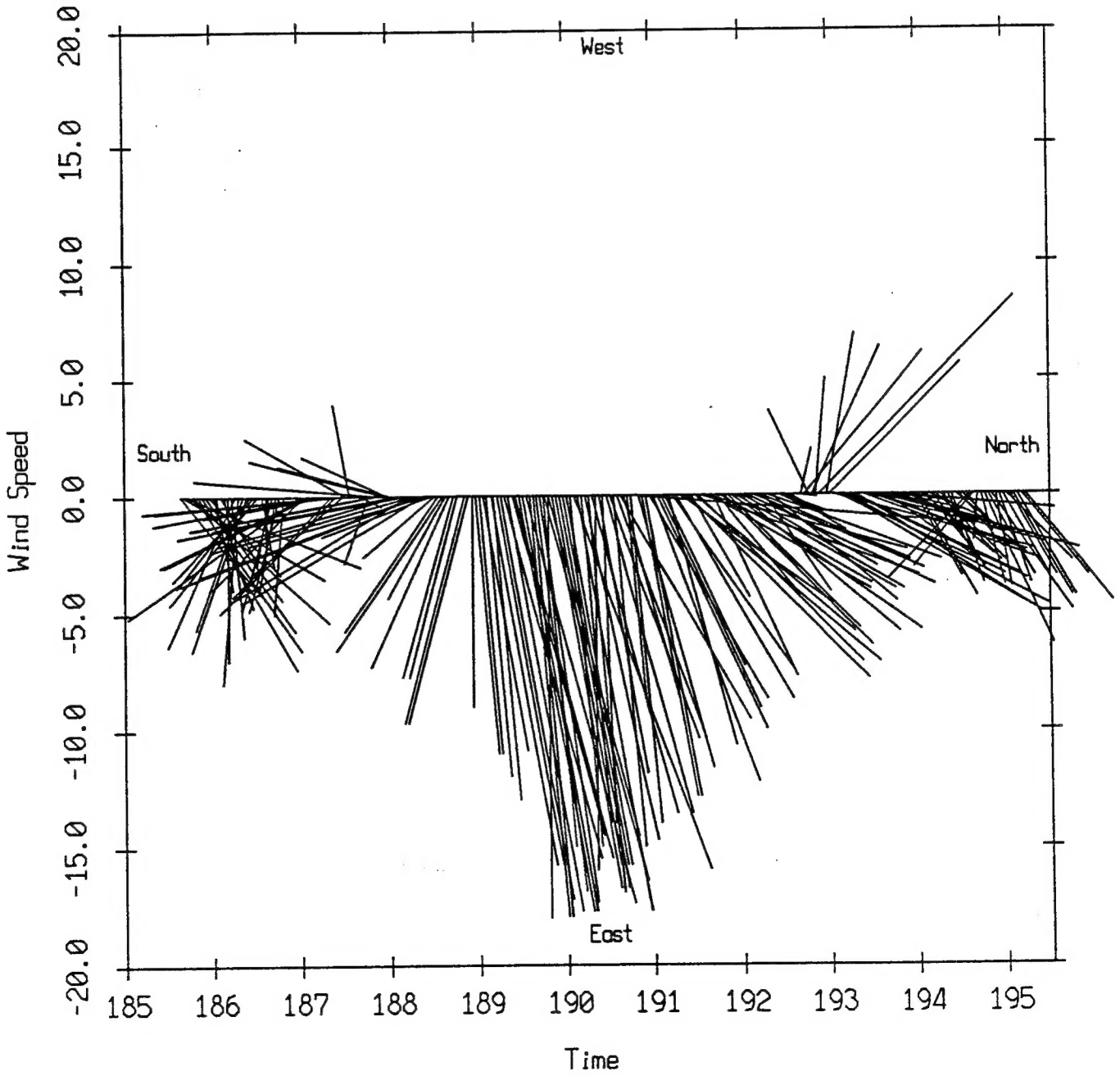

Figure 30: Navigation Block Diagram

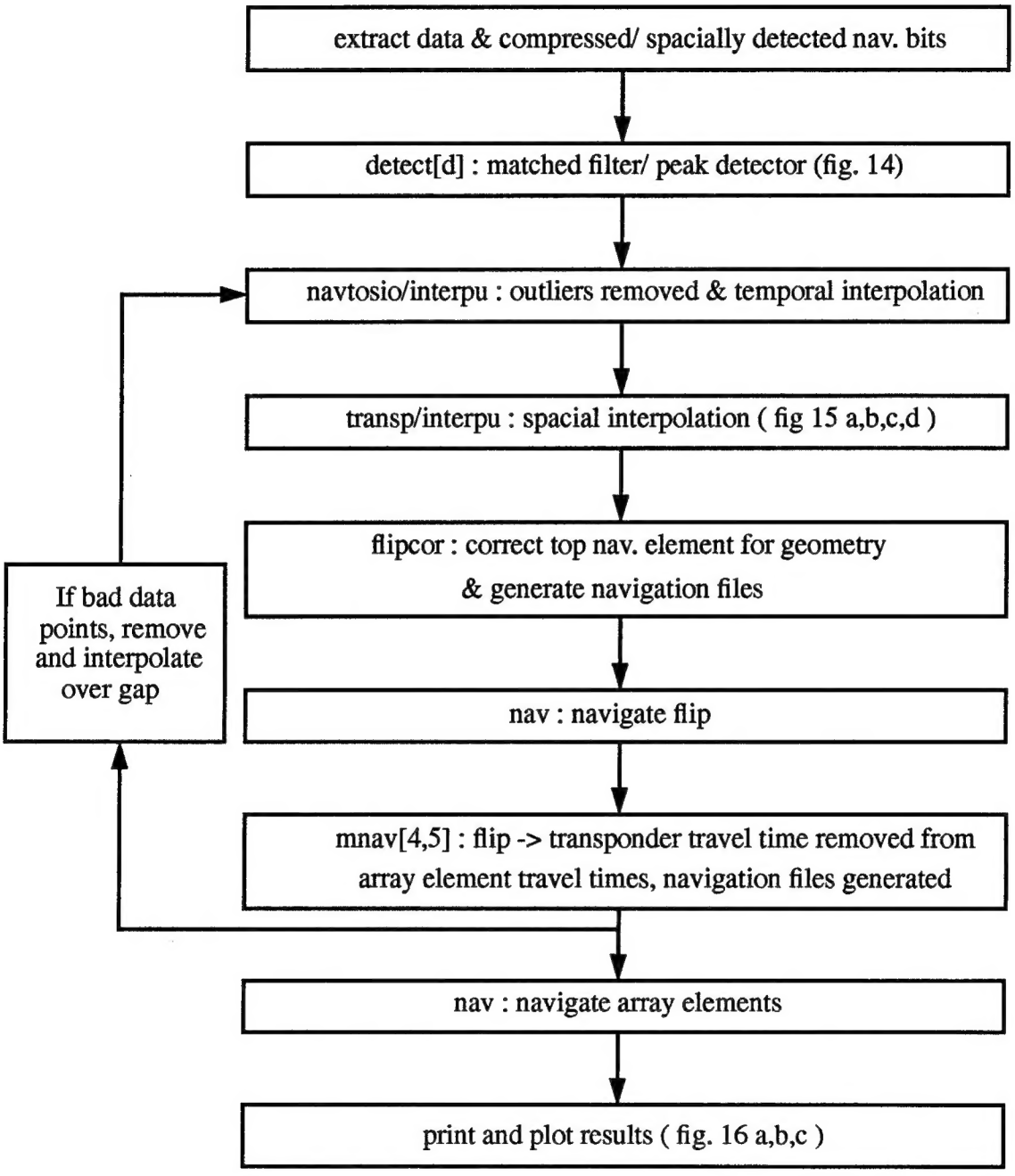

ONR/MPL REPORT DISTRIBUTION

Office of Naval Research (3)
Department of the Navy
Ballston Tower One
800 North Quincy Street
Arlington, VA 22217-5660
Atten: Dr. Richard Doolittle
Code 321

Administrative Grants Officer (1)
Office of Naval Research
Resident Representative
University of California, San Diego, 0234
8603 La Jolla Shores Drive
San Diego, CA 92093-0234

Commanding Officer (2)
Naval Research Laboratory
Atten: Code 2627
Washington, D.C. 20375-5320

Defense Technical Information Center (4)
Building 5, Cameron Station
Alexandria, VA 22304-6145